Dissertation

submitted to the

Combined Faculty of Natural Sciences and Mathematics

of the Ruperto Carola University Heidelberg, Germany

for the degree of

Doctor of Natural Sciences

Presented by

M.Sc. Julia Mändl

born in: Schwandorf, Germany

Oral examination: 09.07.2020

The *Growth Differentiation Factor 15* – a Novel Cellular Target Gene for Oncogenic Human Papillomaviruses

Referees: Prof. Dr. Martin Müller
Prof. Dr. Felix Hoppe-Seyler

Table of Contents

Summary

Persistent infections with oncogenic human papillomaviruses (HPVs) represent a major risk factor for the development of cervical cancer. The viral E6 and E7 proteins are the central driving forces for cervical carcinogenesis by inhibiting important tumor-suppressor pathways in the host cell and by generating genomic instability. Cervical cancer cells are dependent on the continuous expression of *E6/E7* in order to maintain their malignant phenotype ("oncogene addiction"). Therefore, the identification and characterization of so far unknown, E6/E7-regulated factors should enable a better understanding of the mechanisms behind HPV-linked tumorigenesis and could possibly reveal new therapeutic starting points.

The present study shows that the expression of the cellular *growth differentiation factor 15* (*GDF15*) gene, a pro-apoptotic stress response gene, is downregulated by E6 in HPV-positive cervical cancer cells as well as in HPV-immortalized keratinocytes. This GDF15 repression is observed both at the mRNA and protein level, and mechanistically caused by the interference of E6 with the p53-dependent transcriptional activation of the *GDF15* gene. The C/EBP homologous protein (CHOP) was identified as a second major activator of GDF15 expression in HPV-positive cancer cells. While p53 is the key determinant of basal GDF15 levels, it was found that both p53 and CHOP can differentially contribute to the stress-induced upregulation of GDF15 expression, dependently on the type of stress. On the phenotypic level, GDF15 overexpression blocked the capacity of cervical cancer cells to form colonies. Moreover, three anti-proliferative drugs, the ER stressor tunicamycin, the nonsteroidal anti-inflammatory drug sulindac sulfide, and the chemotherapeutic drug cisplatin, increased GDF15 levels in HPV-positive cancer cells. This was linked to the induction of apoptosis, as determined by the detection of apoptosis markers, TUNEL assays, and live cell imaging experiments visualizing Caspase activation. Both *GDF15* knockout by the CRISPR/Cas9 technology and transient downregulation of *GDF15* expression by RNA interference counteracted the pro-apoptotic stress response of HPV-positive cervical cancer cells towards those three agents.

In summary, these results identify *GDF15* as a novel cellular target gene of oncogenic HPVs, which is repressed by the E6 oncoprotein. The findings of the functional studies indicate that the downregulation of GDF15 provides HPV-positive cells with a survival advantage, by increasing their resistance against different forms of cellular stress. From a clinical point of view, it is interesting that GDF15 also plays a role in the induction of apoptosis by cisplatin, the major cytostatic agent used for treating cervical carcinomas. This latter observation points out that the E6-mediated GDF15 repression could contribute to the chemotherapy resistance of HPV-positive cancer cells.

Zusammenfassung

Persistierende Infektionen mit onkogenen humanen Papillomviren (HPV) stellen einen Hauptrisikofaktor für die Entstehung von Gebärmutterhalskrebs dar. Dabei spielen die Virusproteine E6 und E7 eine zentrale Rolle, da sie in der Wirtszelle Signalwege von wichtigen Tumorsuppressoren inhibieren und genomische Instabilität fördern. Zervixkarzinomzellen sind von einer stetigen *E6/E7*-Expression abhängig, um ihren malignen Phänotyp aufrechtzuerhalten („*oncogene addiction*"). Daher sollte die Identifizierung und Charakterisierung von bisher unbekannten, E6/E7-regulierten Faktoren dazu beitragen, die Mechanismen der HPV-assoziierten Karzinogenese besser zu verstehen. Zudem könnten dadurch neue therapeutische Ansatzpunkte aufgedeckt werden.

In der vorliegenden Arbeit wurde gezeigt, dass die Expression des zellulären „*Growth differentiation factor 15*" (*GDF15*)-Gens, ein pro-apoptotisches Gen in Stressantworten, durch E6 in HPV-positiven Gebärmutterhalskrebszellen und -immortalisierten Keratinozyten gehemmt wird. Diese GDF15-Inhibitierung kann sowohl auf der mRNA- als auch auf der Proteinebene festgestellt werden. In mechanistischer Hinsicht verhindert E6, dass p53 transkriptionell das *GDF15*-Gen aktiviert. Das C/EBP homologe Protein (CHOP) wurde als zweiter wichtiger Aktivator der GDF15-Expression in HPV-positiven Krebszellen identifiziert. Während p53 als Schlüsselfaktor die basale GDF-Expression bestimmt, können p53 und CHOP in Abhängigkeit von der vorliegenden Stressart unterschiedlich dazu beitragen, die GDF15-Expression nach Stress anzuheben. Auf phänotypischer Ebene minderte GDF15-Überexpression die Fähigkeit von Krebszellen, Kolonien zu formen. Darüber hinaus erhöhten drei Proliferationsinhibitoren, der ER Stressor Tunicamycin, das nichtsteroidale Antiphlogistikum Sulindac-Sulfid und das Zytostatikum Cisplatin, die GDF15-Level in HPV-positiven Krebszellen. Dies war verknüpft mit der Induktion von Apoptose, wie durch den Nachweis von Apoptosemarker, TUNEL-Versuche und *live cell imaging*-Experimenten, die die Aktivierung von Caspasen sichtbar machten, bestimmt wurde. Sowohl die Deletion des *GDF15*-Gens mit der CRISPR/Cas9 Technologie als auch die transiente Unterdrückung der *GDF15*-Expression durch RNA-Interferenz wirkten der pro-apoptotischen Stressreaktion der HPV-positiven Gebärmutterhalskrebszellen gegenüber den drei Agenzien entgegen.

Zusammenfassend identifizieren diese Ergebnisse *GDF15* als neues zelluläres Zielgen von onkogenen HPV-Typen, das durch das E6 Onkoprotein gehemmt wird. Die Resultate der funktionellen Studien weisen darauf hin, dass die Inhibierung der GDF15-Expression einen Überlebensvorteil für HPV-positive Gebärmutterhalskrebszellen bietet, da sie dadurch ihre Resistenz gegenüber verschiedenen, zellulären Stressarten steigert. Unter klinischen Gesichtspunkten ist es daher interessant, dass GDF15 bei der Apoptose-Induktion durch Cisplatin eine Rolle spielt, das als Zytostatikum standardmäßig gegen Zervixkarzinome

eingesetzt wird. Letzteres deutet darauf hin, dass die E6-vermittelte GDF15-Repression zur Resistenz von HPV-positiven Krebszellen gegenüber Chemotherpaien beitragen könnte.

Acknowledgements

First of all, I would like to thank Prof. Dr. Felix Hoppe-Seyler for the great opportunity to conduct my dissertation in his group, for the valuable feedback, and critical insights into the scientific world and beyond. My sincere thanks also go to Prof. Dr. Karin Hoppe-Seyler for countless profound and productive discussions about the PhD project, motivating words, and novel points of view.

Next, my gratitude goes to Prof. Dr. Martin Müller for being my first referee and for the fruitful debates during my TAC meetings. Moreover, I am also grateful to Prof. Dr. Britta Brügger and Dr. Marco Binder for their supporting role as my Thesis Committee members. Likewise, I would like to acknowledge Prof. Dr. Volker Lohmann and Prof. Dr. Frank Rösl for participating actively in my TAC meetings with critical questions and new ideas.

Importantly, I also wish to thank the whole Hoppe-Seyler group for the great working atmosphere, the omnipresent helpfulness, and the enjoyable times that we have spent together in- and outside of the lab. I highly appreciate how patiently and diligently Claudia Lohrey, Julia Bulkescher, and especially Angela Holzer supported me with all their experience on the technical base. In addition, an infinitely big “thank you” to the former and present lab members Svenja Adrian, Felicitas Boßler, Julia Braun, Kristin Frensemeier, Nora Heber, Anja Herrmann, Bianca Kuhn, Tobias Strobel, Maria Weber, and Dongyun Yang. I would like to acknowledge Thomas Holz as well for his help regarding any IT problem.

Furthermore, I truly would like to thank my group of regular Heidelberg PhD fellows for the great time, their helpfulness, and all the motivating and encouraging conversations. It was also a real pleasure and very instructive to collaborate with my different DKFZ PhD team members in order to organize several successful events. Additionally, I am grateful for all the good friends from school and university who have accompanied me on my way.

Finally, I am deeply indebted to my family. Thank you for your continuous encouragements to achieve my goals and for cheering me up, especially during exhausting moments. I am very lucky to have your support, trust, and love.

Publications and Presentations

Publications

Mändl, J., Holzer, A., Bulkescher, J., Hoppe-Seyler, K., Hoppe-Seyler, F. The *Growth Differentiation Factor 15 (GDF15)* – a Novel Cellular Target Gene for Oncogenic Human Papillomaviruses. Manuscript in preparation.

Hoppe-Seyler, K., Mändl, J., Adrian, S., Kuhn, B. J. & Hoppe-Seyler, F. Virus/Host Cell Crosstalk in Hypoxic HPV-Positive Cancer Cells. *Viruses* **9**, 174 (2017).

Presentations

Mändl, J., Hoppe-Seyler, K., Hoppe-Seyler, F. The *Growth Differentiation Factor 15* is a Novel Cellular Target Gene for Oncogenic Human Papillomaviruses. Retreat of the DKFZ Research Program Infection, Inflammation and Cancer. 25.–27.03.2019, Schöntal, Germany. Oral presentation.

Mändl, J., Hoppe-Seyler, K., Hoppe-Seyler, F. The *Growth Differentiation Factor 15* is a Novel Cellular Target Gene for Oncogenic Human Papillomaviruses. 14th Charles Rodolphe Brupbacher Symposium. 30.01.–01.02.2019, Zurich, Switzerland. Poster presentation.

Mändl, J., Hoppe-Seyler, K., Hoppe-Seyler, F. The *Growth Differentiation Factor 15* is a Novel Cellular Target Gene for Oncogenic Human Papillomaviruses. Helmholtz International Graduate School for Cancer Research 2018 PhD Poster Presentation. 16.11.2018, Heidelberg, Germany. Poster presentation.

Mändl, J., Hoppe-Seyler, K., Hoppe-Seyler, F. The Growth Differentiation Factor 15 is a Novel Target of the Human Papillomavirus E6/E7 Oncoproteins. Helmholtz International Graduate School for Cancer Research 2018 PhD Retreat.16.–18.07.2018, Weil der Stadt, Germany. Oral presentation.

Chapter 1

Introduction

1. Introduction

1.1. Human papillomavirus (HPV)-linked cancer

Worldwide, 18.1 million new cases of cancer and 9.6 million deaths from cancer were estimated for 2018.[1] The global health burden caused by cancer is predicted to rise in the following twenty years, largely due to the growing world population, increasing life span, and changes in lifestyle.

The development of cancer is a complex process, which can take several decades and is triggered by multiple factors. In 1983, Harald zur Hausen and colleagues made a controversially discussed discovery when they firstly reported a close connection between human papillomavirus (HPV) infection and cervical cancer and suggested that pathogens could be involved in the formation of these tumors.[2] Nowadays, it is estimated that infections with viruses, bacteria, or parasites are attributable for 2.2 million new cancer cases per year worldwide.[3] Approximately one third of these cases is linked to oncogenic HPVs, which contribute to the malignant transformation of cervical, other anogenital as well as oropharyngeal cancers. Increasing evidence indicates that HPVs could also be involved in the pathogenesis of non-melanoma skin cancers.[4] Cervical cancer alone accounts for 570,000 new cases and over 300,000 deaths annually.[1]

1.1.1. Classification and life cycle of HPVs

HPVs belong to the family of Papillomaviridae and are small non-enveloped circular double-stranded DNA viruses. Their genome (for a scheme of the HPV18 genome see Figure 1A) consists of approx. 8,000 base pairs and usually encodes eight proteins. These are divided into “early” (E1, E2, E4, E5, E6, and E7) or “late” (L1 and L2) proteins according to their expression pattern during the viral life cycle. Remarkably, not all HPV types encode an E5 protein.[5]

Currently, more than 440 different HPV types are identified according to their *L1* nucleotide sequence and grouped into the five phylogenetic genera “alpha”, “beta”, “gamma”, “mu”, and “nu”.[6,7] HPVs from the alpha genus infect cutaneous or mucosal epithelia and are divided into low- or high-risk HPV types. Low-risk HPV types can cause benign lesions like skin or genital warts, whereas high-risk types can take part in the malignant progression of lesions towards cancer. So far, twelve HPV types have been classified as carcinogenic (HPV16, 18, 31, 33, 35, 39, 45, 51, 52, 56, 58, and 59) and further thirteen have been labelled either as “probably carcinogenic” (HPV68) or “possibly carcinogenic” (HPV26, 30, 34, 55,66, 67, 69, 70, 73, 82, 85, and 97).[8]

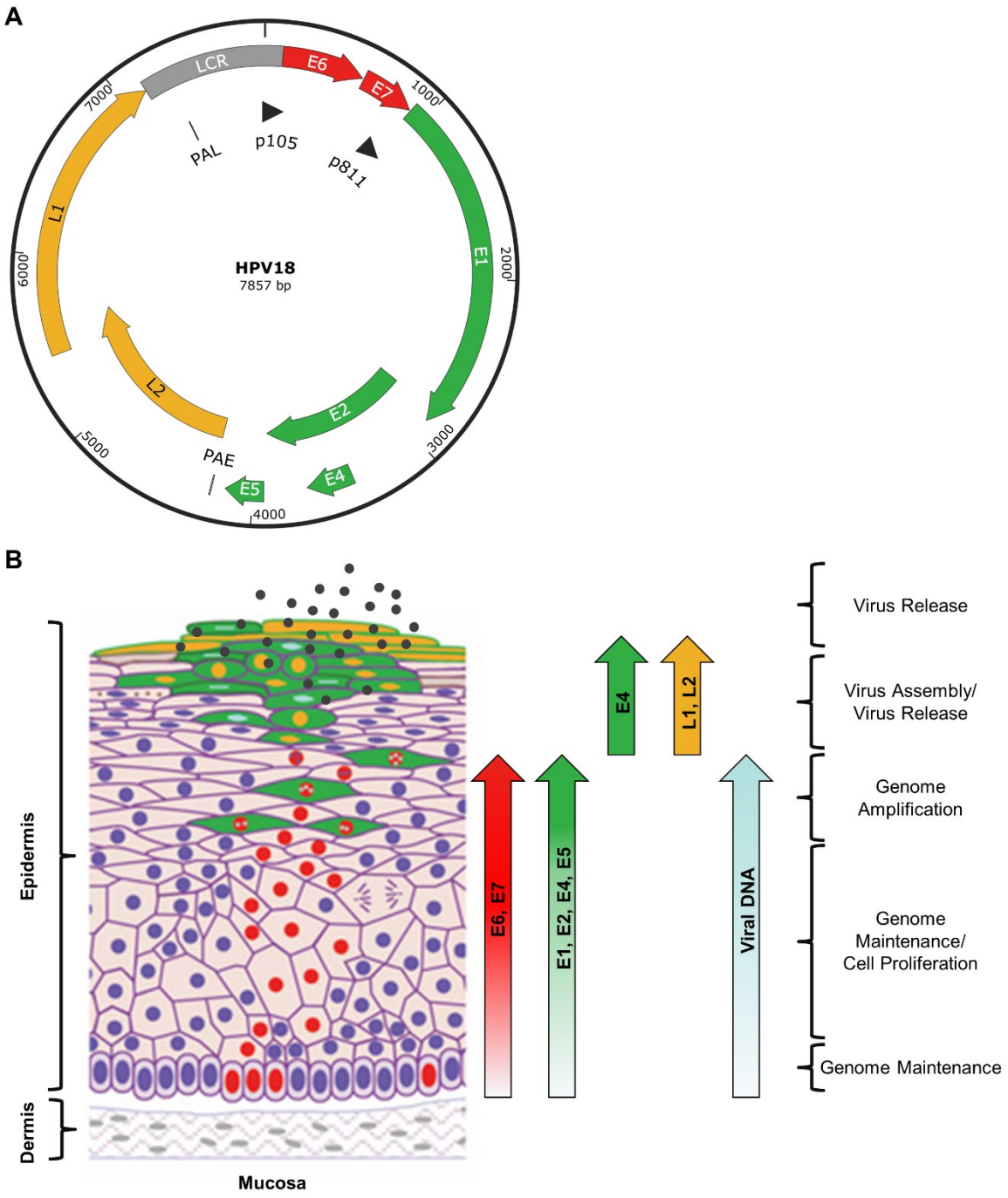

Figure 1 Organization of the HPV genome and the HPV life cycle. (**A**) The HPV18 genome is comprised of 7,857 base pairs. The two viral promoters, p105 and p811 (black arrowheads), are variably active during epithelial differentiation and are regulated by several transcription factors (e.g., AP1 and SP1), which bind to the long control region (LCR, grey box).[9] P105 controls transcription of *E6* and *E7* (red arrows), and p811 the transcription of *E1*, *E2*, *E4*, *E5* (green arrows), *L1,* and *L2* (orange arrows). Expression of the late open reading frames (ORFs) is initiated by alternative splicing, which leads to the switch from the early (PAE) to the late polyadenylation site (PAL). The illustration was created with SnapGene Viewer. (**B**) After basal cells of the epidermis have been infected by HPV, E6 and E7 are expressed and drive cell proliferation beyond the basal layer. In upper epithelial cell layers, increasing expression of E1, E2, E4, and E5 firstly leads to maintenance and later to amplification of the viral genome (light blue). L1 and L2 are expressed in late stages of the HPV life cycle and allow the assembly of virions (black circles). High levels of E4 might promote virus release. Modified from Doorbar *et al.*[10]

Genital HPV types are sexually transmitted. When upper epidermal cell layers are injured, HPVs can infect epithelial basal cells. The replication cycle of HPVs is closely linked to differentiation processes in the infected host cell. This link triggers a distinct chronological order of viral protein expression and promote the amplification of the viral genome (Figure 1B).

During the life cycle of HPVs, the early proteins E1 and E2 support episomal DNA replication: E2 recruits E1, a DNA helicase, to the LCR in the HPV genome to initiate replication.[11,12] Additionally, E2 from genital, oncogenic HPV types can function as a negative regulator of *E6/E7* expression. E6 and E7 promote proliferation by deregulating the cell cycle of the host cell.[13,14] Since they play a major role in the malignant transformation into cervical cancer (see next chapter), they are classified as viral oncoproteins. The transmembrane protein E5 also shows some oncogenic activities like stimulating growth signaling pathways or promoting evasion from host immune responses and apoptosis.[15] However, E5 is not essential for late stages of carcinogenesis because the *E5* gene is often deleted in cervical cancer cells.[16] In final phases of the HPV life cycle, E4 is highly expressed and supports efficient genome amplification, assembly, release as well as transmission of the virus.[17] L1 and L2 are called major and minor capsid protein, respectively. They support packing of viral DNA into capsids and form the icosahedral virion structure.[18,19] After virus release and transmission, L1 binds to heparan sulfate chains of proteoglycans in cell membranes or in the extracellular matrix (ECM) in order to initiate infection and the next replication cycle.[18]

1.1.2. The HPV oncoproteins E6/E7 and cervical carcinogenesis

Approximately 90% of cervical HPV infections are rapidly cleared by the human immune system and are therefore asymptomatic.[20] However, a small proportion of HPV infections can persist and form cervical intraepithelial neoplasia (CIN) even decades after the first contact to HPVs. These squamous lesions are histologically classified into one of three CIN scores according to their grade of dysplasia (CIN1: mild, CIN2: moderate, and CIN3: severe).[21] Only a low percentage of CINs finally give rise to cervical cancer, most commonly in women at the age of 40-60 years.[22] In line with this clinical data, the overexpression of E6/E7 can promote immortalization of keratinocytes *in vitro* but is usually not accompanied by the induction of tumorigenesis.[23] Interestingly, virtually all cervical tumors are HPV-positive.[24] These observations indicate that HPV infections are necessary, but not sufficient to cause cervical carcinomas.

For instance, effective immune evasion, diverse mutations in the host genome, and alterations in epigenetic patterns are linked to the progression of CINs into cervical cancer. Tumorigenesis is usually accompanied by the integration of HPV DNA into the host genome.[25] During this process, large parts of the viral genome can get deleted, which stops the production of new

virions. However, the *E6/E7* ORFs and expression of the HPV oncoproteins E6 and E7 are always retained.[16] Remarkably, the rates of *E6/E7* transcription can rise during tumorigenesis because "super-enhancer-like elements" can form after tandem integration of two viral genome copies into the host DNA.[26] Furthermore, *E6/E7* transcripts can be stabilized by deletion of non-coding AT-rich regions in the 3' end of the viral early region upon viral integration.[27] In addition, disruptions in the high-risk *E2* gene or methylation of E2 binding sites in the LCR can increase *E6/E7* expression.[28] High levels of E6/E7 are maintained during the development and in later stages of cervical cancer; malignant HPV-positive tumors are described as "oncogene-addicted" since inhibition of *E6* or *E7* commonly leads to cell growth arrest by apoptosis or senescence.[29,30] In line with these observations, the proliferation of HPV-positive cervical cancer cells is repressed *in vivo,* in transgenic mice or xenograft models, after interfering with viral oncoprotein expression.[31,32]

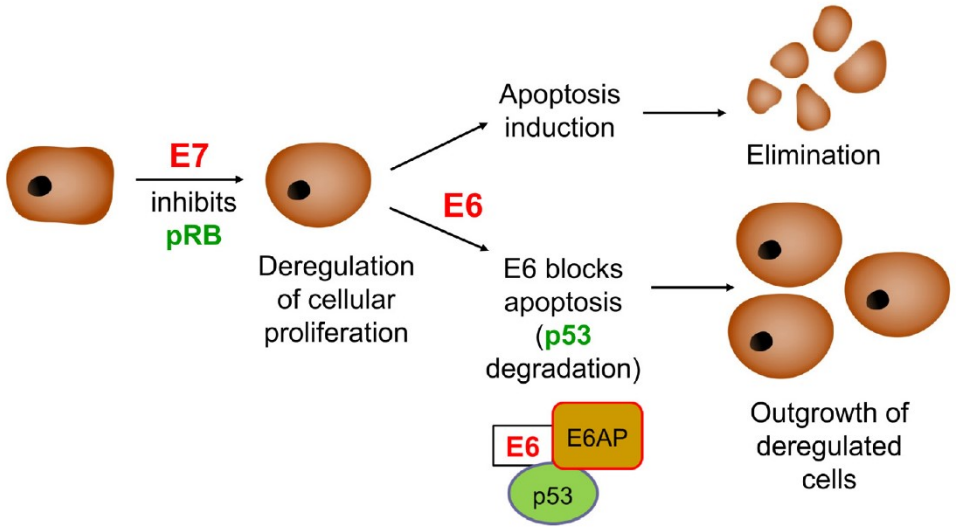

Figure 2 Cooperation of high-risk HPV E6 and E7 in carcinogenesis. E7 dysregulates the cell cycle and drives proliferation of the host cell by inhibiting the retinoblastoma protein (pRB). Such aberrant cellular growth stimuli usually induce pro-apoptotic signaling pathways like the p53 tumor suppressor pathway, which would lead to the elimination of HPV-infected cells. However, E6 blocks this host defense mechanism because it mediates the binding of the ubiquitin ligase E6-associated protein (E6AP) to p53, which results in the proteasomal degradation of p53. The figure is derived from Hoppe-Seyler *et al.*[33]

E6 and E7 are rather small proteins of approx. 150 and 100 amino acids, respectively. They form various complexes with host proteins in order to manipulate important regulatory pathways in the host cell.[34] The E6 and E7 proteins of high-risk HPVs show diverse oncogenic activities and cooperate in the malignant transformation into cervical cancer (Figure 2). Collectively, they increase cell proliferation and also induce genomic instability.[35,36] A high genomic instability can result in an accumulation of mutations in the host genome leading to inactivation of tumor suppressor genes or activation of oncogenes, which finally causes the malignant progress towards cancer.

The best-characterized target for E7 is the tumor suppressor pRB. In healthy cells, pRB is a key cell cycle regulator by binding to E2F transcription factors.[37] For the transition from G1 to S phase, pRB is phosphorylated and releases E2F proteins. Subsequently, the E2F transcription factors activate the expression of further cell cycle regulators like $p16^{INK4A}$, cyclin A and E, and of several proteins required for DNA synthesis.[38] In HPV-infected cells, E7 enforces entry into the S phase by recruiting a ubiquitin ligase complex to pRB, which is subsequently degraded by the proteasome.[39] Consequently, expression of E2F target proteins are enhanced, and high $p16^{INK4A}$ expression can serve as a marker for HPV-positive tissues.
Apart from pRB, E7 binds to related pocket proteins like p107 and p130 and thereby disrupts regulatory mechanisms of the DREAM (dimerization partner, RB-like, E2F and MuvB) complex.[40] This effect further promotes cell proliferation because the main function of the DREAM complex is to suppress expression of cell cycle-related genes when not required. Additionally, E7 promotes aberrant centrosome duplication, which triggers asymmetric distribution of chromosomes during mitosis.[36] This can cause numerical chromosomal abnormalities in cervical cells.
After DNA damage, p53 expression is increased, which leads to the transcriptional upregulation of the cell cycle inhibitor p21 and arrests cells at the G1-S phase checkpoint.[41] This cell cycle arrest is important for efficient DNA repair before the cells move into S phase. Additionally, p53 can induce apoptosis by transcriptional activation of several pro-apoptotic genes like *PUMA* (*p53 upregulated modulator of apoptosis*) and *NOXA* (Latin for damage).[41] In HPV-positive cells, present p53 is steadily marked for degradation in the proteasome because E6 recruits the ubiquitin ligase E6AP to p53.[42]
Apart from repressing p53, E6 binds to PDZ (firstly discovered in post synaptic density protein 95 (PSD95), disc large homolog 1 (Dlg1) and zonula occludens-1 protein (ZO-1)) domain-containing proteins (e.g., DLG1), which regulate cell polarity, migration, and attachment for instance.[43] E6 also stimulates the expression of human telomerase reverse transcriptase (hTERT), the catalytic component of telomerase, and thereby prevents replicative senescence.[44]

1.1.3. Prevention and treatment of cervical cancer

Smoking, the number of full-term pregnancies, and long-term use of hormonal contraceptives were shown to increase the risk of cervical cancer.[45–47] However, the infection with oncogenic HPVs represents the major risk factor because evidence of single or multiple HPV types is found in nearly all cervical tumors.[24] Hence, the development of vaccines against high-risk HPV types should represent a substantial step in the progress of preventing cervical cancer.

Currently, three prophylactic vaccines are approved. They are based on virus-like particles (VLPs) comprised of the major capsid protein L1. The bivalent Cervarix (GlaxoSmithKline Biologicals, Rixensart, Belgium) protects against the two most frequent high-risk HPV types in cervical cancer, HPV16 and HPV18, accounting for 55.8% and 14.3% of the cases, respectively.[48] The quadrivalent Gardasil (MSD Vaccins, Lyon, France) additionally includes antigens against the two low-risk HPV types 6 and 11, which commonly cause genital warts.[49] Since 2015, the nonavalent vaccine Gardasil 9 (MSD Vaccins, Lyon, France) has been approved. It covers the HPV types 6, 11, 16, 18, 31, 33, 45, 52, and 58. All three vaccines show excellent safety profiles and efficiencies in seroconversion, which result in higher antibody titers than observed after natural infection.[49,50] The German Standing Committee on Vaccination at the Robert Koch Institute recommends vaccination against HPVs at the age of 9-14 for girls and, since June 2018, also for boys.[51] In order to protect against a broader range of HPV types, vaccines based on the minor capsid protein L2 are under development, which are expected to be less type-specific.[52]

However, low global vaccination rates represent a major drawback in the prevention of cervical cancer.[53] To reduce the costs of HPV vaccines, could be an important step to raise vaccinations rates. This will be especially helpful in less developed, low-income countries of Africa and Asia, where the highest incidence rates of cervical cancer cases are found.[53,54]

More efficient screening procedures and therapies are needed until a sufficient proportion of the world population and people of all ages are protected against HPV-linked cancer types by vaccination. Cytology-based screening for cervical cancer will be increasingly supplemented or replaced by HPV DNA/RNA testing.[21] Currently, precancerous lesions and early stages of cervical cancer are usually removed by surgery.[55] In more advanced cancers, radiotherapy is recommended and can be combined with or substituted by chemotherapy. Cisplatin is the most frequently used chemotherapeutic drug for cervical carcinomas.[55] However, a major obstacle for successful treatment of cancer patients is the formation of resistance mechanisms against cisplatin in tumor cells.[56]

Since E6 and E7 are essential drivers of cervical cancer cell proliferation and are not expressed in healthy tissues, they represent attractive targets for immunotherapeutic approaches and the development of cancer-specific inhibitors.[57] However, the success of immunotherapeutic strategies has often been limited so far because HPVs have developed several mechanisms to evade the host immune system. For example, they interfere with the antigen-presenting machinery of the host.[58] Dymalla and colleagues showed that E6 can be targeted by peptides that block the E6AP binding pocket of E6 and therefore prevent the degradation of p53.[59] These small E6-specific, inhibitory peptides as well as siRNAs (small interfering RNAs) targeting *E6* or *E6/E7* transcripts, or other known E6/E7-specific inhibitors represent promising

therapeutic strategies, since they can lead to the induction of apoptosis or senescence selectively in HPV-positive cancer cells.[33]

1.1.4. Identification of novel HPV targets

The identification and subsequent characterization of novel downstream targets of E6/E7 could provide deeper insights into the molecular mechanisms how HPVs promote cervical tumorigenesis. This knowledge might also support the development of new therapeutic approaches and explain why some therapeutic strategies fail to efficiently reduce tumor burden.

To this end, Kuner and colleagues knocked down endogenous HPV18 E6/E7 expression in HeLa cells by RNA interference (RNAi).[60] By performing transcriptome analyses, they found more than 600 host genes to be differentially expressed, which indicates that these genes might be direct or indirect targets of the HPV oncoproteins E6 and E7.

Among the 288 identified upregulated genes, the *growth differentiation factor 15* (*GDF15*) gene showed the largest change with a 7-fold increase in mRNA levels. This implies that E6/E7 might strongly repress GDF15 expression in HPV-positive cancer cells.

1.2. The growth differentiation factor 15 (GDF15)

At the turn of the millennium, GDF15 was independently discovered in several laboratories as a cytokine.[61–66] Hence, GDF15 has five alternative names: NSAID-activated gene-1 (NAG-1),[62] placental bone morphogenetic protein (PLAB),[63] placental transformation growth factor beta (PTGFB),[64] prostate-derived factor (PDF),[65] and macrophage inhibitory cytokine-1 (MIC-1).[66] The tissue distribution of basal GDF15 expression differs among species.[65,67,68] In humans, GDF15 is expressed at high levels in the placenta, at medium levels in the prostate and the urinary bladder, and at low levels in the kidney, the colon, the pancreas as well as in parts of the brain (pons, medulla, and hypophysis) (Human Protein Atlas available from http://www.proteinatlas.org).[65,69] Upon cellular stress, GDF15 expression seems to be inducible in almost any tissue or cell type including cervical, ovarian, breast, bone, heart, lung, and liver cells.[68,70–74]

1.2.1. Regulation and biosynthesis of GDF15

The human *GDF15* gene is located on the p-arm of chromosome 19 and consists of two exons, which are separated by a single intron.[75] The structure of the *GDF15* transcriptional promoter is illustrated in Figure 3. The transcription factors p53 and CHOP (C/EBP homologous protein; alternative name: DDIT3 for DNA damage-inducible transcript 3) have been described to boost GDF15 expression, e.g., after etoposide treatment or after inducing endoplasmic reticulum

(ER) stress, respectively.[76–78] Additionally, C/EBPβ (CCAAT enhancer binding protein beta) was found to stimulate *GDF15* transcription upon the exposure to capsaicin, a natural substance in red peppers.[79] As another transcription factor, EGR1 (early growth response protein 1) is known to trigger GDF15 expression after treatment with NSAIDs (non-steroidal anti-inflammatory drugs).[80] NSAIDs include commonly known pain relievers like aspirin, sulindac, and ibuprofen. Sp1 is a transcriptional activator of basal *GDF15* transcription.[80] After NSAID treatment, however, Sp1 retards the positive effect of EGR1 on *GDF15* transcription because they compete for the same binding sites in the *GDF15* promoter.[80,81] The transcriptional activity of the *GDF15* promoter can be strongly inhibited after methylation of two specific CpG islands, which are closely located to the transcription start site.[82]

Figure 3 Structure of the *GDF15* transcriptional promoter. The *GDF15* promoter contains binding sites for p53 (green boxes), CHOP (light grey oval), and C/EBPβ (yellow hexagons). The three binding sites for EGR1 and Sp1 overlap. Additionally, the location of the TATA box (orange box) and two DNA methylation sites (small red circles) are shown. A black arrow marks the start site and the direction of transcription.

Besides transcriptional regulation, posttranscriptional mechanisms are known to affect GDF15 expression.[77,83–86] The 3' untranslated region (UTR) of *GDF15* mRNA contains conserved adenylate-uridylate-rich elements (AREs), which promote the degradation of *GDF15* mRNA.[84] Phosphorylation of the extracellular signal-regulated kinases 1/2 (ERK1/2) or binding of human antigen R (HuR) to the AREs in the 3' UTR inhibit the decay of *GDF15* transcripts.[77,84]

Figure 4 schematically shows how GDF15 is synthesized and processed in cells, starting from a 308 amino acid large pre-pro-protein. After translation, two pro-GDF15 molecules are joined in the C-terminus by a disulfide bridge and can be N-glycosylated at the asparagine residue 70.[87,88] The N-terminal parts of the pro-GDF15 dimer are cleaved off at an RXXR motif (X: random amino acid) in order to form the mature GDF15 dimer.[89] The secondary structure of GDF15 is further characterized by a cysteine knot, which is generated by four intramolecular disulfide bonds.[90] GDF15 can be secreted in its pro- and mature form.[91]

In contrast to cytokines of the TGF-β family,[92,93] neither the N-glycosylation nor the propeptide seem to be required for processing and secretion of GDF15.[91,94] Nevertheless, the propeptide might support correct folding and dimerization of GDF15 and accelerate its secretion.[88,91,95] Secreted pro-GDF15 is reported to bind to the ECM via its propeptide part.[96] Therefore, pro-GDF15 could be secreted in order to form extracellular depots of mature GDF15 and to delay the increase of serum GDF15 levels.[96]

Mature GDF15 does not represent the only active form of GDF15: Min *et al.* showed that pro-GDF15 inhibited the transcriptional activity of Smad (a fusion word formed by Sma and Mad (Mothers against decapentaplegic)) proteins by using a GDF15 mutant (R193A) that cannot be cleaved into mature GDF15.[97] The biological function of the N-glycosylation in pro-GDF15 is still unclear and requires further research.

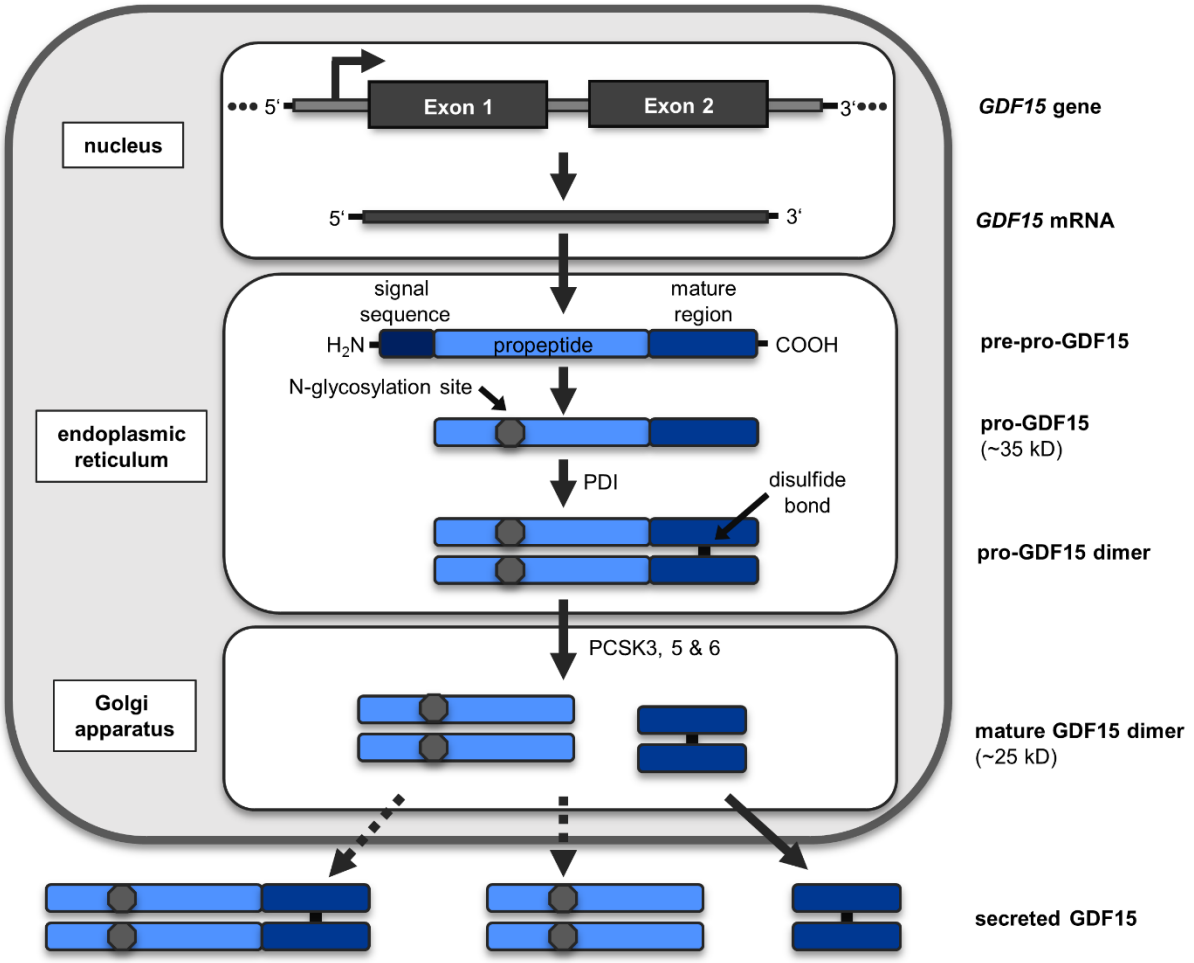

Figure 4 Biosynthesis of GDF15. After transcription in the nucleus, *GDF15* mRNA is transported to the rough ER. There, pro-GDF15 is synthesized and translocated into the ER lumen in its pre-pro-form. Within the ER, the ER signal sequence gets removed fast and pro-GDF15 can be N-glycosylated in its N-terminal propeptide part. The protein disulfide isomerase (PDI) generates pro-GDF15 homodimers by forming a disulfide bond between cysteines in the C-terminus.[66] In the Golgi apparatus, three proteases from the pro-protein convertase subtilisin/kexin (PCSK) family are known to cleave the pro-GDF15 dimer at amino acid 196 into two propeptide molecules and the mature GDF15 dimer: PCSK3 (alias Furin), PCSK5, and PCSK6.[98] GDF15 can be secreted either as pro-GDF15 dimer or mature GDF15 dimer.[66]

1.2.2. Screening for GDF15 receptors

Originally, GDF15 was classified as a divergent member of the transforming growth factor beta (TGF-β) superfamily.[61,63–66] The inclusion of GDF15 into this family was based on similarities in the gene sequence and on a conserved domain consisting of seven cysteine residues.

However, the percentage of homologous sequences is rather low: *GDF15* shows with 37% the highest homology to *BMP8 (Bone morphogenetic protein 8*).[64] Since the discovery of GDF15, there have been conflicting results whether GDF15 signals through TGF-β receptors (TGFBRs) and affects Smad signaling pathways.[99–103] Direct binding of GDF15 to any of the known members of the TGFBR family has not been reported. In this context, it should also be noted that experimental results based on using recombinant GDF15 have to be interpreted with care because several GDF15 preparations were shown to be of low purity and contaminated by TGF-β1.[104]

Recently, GDF15 was ascribed to the GDNF (glial cell-derived neurotropic factor) family after four independent pharmaceutical company laboratories found mature GDF15 to bind to GFRAL (GDNF family receptor α-like) with high affinity.[90,105–107] No association of GDF15 with any TGFBR pair could be observed by these research groups. GFRAL is a transmembrane protein which requires the receptor tyrosine kinase RET as a coreceptor for signal transmission.[90,106,107] When GDF15 binds to GFRAL, RET is autophosphorylated and stimulates AKT (alias protein kinase B (PKB)), ERK, and phosphoinositide phospholipase C gamma (PLC-γ) signaling pathways.[90,106,107] So far, GFRAL expression has only been detected in two regions of the hindbrain, the area postrema and the nucleus of the solitary tract.[90,106,107] The activation of the GDF15/GFRAL/RET complex in these cells leads to reduced food uptake and body weight in mice and primates, indicating a regulatory role of GDF15 in weight homeostasis.[108] On mRNA level, there is some evidence that GFRAL is expressed in the testis.[106] No GFRAL expression was traceable in any of the 32 analyzed cell lines including HeLa or in other examined peripheral tissues.[90,106,107]

After exhaustive screening of all known human transmembrane proteins,[90,105–107] it is unlikely that another – and in particular ubiquitously expressed – cell surface receptor for GDF15 will be found.[108] Since no GFRAL expression is detectable in cervical cells,[106] this thesis mainly focuses on the function of intracellular GDF15 in HPV-positive cancer cells. Changes of intracellular GDF15 levels have been linked to the regulation of important cellular processes such as proliferation, invasion, tumorigenesis, transcriptional regulation, migration, or apoptosis. For example, Tsui and colleagues reported that silencing of GDF15 by siRNA promoted cell proliferation, invasion, and tumorigenesis of bladder carcinoma cells, whereas GDF15 overexpression generated opposing effects.[109] Furthermore, a tetracycline-inducible GDF15 expression cassette repressed several TGF-β target genes like TIMP3 (tissue inhibitor of metalloproteinases 3) and LTBP1 (latent TGFβ-binding protein 1) by interrupting Smad binding to DNA in the osteosarcoma cell line U2OS.[97] Downregulation of GDF15 by shRNAs repressed migration of pancreatic cancer cells after solid stress and induction of apoptosis after ER stress in colorectal cells.[110,111] Further examples can be found in chapter 1.2.3.2.

1.2.3. GDF15 as a stress response protein

Since serum levels of circulating GDF15 can be easily measured and are relatively low in healthy individuals, GDF15 is discussed as a biomarker for diverse pathological states (e.g., cardiovascular diseases, diabetes, rheumatoid arthritis, and cancer).[112–115] However, high GDF15 serum levels alone are rather unspecific and therefore less suitable for diagnostic purposes because a multitude of stress factors is known to stimulate GDF15 expression (see next paragraph). In line with this, serum GDF15 is described as a marker for "all-cause mortality".[116,117] In contrast to this finding, the transgenic expression of human GDF15 has been reported to increase the lifespan of mice.[118] Furthermore, GDF15 plasma concentrations are positively associated with age, body mass index (BMI), smoking, pregnancy, intense exercise, or intake of drugs like NSAIDs.[119–121]

Several stress factors are known to activate GDF15 expression. These include hypoxia,[71] high cell density,[122] radiation,[123] solid stress,[110] and ER stress.[77] Additionally, GDF15 levels are strongly induced by numerous anti-tumorigenic drugs, irrespectively of whether they are from natural origin (resveratrol,[124] capsaicin,[79] genestein,[125] camptothecin,[109] etoposide,[76] etc.) or chemically synthesized (doxorubicin,[123] PPAR-γ (peroxisome proliferator-activated receptor gamma) ligands,[84,126] diverse NSAIDs,[62,127] cisplatin,[123] etc.). At least one of the transcription factors p53, CHOP, and EGR1 is typically involved in the activation of GDF15 transcription after stress.[77,80,122] Furthermore, GDF15 is suspected to regulate its own expression in a paracrine and autocrine manner.[128]

These observations raise the questions whether GDF15 upregulation is a cause or a result of different pathological states, and whether high GDF15 levels worsen or improve the course of a disease. Since GDF15 reveals pleiotropic functions, the answers to these questions are complex and appear to be strongly dependent on the context of the disease.[112,129,130]

1.2.3.1. ER stress and GDF15

The ER is a dynamic tubular network, which fulfils various cellular functions such as storage of intracellular calcium, gluconeogenesis, lipid synthesis, and the production and processing of secretory and membrane proteins.[131] High translation rates or accumulation of un- or misfolded proteins can induce ER stress, which activates signaling pathways of the unfolded protein response (UPR) (Figure 5).[132]

In healthy cells, the UPR attenuates protein synthesis, upregulates expression of chaperons and other proteins involved in protein folding and maturation, and activates proteasomal degradation of misfolded proteins.[131] The latter process is called ERAD (ER-associated degradation). Thereby, UPR reduces ER stress and restores protein homeostasis. When ER stress persists further, the UPR, however, triggers different pro-apoptotic pathways in order to

eliminate irreversibly damaged cells.[133] For instance, the pro-apoptotic protein CHOP is induced by all three major UPR signaling pathways.[134] CHOP can function either as a transcriptional activator or as a repressor, forming heterodimers with other C/EBP family members. In the former case, CHOP directly binds to certain DNA elements in order to activate the expression of its target genes, while in the latter case, CHOP represses the transcriptional activity of other C/EBP family members by binding to them.[135]

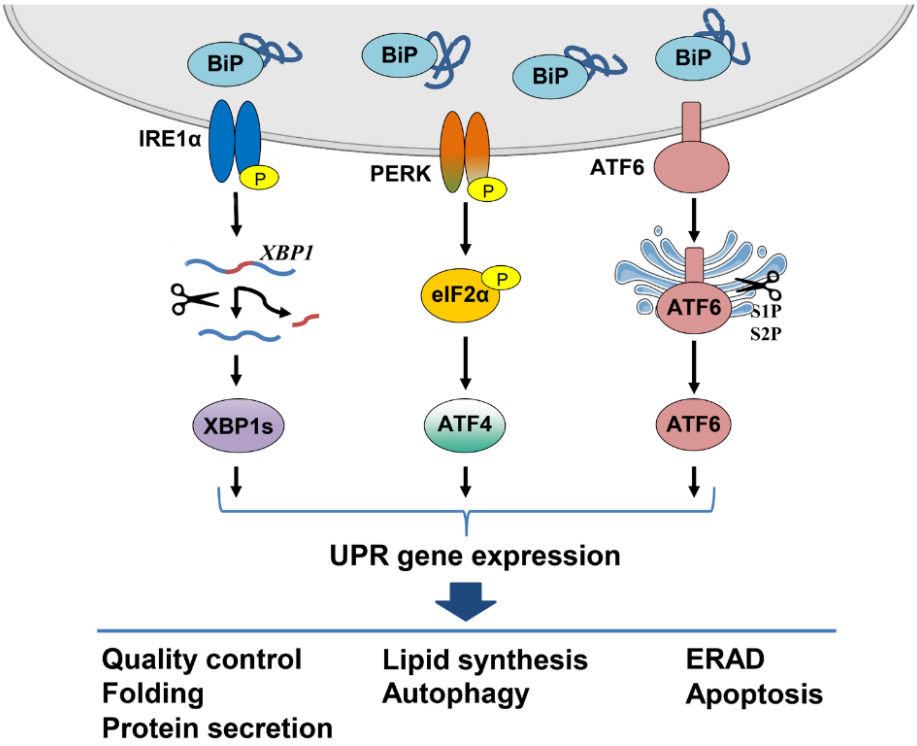

Figure 5 The three major signaling pathways in the UPR. During ER stress, the accumulation of unfolded proteins results in the withdrawal of the ER-resident chaperon BiP (binding immunoglobulin protein; alias glucose-regulated protein 78 (GRP78)) from three signaling receptors. These receptors are located in the ER membrane and are subsequently activated. After stimulation, IRE1α (inositol-requiring enzyme 1 alpha) dimerizes and auto-trans-phosphorylates its own serine/ threonine residues. The autophosphorylation activates the cytosolic RNAse domain of IRE1α, which cleaves the mRNA of *XBP1* (*X-box binding protein 1*). The cleavage of the transcript induces mRNA splicing and expression of XBP1. Like for IRE1α, the loss of BiP binding leads to successive oligomerization and autophosphorylation of PERK (protein kinase R-like ER kinase). Because eIF2α (eukaryotic initiation factor 2 alpha) is phosphorylated by active PERK, global protein translation is inhibited but the translation of some selective mRNAs, e.g., *ATF4* (*activating transcription factor 4*) mRNA, is enhanced. Upon activation, ATF6 (activating transcription factor 6) is transported to the Golgi apparatus. There, the cytosolic fragment of ATF6 is cleaved off and therefore set free by the proteases S1P and S2P. The three transcription factors XBP1, ATF4, and cleaved ATF6 migrate into the nucleus and upregulate the expression of multiple UPR proteins, which reduce the effects of ER stress. However, persistent ER stress induces apoptosis. The illustration was modified from Storm *et al.*[136]

Cancer cells exhibit increased ER stress and UPR levels because of elevated protein synthesis rates, lactic acidosis as well as oxygen and nutrient deprivation.[137] Different anti-tumorigenic drugs like NSAIDs are reported to shift UPR signaling pathways in cancer cells towards the

induction of apoptosis.[138] For instance, the treatment of colorectal cancer cells with the NSAID sulindac sulfide (SSide) activates PERK signaling as well as ATF3 (activating transcription factor 3) and ATF4 expression.[111] ATF3 and ATF4 enhance *CHOP* transcription and subsequently upregulate GDF15 expression. Both CHOP and GDF15 promote apoptosis in colorectal cancer cells after treatment with SSide.[111] NSAIDs can increase GDF15 expression also through ER-stress independent pathways. Namely, NSAIDs support the translocation of the transcription factor ESE1 (alias E74 like ETS transcription factor 3 (ELF3)) into the nucleus, where ESE1 subsequently activates the *EGR1* promoter.[139] Afterwards, EGR1 binds to the *GDF15* promoter (Figure 3) and stimulates its transcription.

1.2.3.2. GDF15 in cancer

In cancer, GDF15 exhibit both pro- and anti-tumorigenic activities, which seem to be dependent on the cell type, the stage of carcinogenesis, and the experimental design (e.g., use of recombinant GDF15, overexpression or knockdown of GDF15, *in vitro* vs. *in vivo* studies).[127,140–142] Additionally, high levels of circulating GDF15 can foster tumor-induced anorexia and weight loss.[101,143] A selection of examples for the pleiotropic functions of GDF15 in cancer is listed in the following paragraphs.

Regarding pro-tumorigenic effects, it has been shown that GDF15 stimulated EMT (epithelial-mesenchymal transition) and metastasis of colorectal cancer cells. This was based on the observation that overexpression of GDF15 repressed E-cadherin and upregulated MMP9 (matrix metallopeptidase 9), Vimentin, and Twist expression.[144] Furthermore, proliferation was enhanced by stable, exogenous expression of GDF15 in the prostate cancer cell line LNCaP, whereas it was reduced after GDF15 silencing in malignant glioma cells.[73,145] Moreover, silencing of GDF15 in melanoma cells reduced their tumorigenicity after injection into athymic mice.[146] Further, GDF15 increased uPA (urokinase-type plasminogen activator) expression and invasiveness of gastric cancer cells.[147]

Concerning its anti-tumorigenic functions, it has been found that GDF15 repressed the expression of EMT markers like SNAIL, SLUG, or N-cadherin and upregulated E-cadherin levels in bladder carcinoma and breast cancer cells.[109,148] Additionally, silencing of GDF15 has been shown to increase migration of breast cancer cells by dephosphorylating p38 mitogen-activated protein kinase (MAPK).[148] In the prostate cancer cell line PC3, exogenous GDF15 expression diminished proliferation.[149] Ectopic overexpression of GDF15 reduced the size of mice.[83,150] The induction of apoptosis represents one mechanism by which GDF15 could act as a tumor suppressor. In this regard, Zhang and colleagues have reported that GDF15 overexpression led to apoptosis of glioblastoma cells in a Smad-dependent manner.[151] Furthermore, GDF15 expression is induced by ER stress and anti-tumorigenic drugs like

NSAIDs, and is involved in their pro-apoptotic effect.[111,138] In line with this, the tumor-preventive action of sulindac was abolished by *GDF15* knockout in a mouse model of intestinal cancer.[152] In gastric cancer cells, GDF15 overexpression increased SSide-mediated apoptosis by upregulating the expression of the death receptors 4 and 5 (DR4 and DR5).[153] Furthermore, GDF15 levels were raised in hepatocellular carcinoma cells after treatment with the flavonoid derivate GL-V9 and induced apoptosis by lowering the mitochondrial membrane potential (MMP).[86]

1.3. Research objectives

A previous transcriptome analysis implies that the expression of the cellular stress response gene *GDF15* might be strongly inhibited by E6/E7. The present thesis aims to explore whether *GDF15* is a novel target gene for oncogenic HPVs and to assess the functional role of GDF15 regulation for the malignant phenotype of HPV-positive cervical cancer cells.

The following major questions will be addressed:

(i) Is GDF15 expression modulated by the HPV E6/E7 oncoproteins? To validate the results of the transcriptome analysis, *E6* or *E6/E7* will be silenced in cervical cancer cells as well as in HPV-immortalized keratinocytes and resulting effects on GDF15 mRNA and protein expression will be assessed.

(ii) Which molecular mechanisms underly the regulation of GDF15 in HPV-positive cells? In this regard, analyses will focus on two key transcriptional activators of *GDF15*, CHOP and p53 (itself a known E6 target). Moreover, it will be studied whether deprivation of nutrients like glucose affect GDF15 expression.

(iii) Does GDF15 affect the proliferation of cervical cancer cells? Proliferation measurements by live cell imaging, colony formation assays, cell cycle analyses, and apoptosis assays will be performed after GDF15 overexpression or knockdown/knockout of *GDF15* using RNAi and CRISPR/Cas9 methodology.

(iv) Do HPV-positive cancer cells modulate GDF15 expression to increase their resistance against different forms of stress? Are p53 or CHOP involved in this process? To address these questions, the effects of two ER stressors, tunicamycin (TM) and thapsigargin (TG), the SSide, and the cytostatic drug cisplatin will be used as exemplary stress inducers. The role of GDF15 for the phenotypic responses of HPV-positive cancer cells towards these agents will be investigated after silencing endogenous GDF15 expression.

It is hoped that these explorations regarding GDF15 expression and function will add to our concepts of HPV-linked tumorigenesis. Elucidating the host cell pathways that are deregulated

by the HPV oncoproteins E6 and E7 is critical to understand how oncogenic HPVs induce and maintain the malignant phenotype of their host cell. This understanding could also form a basis for the development of novel strategies to prevent or treat HPV-positive preneoplasias and cancers.

Chapter 2

Results

2. Results

2.1. Expression of GDF15 in cervical cancer cells

GDF15 may represent a yet unknown target gene of the HPV oncoproteins because *GDF15* mRNA expression was highly increased and represented the top hit of a genome-wide microarray analysis after silencing endogenous *E6/E7* expression in HeLa cells.[60] This result suggests that E6/E7 repress GDF15 expression in cervical cancer cells.

2.1.1. Upregulation of GDF15 expression upon silencing of *E6* or *E6/E7* transcripts

In order to validate this finding by independent methods, E6 alone or E6 and E7 in combination were silenced in HPV16-positive SiHa and MRI-H186 cells as well as in HPV18-positive HeLa cells by RNAi (Figure 6A). This led to increased *GDF15* mRNA expression in all three cervical cancer cells lines as measured by qRT-PCR (Figure 6B). *E7* alone cannot be downregulated by RNAi as discussed elsewhere.[29,30] Sole silencing of *E6* had limited impact on total *E6/E7* transcript levels in SiHa and MRI-H186 cells (Figure 6A). This observation is in line with the report that E6-encoding transcripts represent a minor proportion of total *E6/E7* transcripts in HPV16-positive cancer cells.[154]

Immunoblot analyses of E6 and E7 verified successful downregulation of the oncoproteins by RNAi in SiHa (Figure 6C), MRI-H186 (Figure 6D), and HeLa (Figure 6E) cells. GDF15 protein expression (Figure 6C-E) was elevated in those cells after solely blocking E6 or after combined knockdown of E6 and E7 expression, in line with the regulation of its mRNA levels (Figure 6B). The amplitude of GDF15 upregulation varied between the different cervical cancer cell lines.

The following terminology is used to distinguish the different GDF15 protein forms (Figure 4) in this thesis: GDF15 refers to the total intracellular GDF15 protein, pro-GDF15 represents the approx. 35 kDa pro-form of GDF15, and mature GDF15 denotes the cleaved, 12 kDa form of GDF15. It is explicitly stated when secreted, extracellular GDF15 is referred to.

Interestingly, pro-GDF15 shifted from the faster migrating, non-glycosylated form (34 kDa) towards the slower migrating, N-glycosylated form (36 kDa) after blocking both viral oncoproteins in HeLa cells as detected by immunoblotting (Figure 6E). That observation suggests that HPV18 E7 alone or E6/E7 in combination might inhibit the N-glycosylation of pro-GDF15 in HeLa cells. However, the N-glycosylation of pro-GDF15 seems to be regulated in a cell line-dependent manner because SiHa (Figure 6C) and MRI-H186 (Figure 6D) cells only showed the faster or the slower migrating pro-GDF15 form, respectively. A closer analysis of different pro-GDF15 forms can be found in chapter 2.3.1.1.

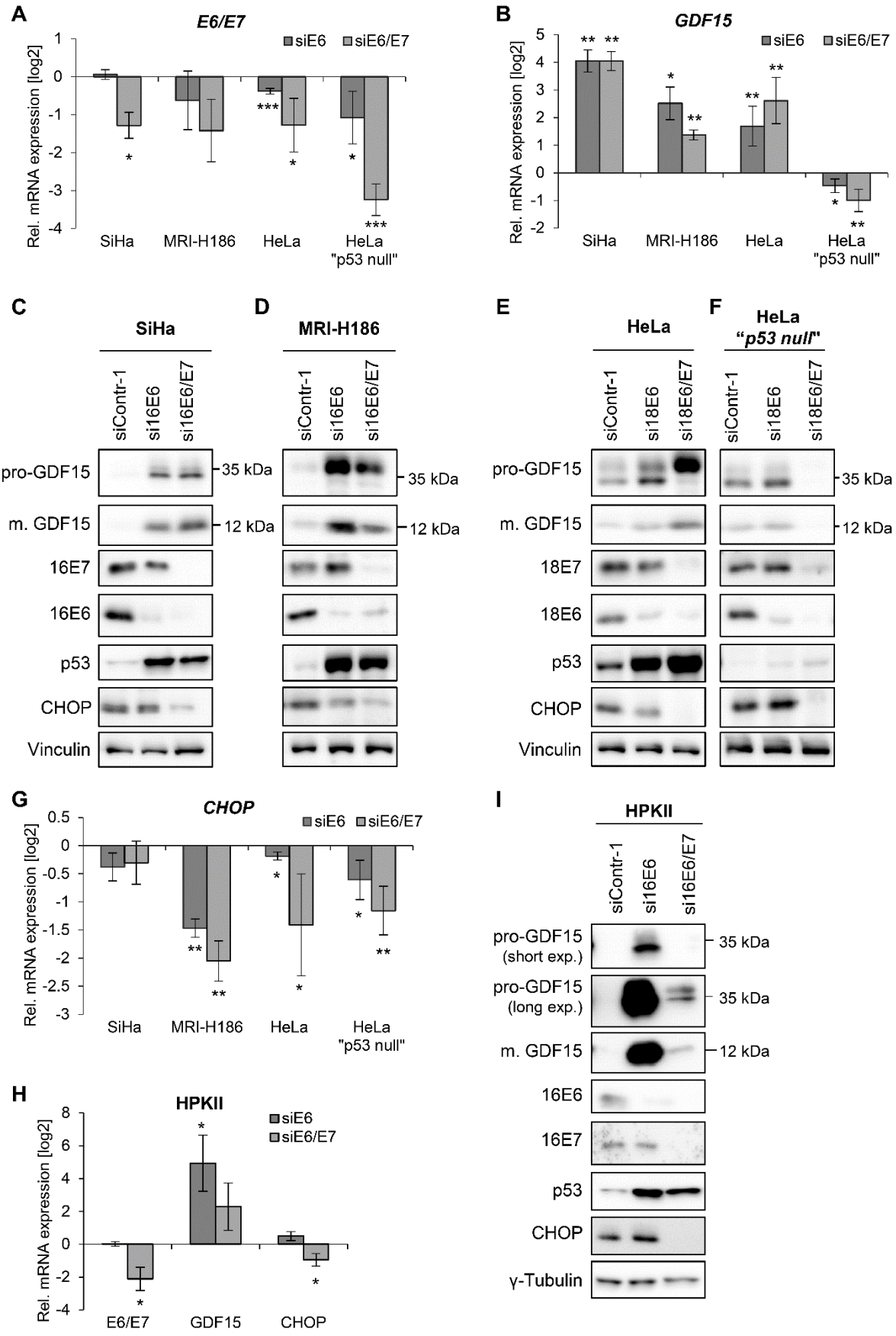

Figure 6 Upregulation of GDF15 expression after silencing E6 or E6/E7 in HPV-positive cells. E6 alone or E6/E7 were downregulated in the HPV-positive cervical cancer cell lines SiHa, MRI-H186,

HeLa, HeLa *"p53 null"* (A-G), and the keratinocyte cell line HPKII (H, I) by RNAi. (**A, B, G, H**) qRT-PCR analyses determining relative transcript levels of HPV16 or HPV18 *E6/E7* (A, H), *GDF15* (B, H), and *CHOP* (G, H). Depicted is the log2 of the mean expression levels relative to siContr-1-transfected cells. Bars represent standard deviations. Asterisks indicate statistically significant differences to control-transfected cells as determined by one-sample *t*-test. *p ≤ 0.05, **p ≤ 0.01, ***p ≤ 0.001. (**C-F, I**) Immunoblot analyses of pro-GDF15, mature (m.) GDF15, E6, E7, p53, and CHOP expression in SiHa (C), MRI-H186 (D), HeLa (E), HeLa *"p53 null"* (F), and HPKII (I) cells. For HPKII, one representative experiment out of two is shown. Vinculin and γ-Tubulin are loading controls.

GDF15 might be repressed through E6-mediated degradation of p53,[155] since silencing of *E6* restored p53 levels and was sufficient to increase GDF15 expression (Figure 6B-E). This hypothesis is supported by the identification of two activating p53 binding sites in the promoter of *GDF15*.[76] To test the contribution of p53, the effect of E6/E7 knockdown was analyzed in the HeLa-derived cell clone HeLa *"p53 null"*, in which p53 is efficiently downregulated by stable expression of a shRNA against the *TP53* mRNA (Figure 6F).[156] GDF15 mRNA and protein levels were not appreciably elevated in HeLa *"p53 null"* cells after transfection of E6 siRNAs. This is in contrast to the strong GDF15 induction observed in all other studied cervical cancer cell lines, which express p53 (Figure 6B-E, also see below). Unexpectedly, GDF15 expression was in fact strongly downregulated when E6 and E7 were concomitantly repressed in HeLa *"p53 null"* cells (Figure 6F). This result points out that E7 or E6/E7 can increase GDF15 amounts in this particular cell line through a p53-independent pathway.

CHOP could also mediate the induction of GDF15 expression after E6/E7 inhibition in HPV-positive cells, since CHOP is another known activator of *GDF15* transcription apart from p53.[111] However, CHOP mRNA and protein levels were decreased after E6/E7 knockdown in all four cervical cancer cell lines analyzed (Figure 6C-F). The extent of downregulation varied between the individual cell lines. CHOP repression was stronger after silencing the expression of both HPV oncoproteins compared to silencing E6 alone (Figure 6C-F), with the exception of *CHOP* mRNA levels in SiHa cells (Figure 6F).

The HPKII cell line is non-cancerous and derived from a human foreskin keratinocyte that was immortalized by spontaneous integration of HPV16 *E6/E7* DNA after transfection.[23] In HPKII cells, GDF15 mRNA (Figure 6H) and protein (Figure 6I) expression was increased after knocking down *E6* and to a lower extent after knocking down *E6/E7* as observed for the cancer cell lines (Figure 6B-E). P53 levels were also restored after E6 repression (Figure 6I). Alike in tumor-derived cell lines (Figure 6C-F), CHOP expression was decreased after E6/E7 downregulation in HPKII cells on mRNA (Figure 6H) and protein level (Figure 6I).

For its cytokine functions, GDF15 can be secreted into the extracellular space.[66] Thus, an alternative explanation for the accumulation of intracellular GDF15 after E6/E7 knockdown could be that the HPV oncoproteins foster the secretion of GDF15. Cell culture supernatants of HeLa and SiHa cells were analyzed for extracellular GDF15 levels after silencing of E6 or

E6/E7: increased amounts of secreted GDF15 were detected for both cell lines by Western blotting (Figure 7).

Interestingly, more complex band patterns were found for pro-GDF15 in the cell culture supernatant than intracellularly. In supernatants of HeLa cells, two pro-GDF15 forms migrated faster or slower, respectively, than the 35 kDa marker protein. The two secreted pro-GDF15 forms of SiHa cells run at molecular weights shortly below 35 kDa. The additional pro-GDF15 forms indicate that pro-GDF15 is further posttranslationally processed during the course of secretion or extracellularly.

Figure 7 Downregulation of *E6* or *E6/E7* increases extracellular levels of GDF15. E6 alone or E6/E7 in combination were downregulated in HeLa and SiHa cells by siRNAs. Immunoblot analyses of cell culture supernatants detecting secreted pro-GDF15 and mature (m.) GDF15 levels. Loading volumes were normalized on amounts of total intracellular protein.

Overall, these results support the notion that intracellular as well as secreted GDF15 levels of HPV-positive cervical cancer cells are downregulated by the viral oncoproteins. The proteasomal degradation of p53 which is promoted by E6 could be a major mechanism underlying the repression of GDF15.

2.1.2. GDF15 expression is induced by glucose deprivation

Since several links between nutritional supply and GDF15 are reported,[157] it is possible that some cell culture conditions influence the expression of the stress protein GDF15 and its transcriptional regulators. Hence, the effects of prolonged cultivation, fetal calf serum (FCS), seeding cell numbers, and glucose supply were analyzed. Standardly in this thesis, cells were cultured in medium supplemented with 5.5 mM glucose (corresponding to physiological glucose concentrations in human serum) and 10% FCS. Medium was usually exchanged at the start of the experiment.

Firstly, the effects of prolonged cultivation and FCS supply were investigated in HeLa and SiHa cells. To this end, medium either lacking or supplemented with 10% FCS was added and cells were harvested at time point zero or after 24h, 48h, and 72h cultivation (Figure 8A).

In FCS-containing medium, increasing GDF15 mRNA and protein levels were observed in both cell lines over time by qRT-PCR (Figure 8B and C) and immunoblot analyses (Figure 8D and E), respectively. After 72h, pro-GDF15 shifted towards the non-glycosylated form in HeLa

cells (Figure 8D). CHOP protein expression was upregulated by prolonged cell cultivation as well (Figure 8D and E). Only minor changes in p53 and E6/E7 protein levels were observed.

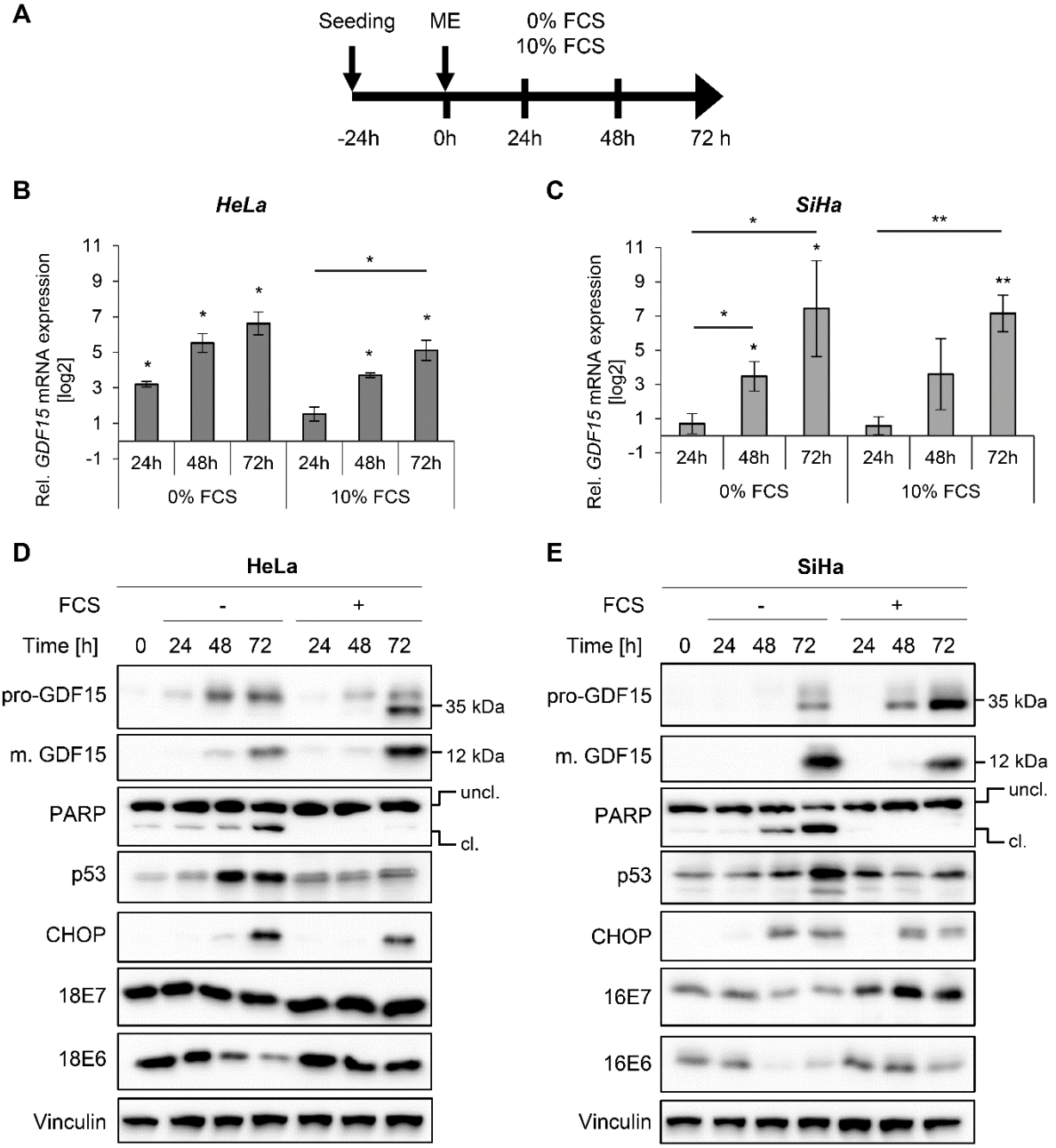

Figure 8 Increase of GDF15 expression under prolonged cell culture. (**A**) Experimental setup. One day after seeding, medium was exchanged to medium supplemented with or lacking 10% FCS. Cells were harvested at time point zero, 24h, 48h, or 72h after medium exchange (ME). (**B, C**) qRT-PCR analyses determining relative mRNA expression levels of *GDF15* in HeLa (B) and SiHa cells (C). For HeLa, the qPCR data are based on two independent experiments. Depicted is the log2 of the mean expression levels relative to cells harvested at time point zero. Bars represent standard deviations. Asterisks indicate statistically significant differences to cells harvested at time point zero (asterisks above bars) or to other samples (asterisks above connecting crossline) as determined by two-sided *t*-test. *p ≤ 0.05, **p ≤ 0.01. (**D, E**) Immunoblot analyses of pro-GDF15, mature (m.) GDF15, PARP (Poly(ADP-ribose) polymerase), p53, CHOP, E7, and E6 expression in HeLa (D) and SiHa cells (E). Uncleaved (uncl.), cleaved (cl.). Vinculin, loading control.

In FCS-free medium, GDF15 mRNA (Figure 8B and C) and protein (Figure 8D and E) levels also raised in both cell lines over time. Alike, p53 and CHOP expression were increased and additionally cleaved PARP indicated the induction of apoptosis (Figure 8D and E). Interestingly, cultivation in FCS-free medium downregulated HPV16 E6/E7 (Figure 8E) and HPV18 E6 (Figure 8D) amounts. HPV18 E7 levels remained constant within the here analyzed time frame (Figure 8D), but also decreased in a comparable experimental setup in which cell density was higher (Figure 27C).

These results suggest that GDF15 expression increases during prolonged cell cultivation, which could be mediated by p53 or by rising CHOP levels. In contrast to GDF15 and CHOP, p53 amounts and PARP cleavage are only boosted in the absence of FCS. The cultivation of HPV-positive cells in FCS-free medium downregulates E6 and later on also E7 expression. The decreased E6 levels could lead to the induction of p53 expression and subsequentially to apoptosis.

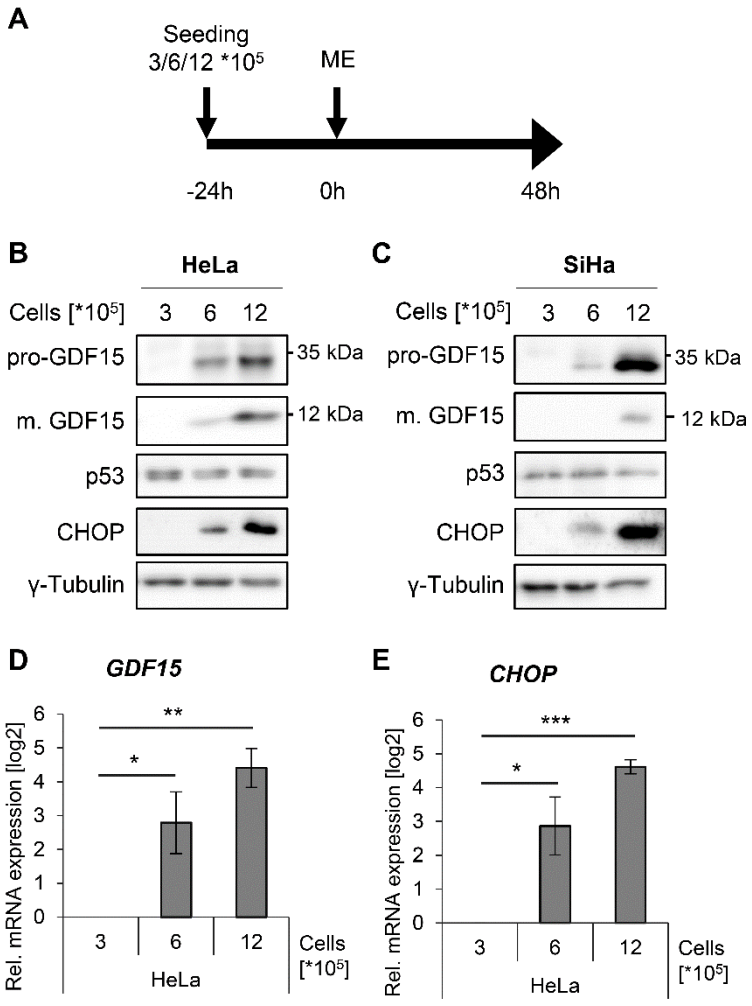

Figure 9 Higher cell seeding numbers increase GDF15 expression. (**A**) Experimental setup. Cells were seeded in three different cell numbers (3 *10^5, 6 *10^5 or 12 *10^5 cells per 6 cm dish). Medium was exchanged (ME) 24h after seeding. Cells were harvested after 48h. (**B, C**) Immunoblot analyses of pro-GDF15, mature (m.) GDF15, p53, and CHOP expression in HeLa (B) and SiHa cells (C). γ-Tubulin, loading control. (**D, E**) qRT-PCR analyses determining relative mRNA expression levels of *GDF15* (D) and *CHOP* (E) in HeLa cells. Depicted is the log2 of the mean expression levels relative to the sample in which 3 *10^5 cells were seeded. Bars represent standard deviations. Asterisks indicate statistically significant differences between samples connected by crosslines as determined by two-sided *t*-test. *p ≤ 0.05, **p ≤ 0.01, ***p ≤ 0.001.

These effects after prolonged cultivation might be linked to increasing cell numbers. Hence, three different cell numbers (3 *10^5, 6 *10^5, or 12 *10^5) of respectively HeLa or SiHa cells were seeded (Figure 9A). Western blot and qPCR analyses showed that high cell seeding numbers elevated GDF15 and CHOP protein (Figure 9B and C) and mRNA amounts (Figure 9D and E) while p53 protein levels (Figure 9B and C) remained unchanged in both cell lines.

Limited nutrient supply resulting from increased cell densities, e.g., glucose deprivation, could cause the observed stimulation of GDF15 and CHOP expression. Therefore, HeLa and SiHa cells were grown in medium containing no, physiological or excessive amounts of glucose (0 mM, 5.5 mM, and 25 mM, respectively). Cell lysates and culture supernatants were harvested after 24h and 48h and analyzed by qPCR and immunoblotting (Figure 10A).

A positive correlation was observed between glucose deprivation and *GDF15, CHOP* as well as *TP53* expression in HeLa and SiHa cells. *GDF15* (Figure 10B and C) and *CHOP* (Figure 10D and E) mRNA levels were strongly upregulated in cells cultivated in glucose-lacking medium. After 48h, *GDF15* (Figure 10B and C) and *CHOP* (Figure 10D and E) transcripts were also increased after cultivation in 5 mM compared to 25 mM glucose medium, probably due to glucose depletion. Alike, decreasing glucose concentrations also raised *TP53* mRNA expression (Figure 10F and G) although this positive effect was less pronounced (~ twofold) than the effects on *GDF15* (Figure 10B and C) and *CHOP* expression (Figure 10D and E) (both up to 32-fold).

In accordance to the mRNA data (Figure 10B-E), GDF15 and CHOP protein levels were also upregulated in HeLa (Figure 11A) and SiHa cells (Figure 11B) by glucose deprivation. Whereas SiHa cells cultivated in 25 mM glucose medium showed the N-glycosylated form of pro-GDF15, cells lacking glucose presented the non-glycosylated form (Figure 11B). This probably is a direct consequence of missing glucose molecules because they are needed for the biosynthesis of carbohydrate chains which are linked to proteins.[158] P53 expression was only slightly induced after 48h in the absence of glucose (Figure 11A and B), which matches the limited changes of its transcript levels (Figure 10F and G).

To sum up, the lack of FCS during cultivation seems to barely affect regular GDF15 expression. However, FCS deficiency can downregulate firstly E6 and later on E7 levels and induce apoptosis over time. In contrast to that, glucose deprivation strongly increases GDF15 mRNA and protein levels in cervical cancer cells explaining why GDF15 amounts are elevated after prolonged cultivation and in samples with high seeding cell numbers. CHOP and/or p53 levels are regulated similarly to GDF15 expression indicating that they could activate GDF15 expression in this context. The rise of p53 expression after glucose deprivation is low suggesting that rather an increase in p53 activity than in its expression levels might be important for GDF15 upregulation.

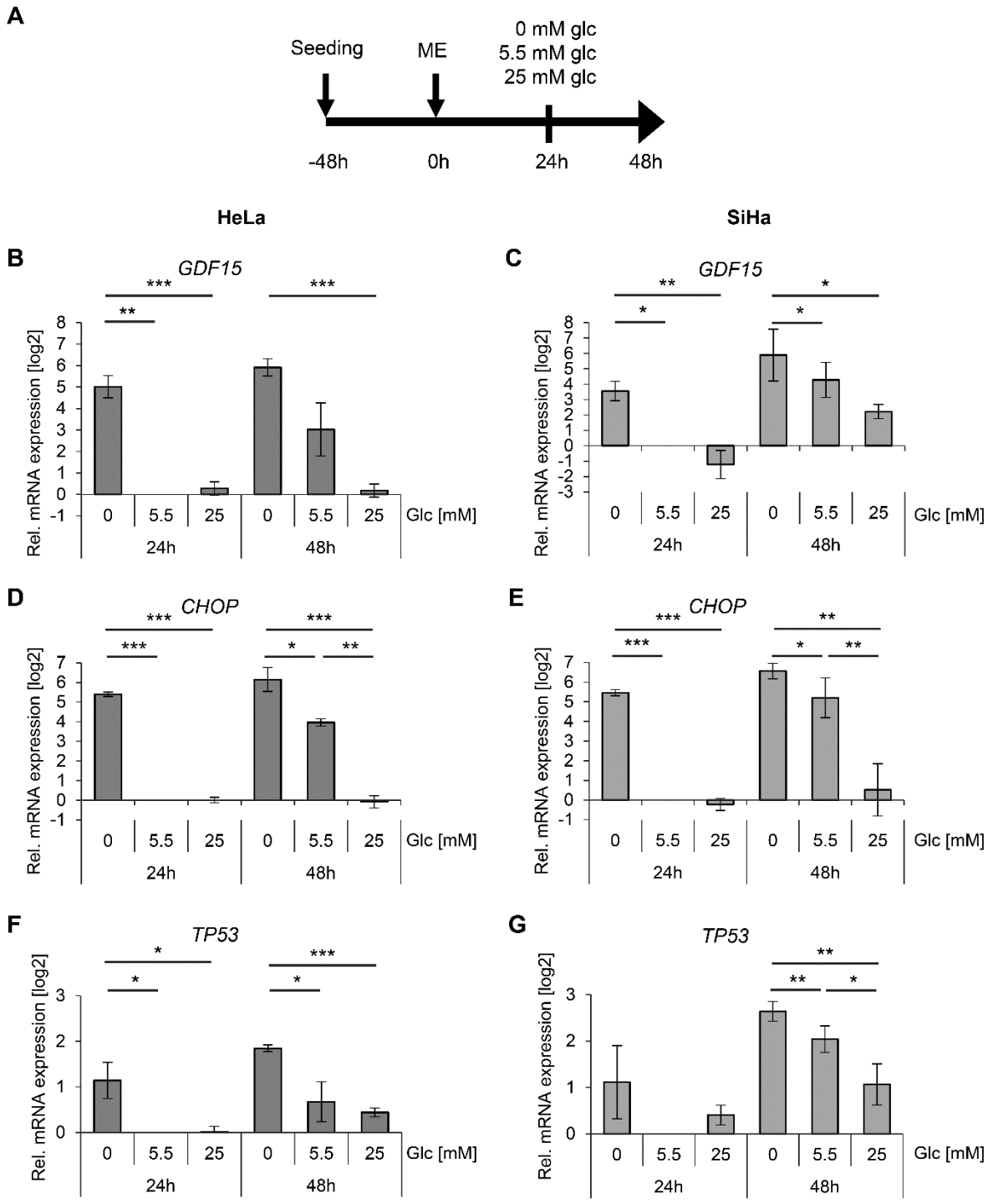

Figure 10 Glucose deprivation upregulates *GDF15* transcript levels. (**A**) Experimental setup. Two days after seeding, medium was exchanged (ME) to medium containing either 0 mM, 5.5 mM, or 25 mM glucose. Cells were harvested 24h or 48h after medium exchange. (**B-G**) qRT-PCR analyses determining relative mRNA expression levels of *GDF15* (B, C), *CHOP* (D, E), and *TP53* (F, G) in HeLa (left column) and SiHa cells (right column). Depicted is the log2 of the mean expression levels relative to cells cultured in medium with 5.5 mM glucose and harvested 24h after medium exchange. Bars represent standard deviations. Asterisks indicate statistically significant differences between samples connected by crosslines as determined by two-sided *t*-test. *p ≤ 0.05, **p ≤ 0.01, ***p ≤ 0.001.

Because of these findings, it is important to consider glucose-related effects in GDF15 expression analyses, especially when samples with divergent cell numbers are compared (e.g., control vs. drug-treated samples, see Figure 28A and C).

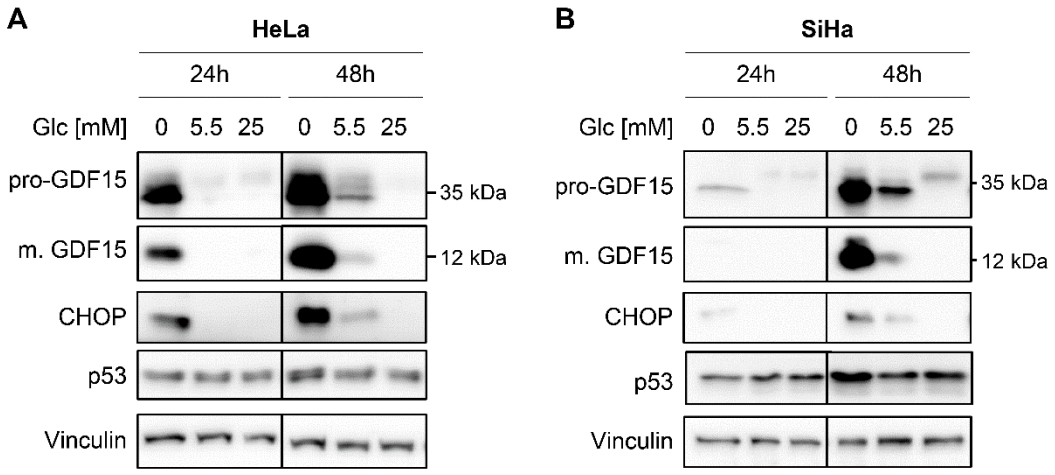

Figure 11 Glucose deprivation increases GDF15 protein levels. Two days after seeding, medium was replaced by medium containing either 0 mM, 5.5 mM, or 25 mM glucose. Cells were harvested 24h or 48h after medium exchange. The experimental setup is depicted in Figure 10A. (**A, B**) Immunoblot analyses of pro-GDF15, mature (m.) GDF15, CHOP, and p53 expression in HeLa (A) and SiHa cells (B). For each protein, cuttings from the same blot and exposure time are shown. Vinculin, loading control.

2.1.3. CHOP and p53 are activators of GDF15 expression after glucose deprivation

The correlation between GDF15, CHOP, and p53 levels suggests that CHOP and/or p53 affect basal GDF15 expression in cervical cancer cells (Figure 6) and increase GDF15 levels during glucose deprivation (Figure 10 and Figure 11). To test this hypothesis, *TP53* and *CHOP* expression were knocked down individually or in combination by RNAi in HeLa cells. Cells were cultivated in medium either supplemented or lacking 5.5 mM glucose.

The successful silencing of *TP53* and *CHOP* expression was validated by qPCR (Figure 12A and B) and immunoblotting (Figure 12D). After cultivation in standard cell culture medium (supplemented with 5.5 mM glucose), *GDF15* transcripts were strongly (sixfold) or slightly (twofold) decreased upon downregulation of p53 or CHOP, respectively (Figure 12C). The decline of GDF15 amounts was minimal larger after combined p53 and CHOP knockdown than after silencing *TP53* mRNA alone.

Cultivation of HeLa cells in glucose-free medium increased *TP53* (Figure 12A), *CHOP* (Figure 12B), and *GDF15* (Figure 12C) mRNA expression as observed before (Figure 10 left column). This upregulation of *GDF15* transcripts turned out lower after silencing p53 or CHOP alone and was completely erased after simultaneous knockdown of both transcription factors (Figure 12C).

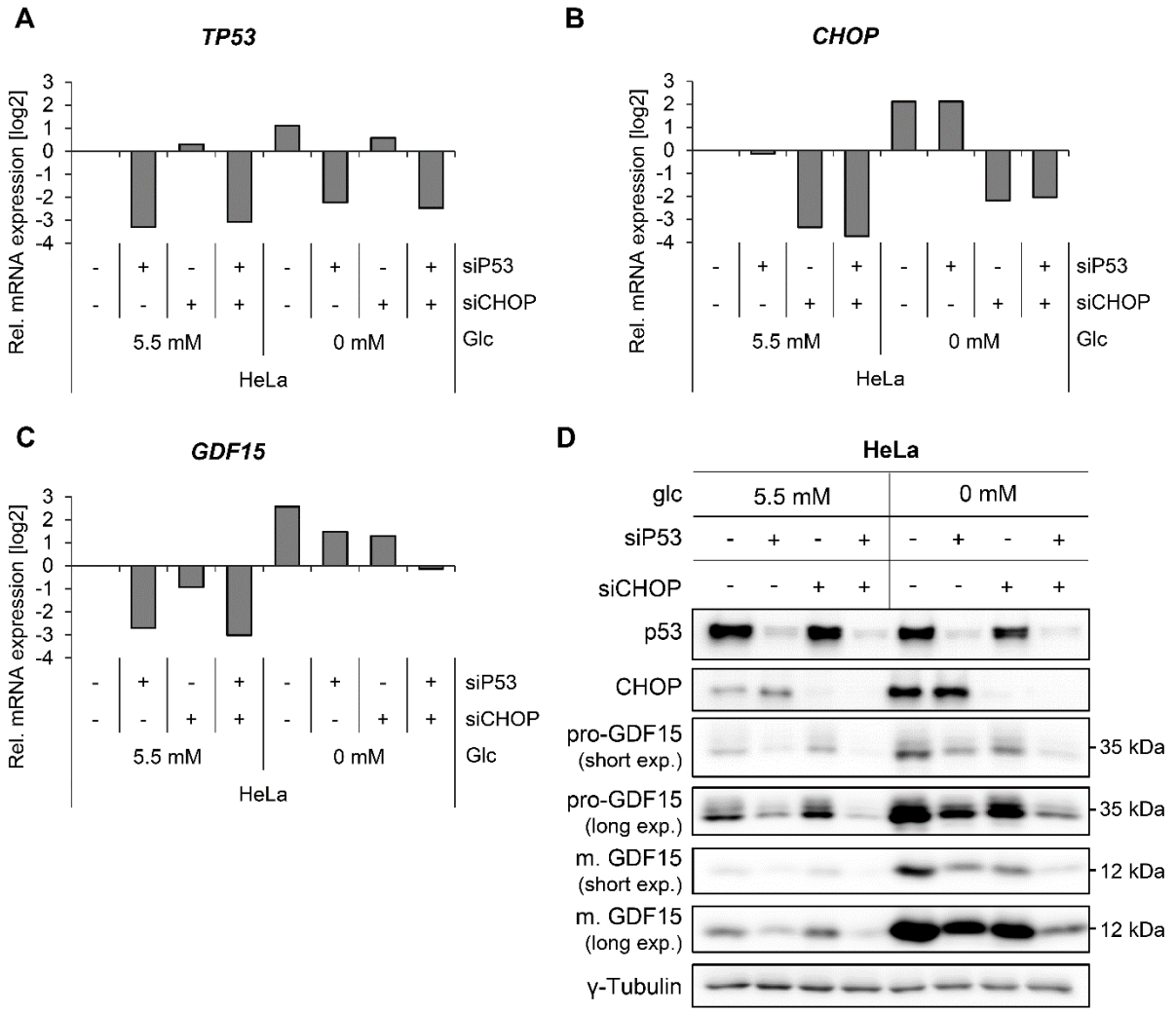

Figure 12 P53 and CHOP activate GDF15 expression in HeLa cells after glucose deprivation. P53 and CHOP were downregulated in HeLa cells by RNAi either alone or in combination. Two days before harvest, medium was exchanged to medium either with or without 5.5 mM glucose. Results of a representative experiment are presented. (**A-C**) qRT-PCR analyses determining relative mRNA expression levels of *TP53* (A), *CHOP* (B), and *GDF15* (C). Depicted is the log2 of the mean expression levels relative to siContr-1-transfected cells cultured in medium supplemented with 5.5 mM glucose. (**D**) Immunoblot analyses of p53, CHOP, pro-GDF15, and mature (m.) GDF15 expression. For both GDF15 forms, a shorter (short exp.) and longer exposition (long exp.) of the blots are shown. γ-Tubulin, loading control.

GDF15 and CHOP protein levels sharply raised during cultivation in medium without glucose in contrast to p53 levels, which remained unchanged (Figure 12D). Silencing of p53 alone or in combination with CHOP strongly diminished basal GDF15 expression and inhibited the glucose deprivation-induced GDF15 upregulation (Figure 12D). This further supports the notion that p53 activity (rather than p53 amounts) might be increased in HPV-positive cells during glucose deficiency. CHOP knockdown did not appreciably affect basal GDF15 levels but attenuated the induction of GDF15 after lacking glucose (Figure 12D). Downregulation of both p53 and CHOP completely abolished GDF15 induction after glucose deprivation.

Collectively, these results indicate that basal *GDF15* transcription in cervical cancer cells is primarily activated by p53 and only to a minor extent by CHOP. However, p53 and CHOP seem to cooperate in the upregulation of GDF15 levels after glucose deprivation.

2.1.4. GDF15 does not affect expression of HPV oncoproteins, p53, or CHOP

GDF15 is reported to modulate gene transcription,[97] including the expression of its own gene in an autocrine manner.[128] Hence, it was next investigated whether GDF15 may influence the expression of its regulators in a feedback mechanism. To this end and for following analyses of GDF15 functions (section 2.2 and 0), several tools (siRNAs targeting *GDF15* mRNA, episomal vectors for overexpression of GDF15 and *GDF15* knockout (KO) cells) were generated.

Applying the CRISPR/Cas9 technique to introduce a *GDF15* knockout in HeLa and SiHa cells, three different guide RNAs (gRNAs) were used to establish three KO clones per cell line. All used gRNAs targeted the first exon of the *GDF15* locus. The successful knockout of GDF15 expression was validated on protein level by immunoblot analyses (Figure 13). To this end, cells were cultured for three days without medium exchange to rise potential GDF15 expression by glucose depletion. GDF15 expression was neither detected in the three HeLa (Figure 13A) nor in the three SiHa *GDF15* KO clones (Figure 13B).

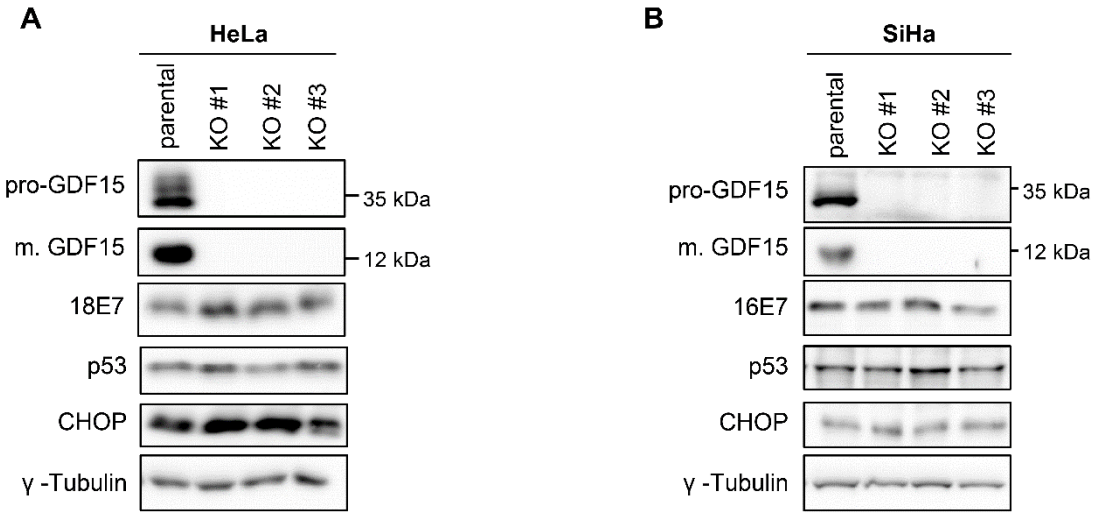

Figure 13 *GDF15* knockout does not alter E7, p53, or CHOP levels in cervical cancer cells. *GDF15* was knocked out in HeLa and SiHa cells by the CRISPR/Cas9 system. Three *GDF15* knockout clones (KO #1-3) were established per cell line. Same cell numbers were seeded for parental cell lines and *GDF15* KO clones. Medium was exchanged on the next day, and cells were harvested 72h later. Immunoblot analyses of pro-GDF15, mature (m.) GDF15, E7, p53, and CHOP expression in HeLa (**A**) and SiHa cells (**B**). γ-Tubulin, loading control.

GDF15 seemed not to regulate CHOP, p53, or E6/E7 expression in HPV-positive cancer cells. Firstly, E7, p53, and CHOP amounts remained unchanged in both HeLa and SiHa cells after

knockout of *GDF15* (Figure 13) or transient downregulation of endogenous *GDF15* expression using siRNAs (Figure 14A). Secondly, HeLa cells were transfected with an episomal vector expressing GDF15. The overexpression of GDF15 did also not affect E7, p53, and CHOP levels as determined by Western blot (Figure 14B). P53 amounts can serve as a surrogate for E6 expression in cervical cancer cells because E6 strongly promotes the degradation of p53. Hence, the unchanged p53 levels after permanent (Figure 13) or transient (Figure 14A) knockdown of *GDF15* expression or after GDF15 overexpression (Figure 14B) indicated that GDF15 does not influence E6 levels.

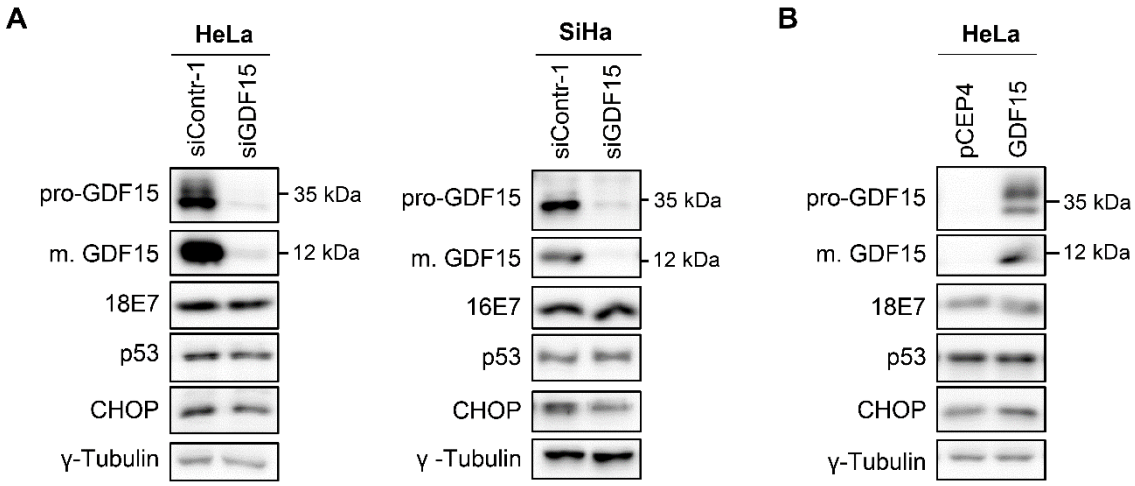

Figure 14 Transient knockdown or overexpression of GDF15 do not modulate E7, p53, and CHOP expression. (**A**) Cervical cancer cells (left panel: HeLa, right panel: SiHa) were transfected with a control siRNA (siContr-1) or with an siRNA pool against GDF15 (siGDF15). Cells were harvested three days after transfection. Immunoblot analyses of pro-GDF15, mature (m.) GDF15, E7, p53, and CHOP expression. γ-Tubulin, loading control. (**B**) HeLa cells were transfected with either 0.1 µg empty pCEP4 vector as control or 0.1 µg pCEP4_GDF15 for overexpression of GDF15. Cells were harvested two days after transfection. Immunoblot analyses of pro-GDF15, mature (m.) GDF15, E7, p53, and CHOP expression. γ-Tubulin, loading control.

2.2. Effects of GDF15 on proliferation of cervical cancer cells

Next, the question was addressed whether GDF15 repression by the HPV oncoproteins contributes to the malignant phenotype of cervical cancer cells. To this end, the proliferation of cervical cancer cells was analyzed by two different technical approaches, live cell imaging and colony formation assays (CFAs).

2.2.1. GDF15 is not a key regulator of cervical cancer cell proliferation in live cell imaging analyses

HeLa mCherry H2B and SiHa mCherry H2B cells stably express a nuclear red fluorophore, which enables quantification of proliferation by live cell imaging with the IncuCyte system.

Proliferation rates of HeLa (Figure 15A) and SiHa (Figure 15B) mCherry H2B cells were not altered by GDF15 knockdown via RNA. In addition, the proliferation of the respective HeLa (Figure 15C) or SiHa (Figure 15D) *GDF15* KO clones, which were generated by the CRISPR/Cas9 methodology (chapter 2.1.4), was not affected by the knockout except for two clones. HeLa *GDF15* KO clone #3 and SiHa *GDF15* KO clone #1 grew slightly slower in comparison to the parental cells, possibly due to some peculiarities of these clones which are independent of their GDF15 expression.

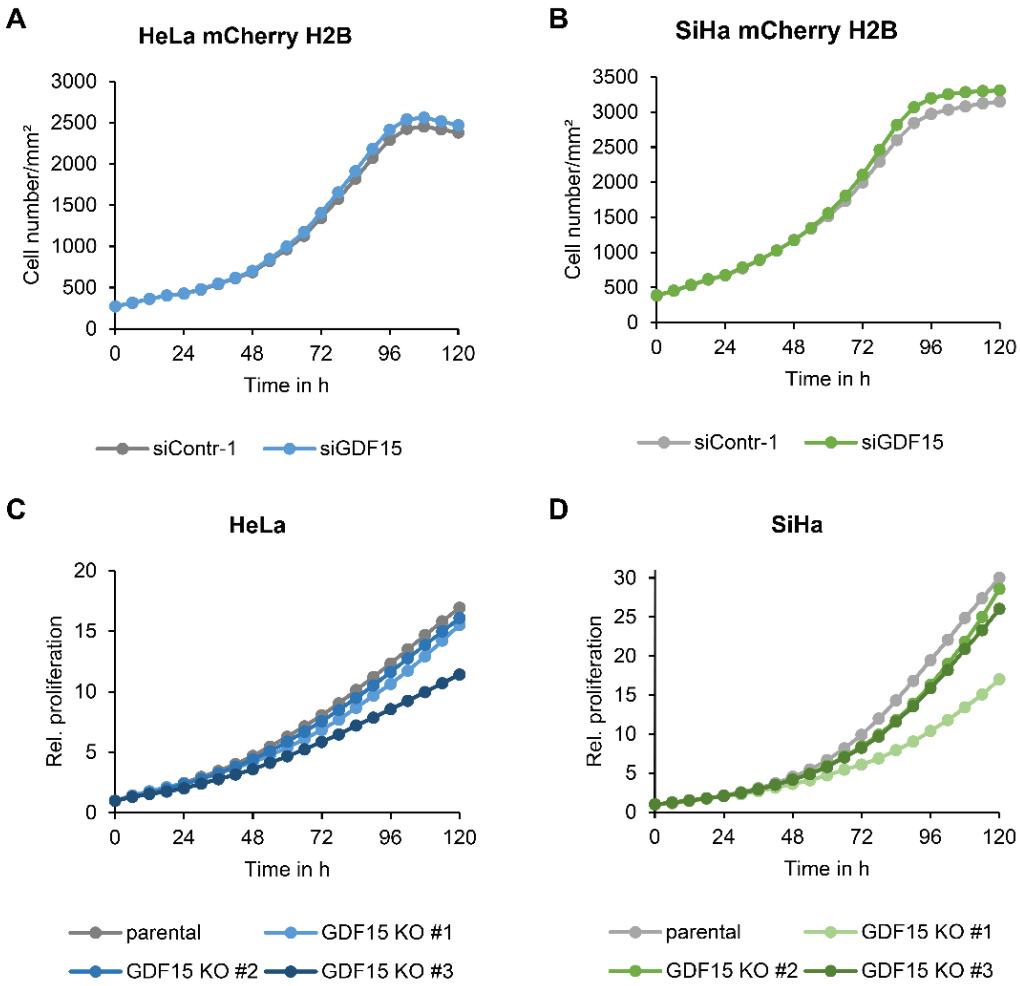

Figure 15 GDF15 is not essential for the proliferation of cervical cancer cells in live cell imaging analyses. (**A, B**) One day after seeding, HeLa mCherry H2B (A) and SiHa mCherry H2B cells (B) were transfected with a control siRNA (siContr-1) or an siRNA pool against *GDF15* mRNA (siGDF15) (for knockdown efficiency see Figure 14A). Medium was exchanged 24h post transfection. Afterwards, cell numbers were determined with the IncuCyte system (every 6 hours for 5 days). (**C, D**) Cells from parental cell lines and derived *GDF15* KO clones #1-3 were seeded in the same cell number, and relative proliferation of HeLa (C) and SiHa cells (D) was determined with the IncuCyte system (every 6 hours for 5 days). Relative proliferation rates were calculated by normalizing the current cell confluence of each cell line on its initial confluence at time point zero. For SiHa, a representative experiment out of two is shown.

In summary, these results indicate that GDF15 expression is not a key determinant for the basal proliferation rate of cervical cancer cells. This was further substantiated that transient silencing of *GDF15* expression by RNAi did not appreciably modulate the cell cycle profile of HeLa cells (Figure 16).

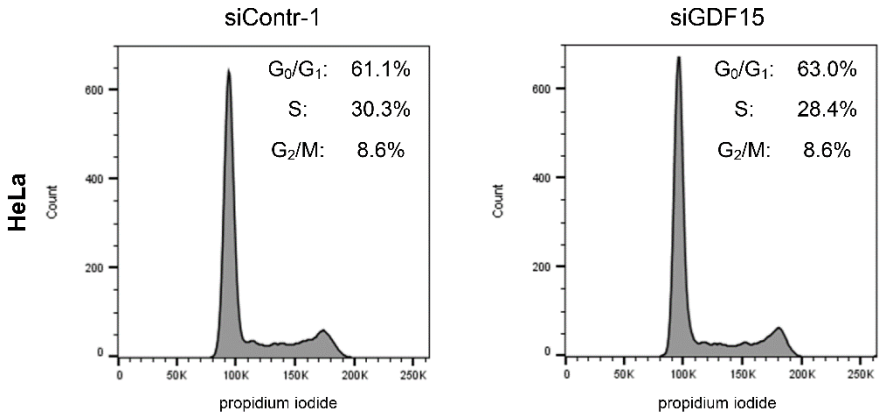

Figure 16 Silencing of GDF15 does not affect the cell cycle distribution of HeLa cells. Cells were transfected with either a control siRNA (siContr-1) or with an siRNA pool against *GDF15* mRNA (siGDF15) (for knockdown validation see Figure 14A), and harvested 72h after transfection. Cell cycle profiles were measured after DNA staining with propidium iodide by flow cytometry analyses. The Watson model[159] was applied to determine the cell cycle distributions.

2.2.2. Both a de- and an increase of GDF15 levels can reduce colony formation of cancer cells

Furthermore, the effect of GDF15 on proliferation of cervical cancer cells was analyzed by CFAs. For this purpose, episomal pCEP vectors which encode shRNAs targeting *GDF15* mRNA were designed. The efficiency of GDF15 downregulation was evaluated by immunoblotting. The pCEP constructs expressing shGDF15.1 and shGDF15.5 were selected for further use because they showed the highest knockdown efficiency (Figure 17A).

The knockdown of GDF15 reduced the colony formation capability of the cervical cancer cell lines HeLa, SiHa, and MRI-H186 (Figure 17B) as well as of the colorectal cancer cell line HCT-116 (Figure 17C). For the analysis of HCT-116 cells, a pCEP construct carrying the empty shRNA expression cassette (pCEP_sh) was used as negative control (Figure 17C) because pilot experiments indicated that shNeg inhibits the colony formation capability of HCT-116 cells. Importantly, less colonies were also formed after GDF15 overexpression in HeLa, SiHa (Figure 17E), and HCT-116 cells (Figure 17F) compared to control-transfected cells.

These findings raise the possibility that a narrow corridor for GDF15 expression exists and either too high or too low levels are detrimental for long-term cellular proliferation. This seems not to be a peculiarity of HPV-positive cells, as it was observed both in cervical cancer cell lines and in HPV-negative, colorectal HCT-116 cells.

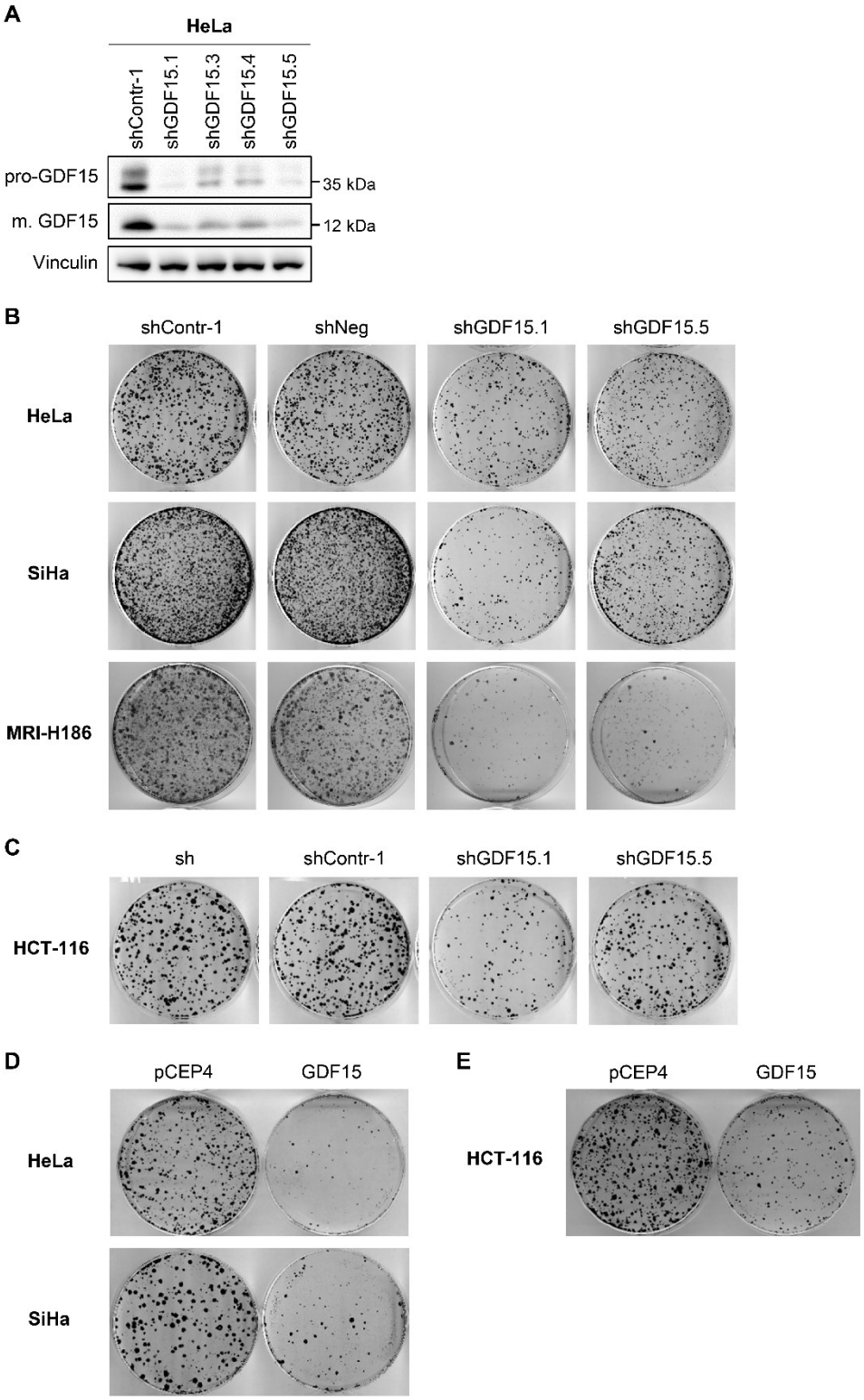

Figure 17 Knockdown as well as overexpression of GDF15 downregulate colony formation capabilities of cervical and colon cancer cells. (**A**) HeLa cells were transfected with pCEP constructs that encode either a control shRNA (shContr-1) or shRNAs targeting *GDF15* mRNA (shGDF15.1, shGDF15.3, shGDF15.4, or shGDF15.5). Cells were harvested 72h post transfection. Validation of GDF15 knockdown by immunoblot analyses of pro-GDF15 and mature (m.) GDF15 expression. Vinculin, loading control. (**B, C**) Colony formation assays of cells transfected with either control pCEP vectors, pCEP_shGDF15.1, or pCEP_shGDF15.5. (B) As control samples, HeLa (upper

panel), SiHa (middle panel), and MRI-H186 cells (lower panel) were transfected with pCEP plasmids coding for control shRNAs, i.e. shContr-1 and shNeg. (C) HCT-116 cells were control transfected either with pCEP_shContr-1 or with pCEP_sh, which contains an empty shRNA expression cassette. (**D**, **E**) Colony formation assays of HeLa (D, upper panel), SiHa (D, lower panel), and HCT-116 cells (E) that were transfected with either 1 µg empty pCEP4 vector as control or with 1 µg pCEP4_GDF15 for the overexpression of GDF15. Validation of GDF15 overexpression vector can be found in Figure 14B.

2.2.3. GDF15 does not protect against low, anti-proliferative levels of DNA damage

The reduced colony formation capabilities of HeLa and SiHa cells after silencing GDF15 (Figure 17B) seem to contrast the results of live cell imaging experiments, where the knockdown of GDF15 did not attenuate the proliferation of HeLa (Figure 15A) and SiHa (Figure 15B) cells. One important difference between the two methods is that the proliferation of transfected cells in CFAs is monitored over a period of 1.5-3 weeks under hygromycin B (HygB) selection. Hence, cervical cancer cells may benefit from moderate GDF15 levels in the presence of HygB. HygB is commonly used as an antibiotic against pro- and eukaryotic cells because it inhibits protein translation by blocking ribosomal translocation.[160] However, HygB was also found to induce DNA damage, which could result in decreased proliferation or survival of cells when DNA repair is disturbed.[161,162] Hence, it was investigated whether GDF15 is needed in response to DNA damage by HgyB, Camptothecin (CPT), cisplatin, or doxorubicin (Doxo). Each agent generates DNA damage by a different mode of action: HygB alkylates purines,[161] CPT inhibits the DNA topoisomerase I,[163] cisplatin preferentially crosslinks neighboring guanines,[164] and Doxo blocks the topoisomerase II by intercalating into DNA strands.[165] Firstly, GDF15 expression was silenced in HeLa mCherry H2B and SiHa mCherry H2B cells. Then, cells were treated with sublethal doses of the DNA-damaging agents and cell proliferation was measured for five days by live cell imaging with the IncuCyte system.

The selected low doses of DNA-damaging agents still allowed the cells to proliferate after treatment, although the proliferation rates were clearly reduced (Figure 18). GDF15 knockdown did not alter this drug-induced retardation of proliferation in HeLa mCherry H2B cells (Figure 18 left column). Similarly, no difference in proliferation was seen between control- and siGDF15-transfected SiHa mCherry H2B cells after adding cisplatin (Figure 18F) or doxorubicin (Figure 18H). Analyzing the effects of HygB (Figure 18B) and CPT (Figure 18D), treated, but also untreated SiHa mCherry H2B cells in which GDF15 expression was downregulated proliferated slightly better at late time points.

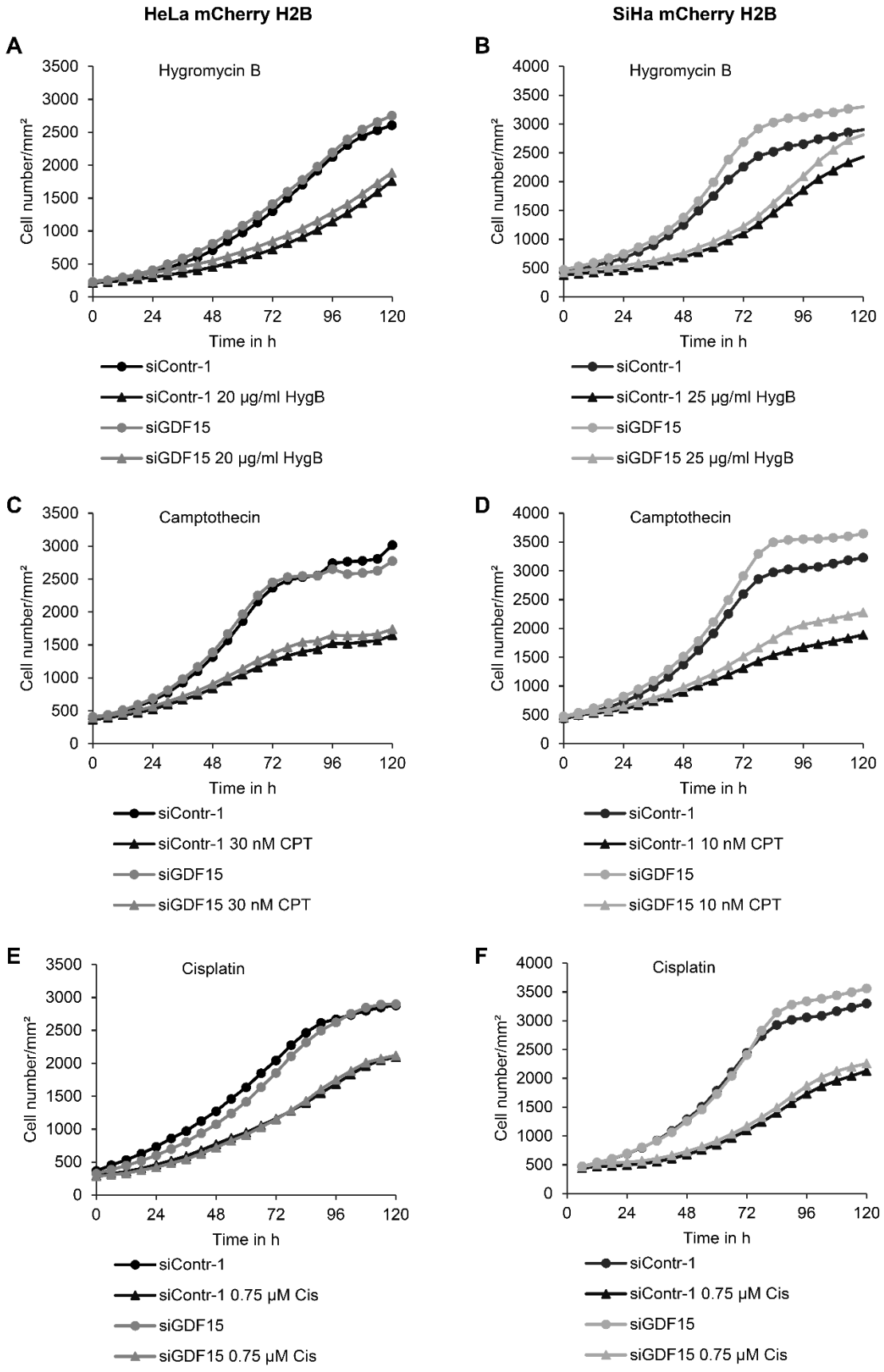
HeLa mCherry H2B
SiHa mCherry H2B
A
Hygromycin B
Cell number/mm²
Time in h
siContr-1
siContr-1 20 µg/ml HygB
siGDF15
siGDF15 20 µg/ml HygB
B
Hygromycin B
Cell number/mm²
Time in h
siContr-1
siContr-1 25 µg/ml HygB
siGDF15
siGDF15 25 µg/ml HygB
C
Camptothecin
Cell number/mm²
Time in h
siContr-1
siContr-1 30 nM CPT
siGDF15
siGDF15 30 nM CPT
D
Camptothecin
Cell number/mm²
Time in h
siContr-1
siContr-1 10 nM CPT
siGDF15
siGDF15 10 nM CPT
E
Cisplatin
Cell number/mm²
Time in h
siContr-1
siContr-1 0.75 µM Cis
siGDF15
siGDF15 0.75 µM Cis
F
Cisplatin
Cell number/mm²
Time in h
siContr-1
siContr-1 0.75 µM Cis
siGDF15
siGDF15 0.75 µM Cis

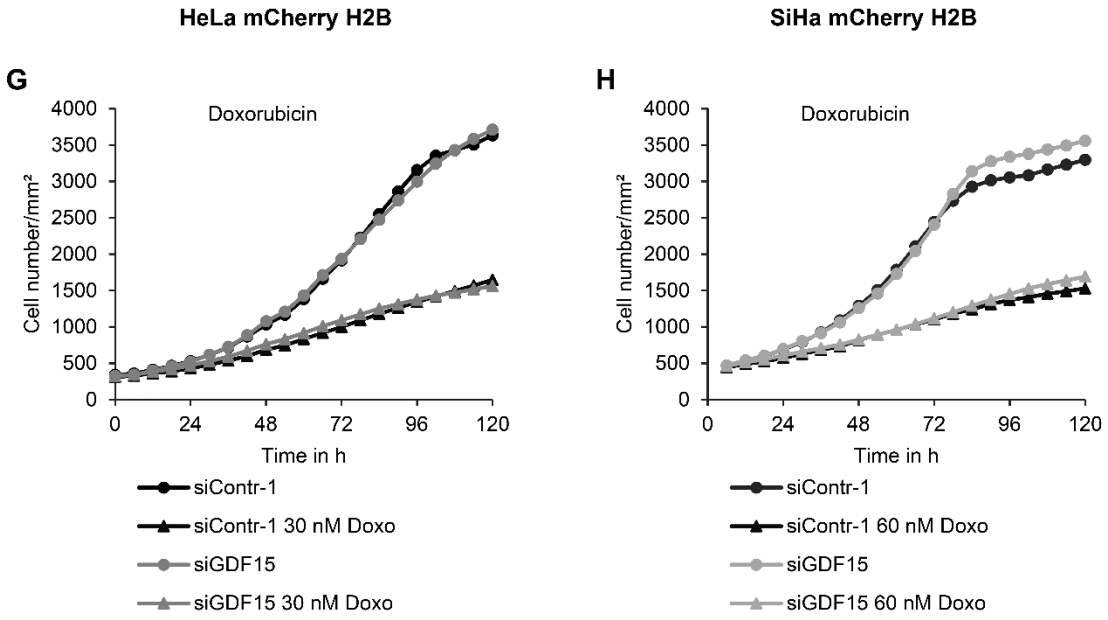

Figure 18 GDF15 knockdown does not sensitize cervical cancer cells towards low, antiproliferative levels of DNA damage. HeLa mCherry H2B (left column) or SiHa mCherry H2B cells (right column) were transfected with a control siRNA (siContr-1) or with an siRNA pool against *GDF15* mRNA (siGDF15) (for knockdown efficiency see Figure 14A). One day later, the cells were treated with sublethal doses of HygB (**A, B**), cisplatin (Cis) (**C, D**), CPT (**E, F**), or Doxo (**G, H**), respectively. Data for F and H were derived from the same experiment and therefore share proliferation curves for untreated samples. Proliferation was monitored by live cell imaging with the IncuCyte system every 6 hours for 5 days.

These observations lead to the conclusion that GDF15 does not protect cancer cells against antiproliferative effects of DNA-damaging agents like HygB. Therefore, the application of HygB as an antibiotic in CFAs does not explain the divergent results of CFAs and live cell imaging experiments after silencing GDF15 expression.

2.3. A functional role for GDF15 in stress-induced apoptosis of cervical cancer cells

Evidence from the literature shows that GDF15 expression is strongly upregulated in cancer cells after diverse, pro-apoptotic stress types and that GDF15 contributes to the observed induction of apoptosis.[62,86,111,124] Additionally, very high GDF15 levels led to reduced colony formation capabilities in HPV-positive cervical cancer cells (Figure 17E) as well as in HCT-116 colon carcinoma cells (Figure 17F). Hence, it was interesting to investigate whether the downregulation of GDF15 represents a growth advantage for cervical cancer cells under lethal stress conditions. The role of GDF15 for the survival of cervical cancer cells that suffer from excessive ER stress or are treated with the NSAID SSide or the chemotherapeutic agent cisplatin was examined. Both drugs are reported to stimulate UPR signaling pathways (Figure 5) in order to induce apoptosis.[111,166]

2.3.1. ER stress-induced apoptosis involves GDF15 in cervical cancer cells

Several external factors like hypoxia or nutrient deprivation can alter protein homeostasis of tumor cells and induce ER stress. In order to cope with this imbalance, tumor cells take advantage of a cytoprotective mechanism, the UPR (described in 1.2.3.1). Signaling pathways of the UPR promote cell survival by attenuation of protein synthesis, stimulation of chaperon expression, and activation of ER-associated degradation of misfolded proteins.[131] However, prolonged UPR can lead to the induction of apoptosis. This principle is used in several therapeutic approaches against cancer, including cervical cancer.[167] Therefore, GDF15 repression by E6 might present a strategy of cervical cancer cells to increase their resistance against apoptosis induced by excessive ER stress.

2.3.1.1. Increase of GDF15 expression during ER stress

Both TM and TG induced ER stress in HeLa (Figure 19A) and SiHa (Figure 19B) cells as indicated by rising BiP and CHOP levels in Western blot analyses. Total GDF15 expression and PARP cleavage were upregulated after 48h TM or TG treatment whereby HeLa cells seemed to be more sensitive towards TG (Figure 19A) and SiHa cells towards TM treatment (Figure 19B). In later experiments, HeLa cells were treated with a higher TM concentration (5 µM) to enhance apoptosis levels. TM and TG downregulated HPV18 E6 in HeLa (Figure 19A) and TM HPV16 E6 in SiHa cells (Figure 19B), which correlated with a rise in p53 levels. E7 expression was not appreciably altered by ER stress.

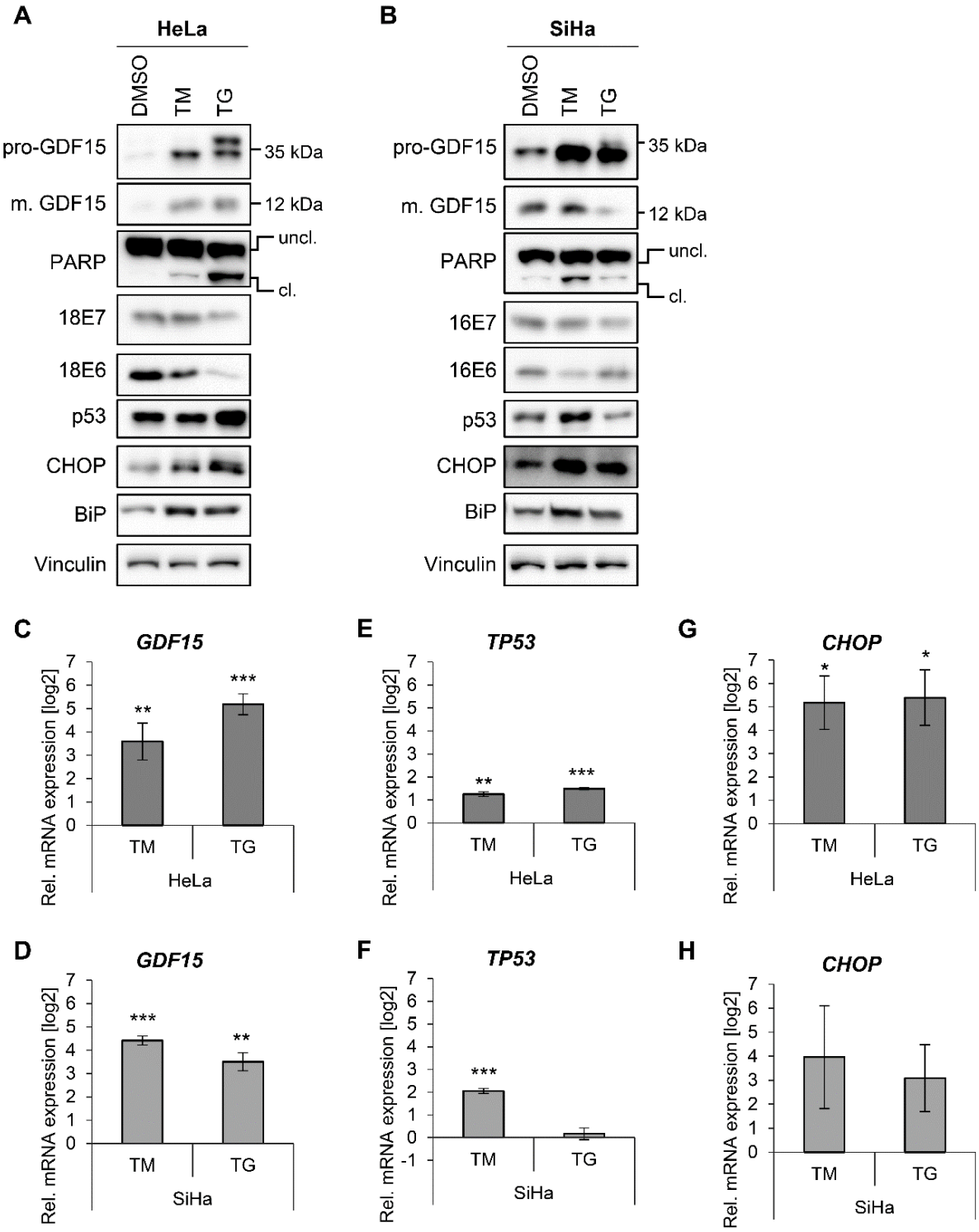

Figure 19 Intracellular GDF15 levels are upregulated by ER stress in cervical cancer cell lines. Cervical cancer cells were treated with solvent control (dimethyl sulfoxide, DMSO), 1 µM TM, or 0.5 µM TG. They were harvested either after 48h for immunoblot analyses of cell lysates (A, B) or after 24h for qRT-PCR analyses (C-H). (**A, B**) Immunoblot analyses of pro-GDF15, mature (m.) GDF15, PARP, E7, E6, p53, CHOP, and BiP expression in cell lysates from HeLa (A) and SiHa cells (B). Uncleaved (uncl.), cleaved (cl.). Vinculin, loading control. (**C-H**) qRT-PCR analyses determining relative mRNA expression levels of *GDF15* (C, D), *TP53* (E, F), and *CHOP* (G, H) in HeLa and SiHa cells. Depicted is the log2 of the mean expression levels relative to DMSO-treated cells. Bars represent

standard deviations. Asterisks above bars indicate statistically significant differences to DMSO-treated cells as determined by one-sample *t*-test. *p ≤ 0.05, **p ≤ 0.01, ***p ≤ 0.001.

The increased levels of the transcription factors CHOP and p53 implied that GDF15 expression might be induced on the mRNA level. This assumption was supported by qRT-PCR analyses of TM- or TG-treated HeLa (Figure 19C) and SiHa (Figure 19D) cells. Both cervical cancer cell lines also showed upregulated *TP53* (Figure 19E and F) and *CHOP* transcript levels (Figure 19G and H) during ER stress. Only SiHa cells did not show higher *TP53* expression after TG treatment (Figure 19F).

In contrast to the increase of intracellular GDF15 protein levels (Figure 19A), TM and TG treatment of HeLa cells decreased total levels of secreted GDF15 (Figure 20). Remarkably, only pro-GDF15 forms below 35 kDa were found intra- (Figure 19A) or extracellularly (Figure 20) after adding TM to HeLa cells, while faster and slower migrating pro-GDF15 forms were observed after TG-induced ER stress (Figure 19A and Figure 20). The two ER stressors have different modes of action in order to generate ER stress: TM blocks the first step of N-glycosylation,[168] whereas TG inhibits a calcium pump in the ER.[169] Hence, the bands below and above 35 kDa may represent the unmodified and N-glycosylated forms of pro-GDF15, respectively.[87]

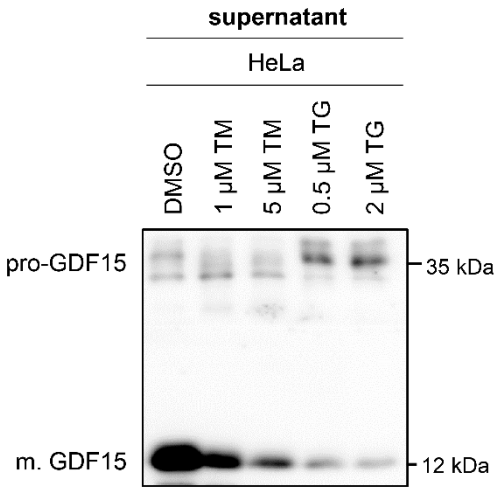

Figure 20 TM or TG treatment decrease total extracellular levels of GDF15. HeLa cells were treated with solvent control (DMSO), 1 µM TM, 5 µM TM, 0.5 µM TG, or 2 µM TG. Cell culture supernatants were harvested after 48h. Immunoblot analysis of cell culture supernatants from HeLa cells is shown detecting secreted pro-GDF15 and mature (m.) GDF15 expression at the same exposure time. Loading volumes were normalized on amounts of total intracellular protein.

To investigate this notion, GDF15 or its mutant N70A, which cannot be N-glycosylated anymore, were overexpressed in HeLa cells and analyzed by immunoblotting (Figure 21A). The expression levels of GDF15 and its mutant N70A were comparable. Both pro-GDF15 bands were found after ectopic expression of GDF15 wildtype, while only the 34 kDa band was detected after overexpressing the GDF15 mutant (Figure 21A). The band pattern was analogous to that after TM treatment of HeLa cells (Figure 19A). Remarkably, mutation of the N-glycosylation site in pro-GDF15 also reduced levels of extracellular GDF15, in particular in the case of the GDF15 pro-form as shown by immunoblotting of HeLa cell culture supernatants (Figure 21B).

To sum up, intracellular GDF15 levels are upregulated by ER stress in cervical cancer cells. This stimulation could be mediated by p53 and CHOP, which both can also be activated by TM or TG treatment. Addition of TM or TG as well as mutation of the N-glycosylation site in pro-GDF15 downregulate the amounts of secreted GDF15. Furthermore, GDF15 could be involved in the induction of apoptosis after ER stress because upregulated GDF15 expression largely correlates with increased PARP cleavage.

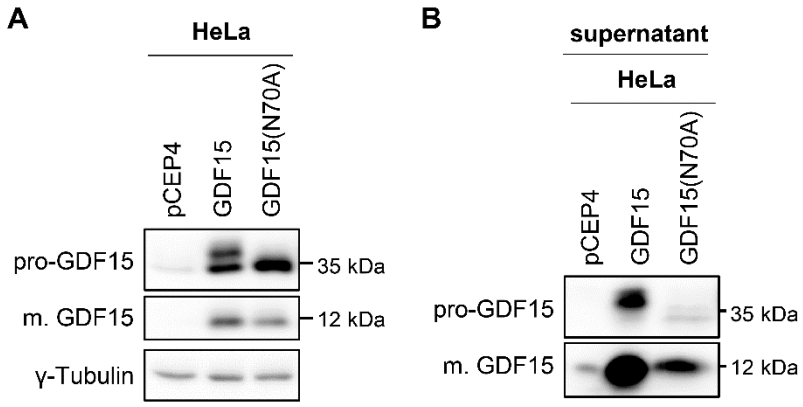

Figure 21 Inhibition of N-glycosylation reduces extracellular levels of GDF15. HeLa cells were transfected with 0.1 µg empty pCEP4, pCEP4_GDF15, or pCEP4_GDF15(N70A). Cell lysates or culture supernatants were harvested 48h post transfection. (**A**) Immunoblot analysis of intracellular pro-GDF15 and mature (m.) GDF15 expression. γ-Tubulin, loading control. (**B**) Immunoblot analysis of cell culture supernatants from HeLa cells detecting secreted pro-GDF15 and mature (m.) GDF15 levels. Loading volumes were normalized on amounts of total intracellular protein. A representative blot out of two independent experiments is shown.

2.3.1.2. CHOP contributes to the upregulation of GDF15 levels during ER stress

In colorectal cancer cell lines, Yang *et al.* identified CHOP as an important activator of GDF15 expression after ER stress.[77] HCT-116 and HeLa cells were treated with TM or TG after silencing *CHOP* mRNA to validate this finding. The ER stressors were also added to p53-deficient HeLa *"p53 null"* and HCT-116 $p53^{-/-}$ cells, since p53 seems to play a major role in GDF15 regulation and can be induced during ER stress as well.

P53 levels were elevated 48h after TM and TG treatment of HeLa cells (Figure 22A). However, p53 is probably not essential for the upregulation of GDF15 because GDF15 protein (Figure 22A) and mRNA expression (Figure 22B) was increased after inducing ER stress in both p53-expressing HeLa and in HeLa *"p53 null"* cells. Additionally, HCT-116 and HCT-116 $p53^{-/-}$ cells showed comparable, elevated GDF15 protein levels after adding ER stressors (Figure 22C). Lacking p53 expression did also not prevent ER stress-mediated activation of CHOP and BiP expression in HeLa cells (Figure 22A). Similar CHOP induction was also observed in both HCT-116 and HCT-116 $p53^{-/-}$ cells after adding TM or TG for 24h (Figure 22C). Notably, HeLa *"p53 null"* cells exhibited increased PARP cleavage after 48h when solely DMSO was

added as solvent control (Figure 22A). Thus, they in general appeared to be more sensitive towards induction of apoptosis.

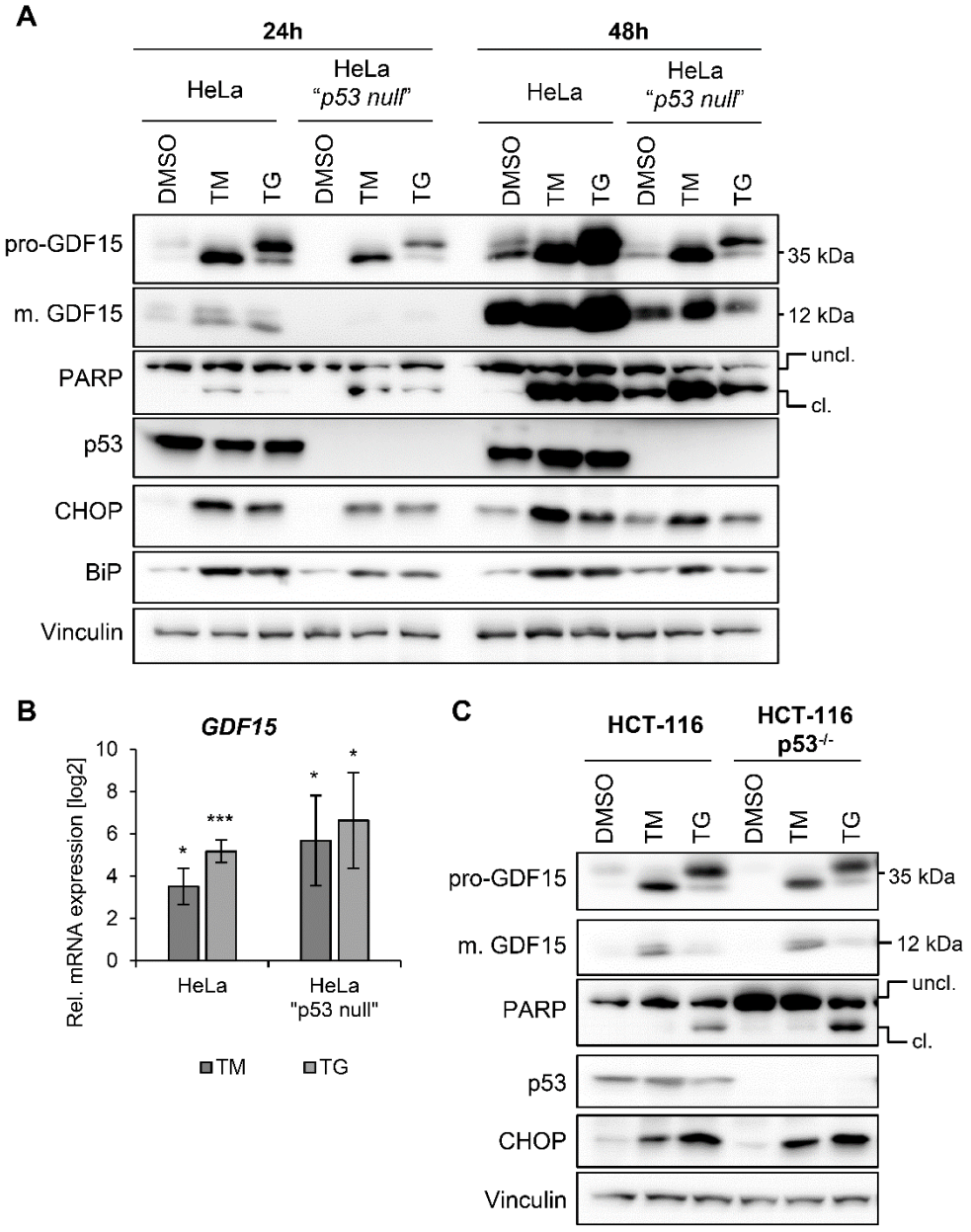

Figure 22 P53 is not essential for the upregulation of GDF15 expression after ER stress. (**A, B**) HeLa or HeLa *"p53 null"* cells were treated with solvent control (DMSO), 5 µM TM, or 0.5 µM TG. (A) Immunoblot analyses of pro-GDF15, mature (m.) GDF15, PARP, p53, CHOP, and BIP expression after 24h or 48h treatment. Uncleaved (uncl.), cleaved (cl.). Vinculin, loading control. (B) qRT-qPCR analyses determining relative mRNA expression levels of *GDF15* 24h after treatment. Depicted is the log2 of the mean expression levels relative to DMSO-treated cells. Bars represent standard deviations. Asterisks indicate statistically significant differences to DMSO-treated cells as determined by one-sample *t*-test. *p ≤ 0.05, ***p ≤ 0.001. (**C**) HCT-116 and HCT-116 p53$^{-/-}$ cells were treated with DMSO, 5 µM TM, or 0.5 µM TG for 24h. Immunoblot analyses of pro-GDF15, mature (m.) GDF15, PARP, p53, and CHOP expression. Uncleaved (uncl.), cleaved (cl.). Vinculin, loading control.

Silencing of *CHOP* by RNAi (Figure 23A and B) reduced GDF15 protein expression (Figure 23A) in TM- and TG-treated HeLa and HeLa *"p53 null"* cells. On mRNA level, CHOP downregulation only decreased *GDF15* expression after TG, but not after TM treatment (Figure 23C). This findings indicates that CHOP might not only be a transcriptional activator of the *GDF15* gene but has additional regulatory effects on GDF15 expression in HPV-positive cancer cells. This notion is further supported because GDF15 expression levels were even slightly raised in control-treated cells after CHOP knockdown (Figure 23B and D), which could also be observed in other experiments of this thesis (Figure 29B and D; Figure 33B and D). Furthermore, CHOP downregulation reduced p53 protein (Figure 23A) and mRNA levels (Figure 23D) in TM- and TG-treated HeLa cells.

In conclusion, these results indicate that CHOP has an important role for the increased GDF15 expression in cancer cells under ER stress.

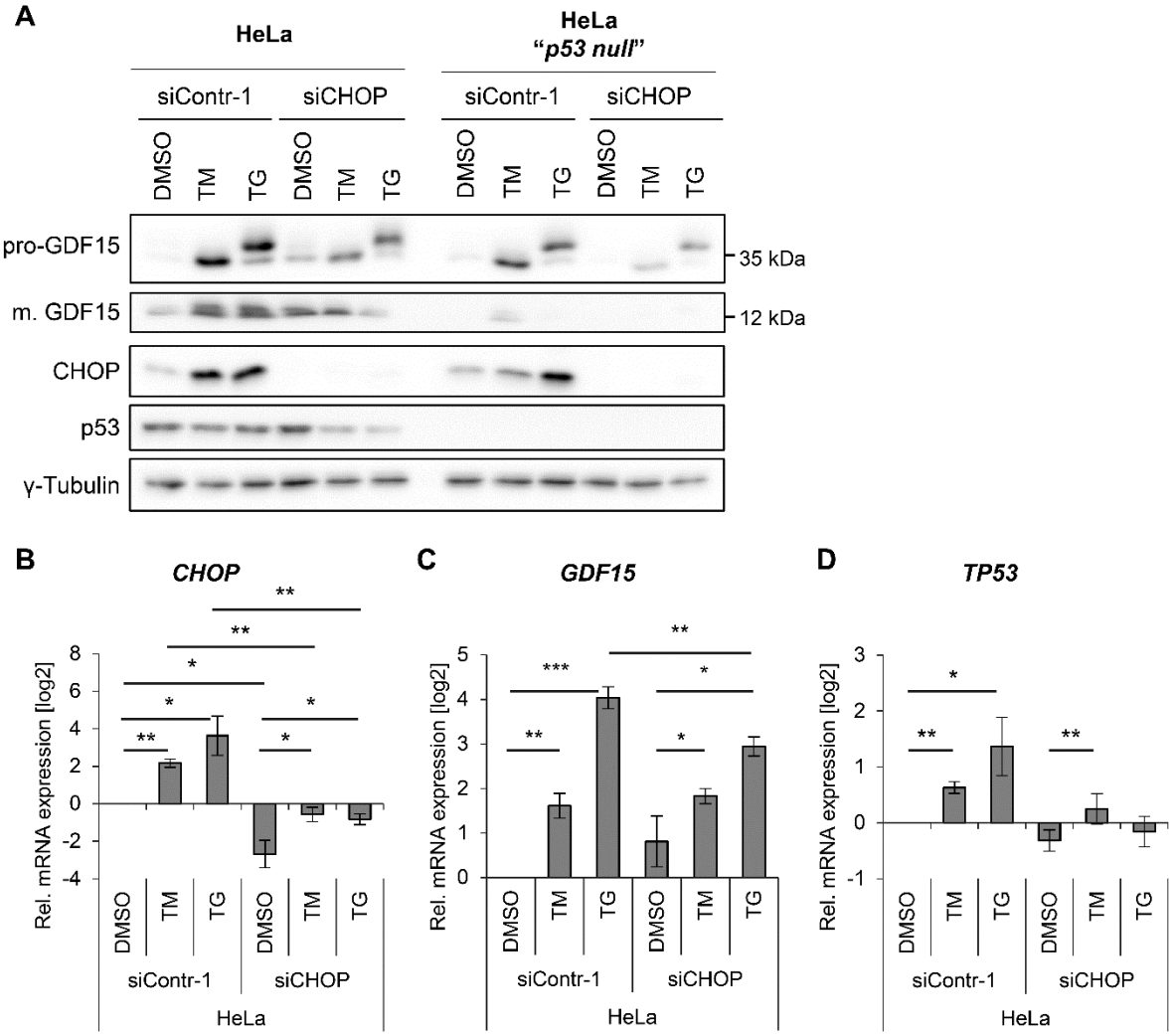

Figure 23 CHOP upregulates GDF15 expression after ER stress. HeLa or HeLa *"p53 null"* cells were transfected with control siRNA (siContr-1) or with an siRNA pool targeting *CHOP* mRNA (siCHOP). Two days after transfection, cells were treated with solvent control (DMSO), 5 µM TM, or 0.5 µM TG for 24h. (**A**) Immunoblot analyses of pro-GDF15, mature (m.) GDF15, CHOP, and p53

expression. γ-Tubulin, loading control. (**B-D**) qRT-analyses determining relative mRNA expression levels of *CHOP* (B), *GDF15* (C), and *TP53* (D). Depicted is the log2 of the mean expression levels relative to DMSO-treated and siContr-1-transfected cells. Bars represent standard deviations. Asterisks indicate statistically significant differences between samples connected by crosslines as determined by two-sided *t*-test. *p ≤ 0.05, **p ≤ 0.01, ***p ≤ 0.001.

2.3.1.3. *GDF15* knockout increases the resistance of HeLa cells against ER stress-induced apoptosis

Next, it was analyzed whether GDF15 downregulation can protect HPV-positive cervical cancer cells against ER stress-induced apoptosis.

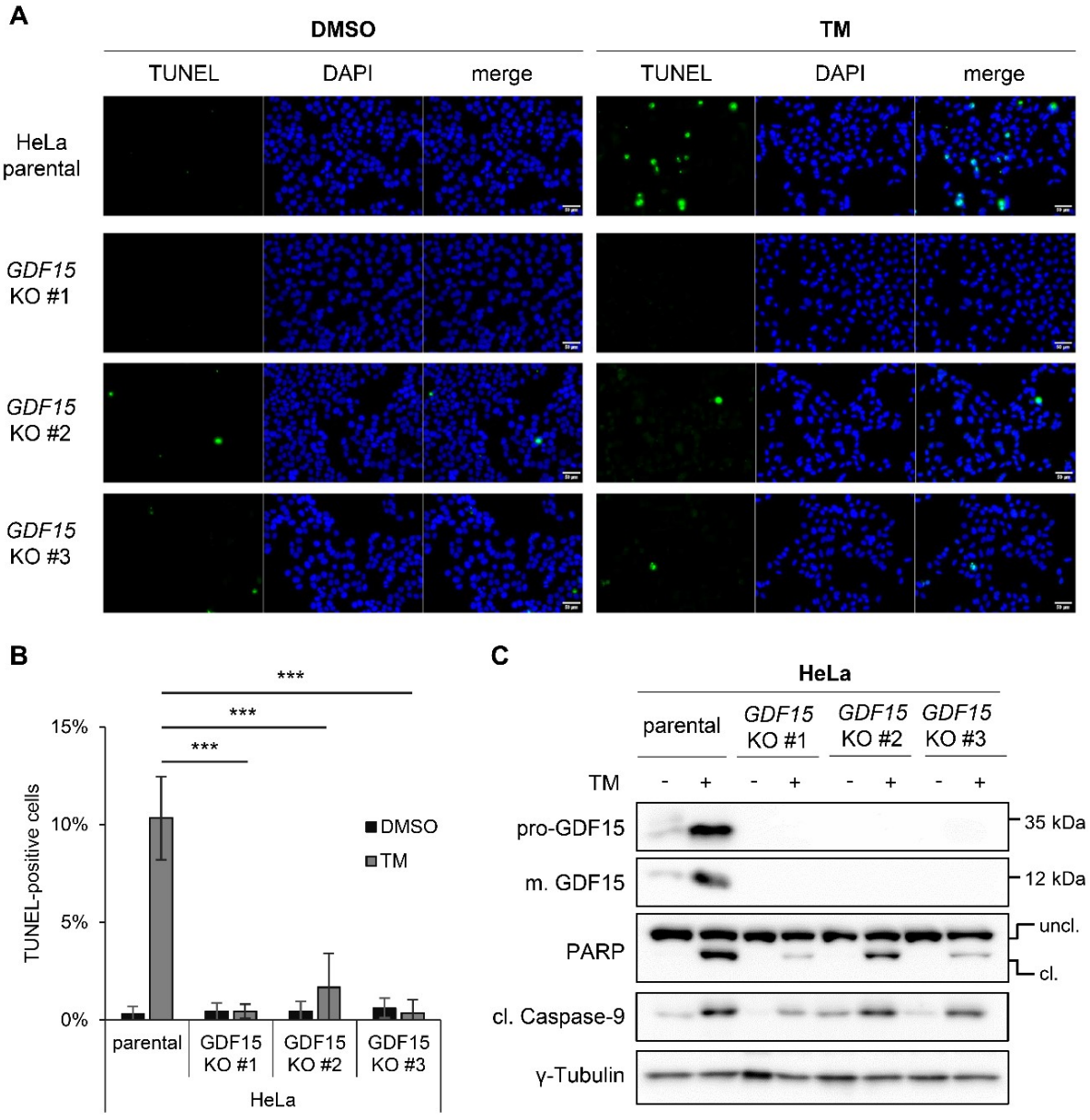

Figure 24 *GDF15* knockout increases resistance of HeLa cells against ER stress-induced apoptosis. Parental HeLa cells or HeLa *GDF15* KO clones #1-3 were treated with solvent control (DMSO) or with 5 µM TM for 48h. (**A**) Representative images after TUNEL and DAPI staining (apoptotic cells: green, cell nuclei: blue). Scale bar: 50 µM. **(B**) Rel. quantification of TUNEL-positive cells on total cell number. Shown are means of at least five images per sample from a representative

replicate. Bars represent standard deviations. Asterisks indicate statistically significant differences between samples connected by crosslines as determined by two-sided *t*-test. ***p ≤ 0.001. (**C**) Immunoblot analyses of pro-GDF15, mature (m.) GDF15, PARP, and cleaved Caspase-9 expression. Uncleaved (uncl.), cleaved (cl.). γ-Tubulin, loading control.

Firstly, a higher percentage of parental HeLa cells than of HeLa *GDF15* KO clones #1-3 were stained positive for apoptosis in TUNEL assays after TM treatment (Figure 24A and B). Secondly, less PARP and Caspase-9 cleavage was detected by immunoblot analyses after *GDF15* KO in TM-treated cells (Figure 24C).

Altogether, these results provide strong experimental evidence that GDF15 repression protects cervical cancer cells against apoptosis via ER stress pathways. Notably, several anti-tumorigenic agents are known to alter ER stress signaling pathways in cancer cells.[138,167] This raises the question whether GDF15 repression also provides resistance to HPV-positive cells against chemopreventive or -therapeutic drugs.

2.3.2. GDF15 can sensitize cervical cancer cells towards SSide treatment

In the past years, increasing evidence has shown that – particularly regular – intake of NSAIDs may reduce the risk of various cancer types, including cervical cancer.[170,171] Among other modes of action, NSAIDs induce apoptosis of cancer cells by stimulating ER stress signaling pathways, which lead to an increase of the pro-apoptotic protein CHOP.[111,172] GDF15 was also reported to mediate apoptosis after NSAID treatment in the colorectal cancer cell line HCT-116.[62]

As a prototype NSAID, SSide was used to assess the effects of NSAIDs on proliferation of HPV-positive cancer cells. SSide is the active metabolite of the prodrug Sulindac, which has been reported to promote growth arrest and apoptosis in cervical carcinoma cells.[173] For all following SSide experiments, cells were cultivated in FCS-free medium because SSide is known to bind to serum albumin.[174] SSide treatment (50 µM) blocked the proliferation of HeLa mCherry H2B (Figure 25A) and SiHa mCherry H2B cells (Figure 25B) in live cell imaging experiments with the IncuCyte system. Untreated control cells proliferated in FCS-free medium for several days (Figure 25), although proliferation of SiHa mCherry H2B cells stopped between two and three days after start (Figure 25B).

2.3.2.1. SSide activates GDF15 expression and induces apoptosis in HPV-positive cancer cells

Historically, GDF15 was identified as NSAID activated gene-1 (NAG-1), which mediated the induction of apoptosis in NSAID-treated colorectal cells.[62] The strongest activating effect on GDF15 expression could be observed after SSide treatment of HCT-116 cells.[62] In line with this, GDF15 levels were also upregulated with increasing SSide concentration in HeLa (Figure

26A), SiHa (Figure 26B), and MRI-H186 (Figure 26C) cells as detected by immunoblotting. Notably, SSide preferentially promoted the N-glycosylated form of pro-GDF15 in HeLa (Figure 26A) and SiHa cells (Figure 26B). MRI-H186 cells showed both pro-GDF15 forms after adding 50 µM SSide (Figure 26C). *GDF15* mRNA expression was also increased in SSide-treated HeLa (Figure 26D) and SiHa cells (Figure 26E) as analyzed by qRT-PCR. In contrast, SSide treatment reduced the levels of extracellular GDF15 as shown by Western blotting of HeLa cell culture supernatants (Figure 26F).

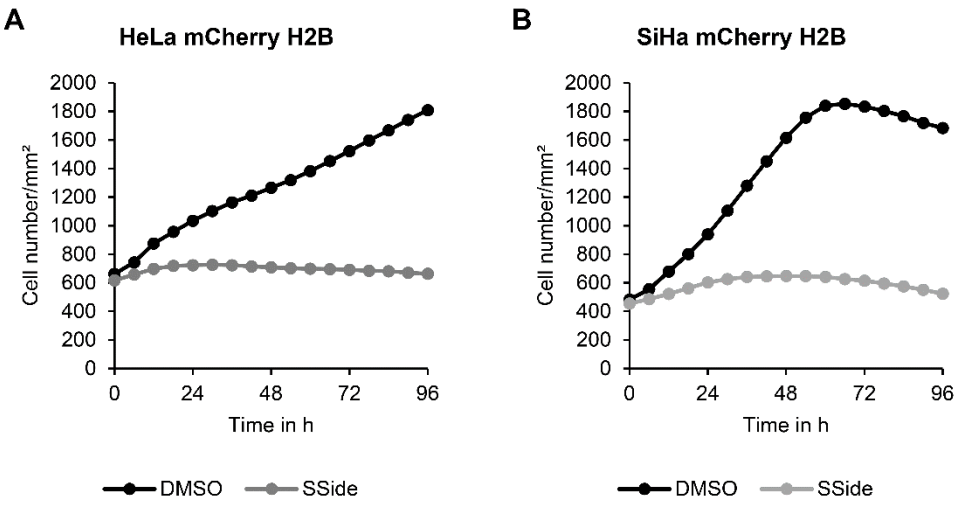

Figure 25 SSide inhibits proliferation of cervical cancer cells. HeLa mCherry H2B (A) and SiHa mCherry H2B cells (B) were treated with solvent control (DMSO) or 50 µM SSide in FCS-free medium. Cell proliferation was monitored for 4 days every 6 hours by live cell imaging with the IncuCyte system.

In all three investigated cervical cancer cell lines, high concentrations of SSide induced apoptosis, which was indicated by PARP cleavage (Figure 26A-C). Furthermore, SSide treatment activated p53 and CHOP expression (Figure 26A-C). After 24h, SSide treatment showed remarkably different effects on HPV oncoprotein levels between the individual cervical cancer cell lines. HPV16 E6/E7 expression was upregulated in SiHa cells (Figure 26B). In HeLa cells, E7 levels remained largely unchanged, whereas E6 levels decreased (Figure 26A). Both E6 and E7 amounts were diminished in MRI-H186 cells (Figure 26C).

In order to analyze how SSide influences the expression of GDF15 and E7 in more detail, parallel time courses with solvent control (DMSO) or SSide were performed in HeLa (Figure 27) and SiHa cells (Figure 28). SSide stimulated *GDF15* mRNA expression immediately after treatment start and maintained high expression levels in HeLa (Figure 27A) and SiHa cells (Figure 28A) over the whole course of the kinetics. In DMSO-treated cervical cancer cells, *GDF15* mRNA levels increased with time (Figure 27A and Figure 28A). This could result from the observation that control cells further proliferate in contrast to SSide-treated cells (Figure 25) and therefore have a higher demand for glucose. At late time points, control cells may

strongly induce GDF15 expression (Figure 25B) because of glucose depletion as described in chapter 2.1.2.

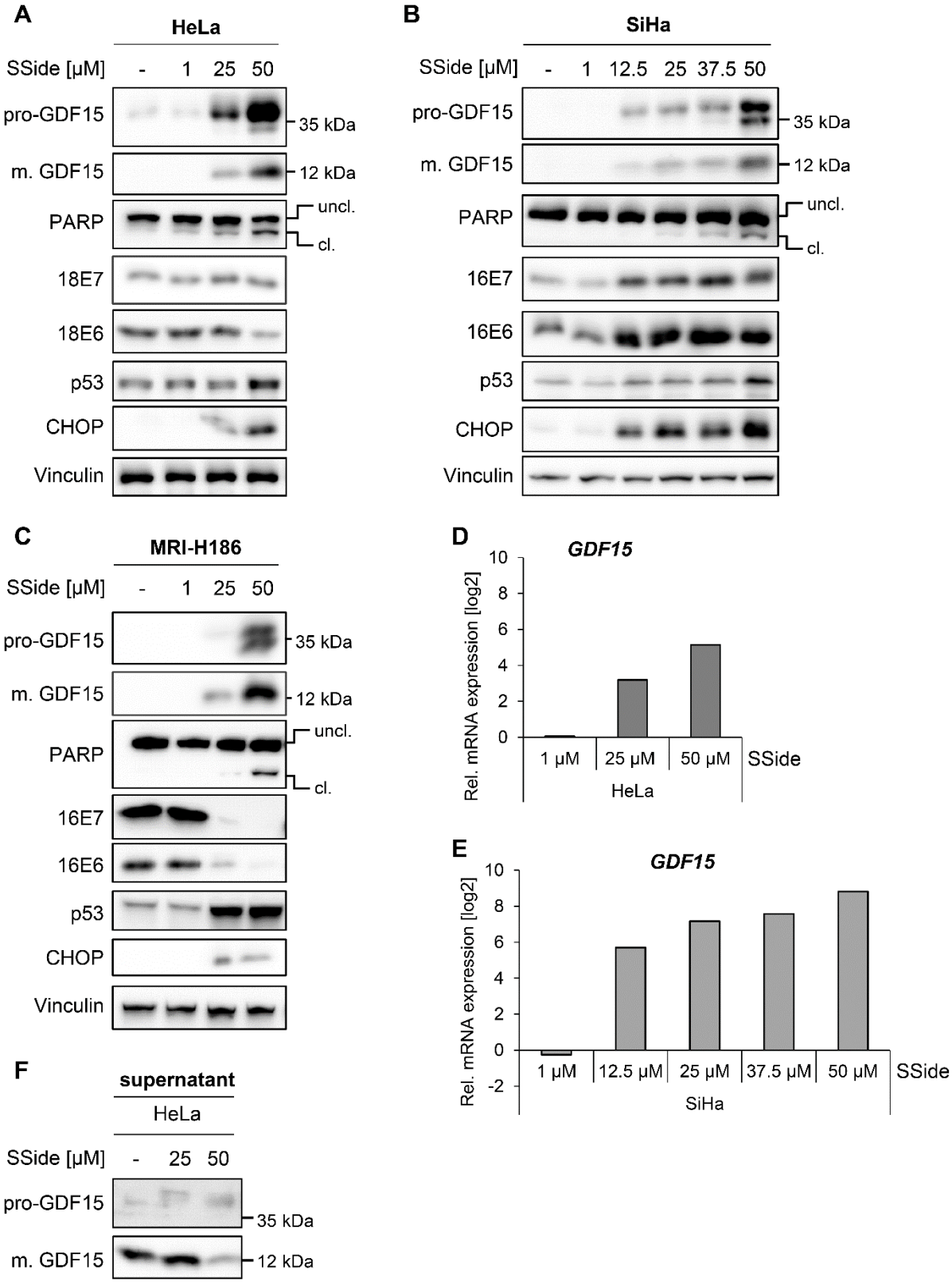

Figure 26 Intracellular GDF15 levels are increased in cervical cancer cells by SSide. Cells were treated with DMSO (solvent control) or with SSide in the indicated concentrations for 24h in FCS-free

medium. (**A-C**) Immunoblot analyses of pro-GDF15, mature (m.) GDF15, PARP, E7, E6, p53, and CHOP expression in cell lysates from HeLa (A), SiHa (B), and MRI-H186 cells (C). For HeLa and MRI-H186, representative blots are shown out of two independent experiments. Uncleaved (uncl.), cleaved (cl.). Vinculin, loading control. (**D, E**) qRT-PCR analyses determining relative *GDF15* mRNA expression in HeLa (D) and SiHa cells (E). Depicted is the log2 of the expression relative to DMSO-treated cells. Shown data are representative for two or three experiments conducted in HeLa or SiHa cells, respectively. (**F**) Immunoblot analysis of cell culture supernatants from HeLa cells detecting secreted pro-GDF15 and mature (m.) GDF15 levels. Loading volumes were normalized on amounts of total intracellular protein.

The regulation of the HPV oncogene transcripts was also time-dependent (Figure 27B and Figure 28B). In HeLa cells, SSide treatment induced *E6/E7* expression after 12h and then started to repress it after 36h (Figure 27B). While *E6/E7* transcripts were upregulated in SSide-treated SiHa cells until 24h, they were strongly downregulated between 36h and 60h (Figure 28B).

On protein level, GDF15 expression increased slightly in DMSO-treated HeLa cells and was strongly upregulated by SSide treatment throughout the time course (Figure 27C). Additionally, SSide induced high levels of cleaved PARP in HeLa cells (Figure 27C). A slight increase in PARP cleavage could also be detected in control cells after 60h, probably caused by the long-term FCS-free cultivation. After an initial induction, SSide treatment downregulated HPV18 E7 levels after 36h (Figure 27C). E7 amounts were also reduced 48h and 60h after adding DMSO to HeLa cells, likely due to cultivation in FCS-lacking medium.

In time course experiments of SiHa cells, GDF15 protein amounts were upregulated by SSide, too (Figure 28C). After 36h, GDF15 levels strongly increased in DMSO-treated SiHa cells and even surpassed the SSide-induced GDF15 levels after 48h. While N-glycosylated pro-GDF15 was observed after adding SSide, the non-glycosylated pro-form of GDF15 dominated in control cells (Figure 28C). PARP cleavage indicated that SSide induced high levels of apoptosis in SiHa cells after 60h (Figure 28C). In addition, control cells started to die of apoptosis after 36h. These effects in DMSO-treated SiHa cells could be due to their ongoing proliferation (Figure 25B), which leads to an increasing deficiency of nutrients and finally to cell death.

After an initial induction by SSide, HPV16 E7 expression was downregulated after 24h in both DMSO- and SSide-treated SiHa cells (Figure 28C). At late time points in control cells, *E6/E7* mRNA levels (Figure 28B) were stimulated, while protein levels (Figure 28C) were repressed. This divergence points towards the involvement of mechanisms that negatively affect E7 translation or protein stability.

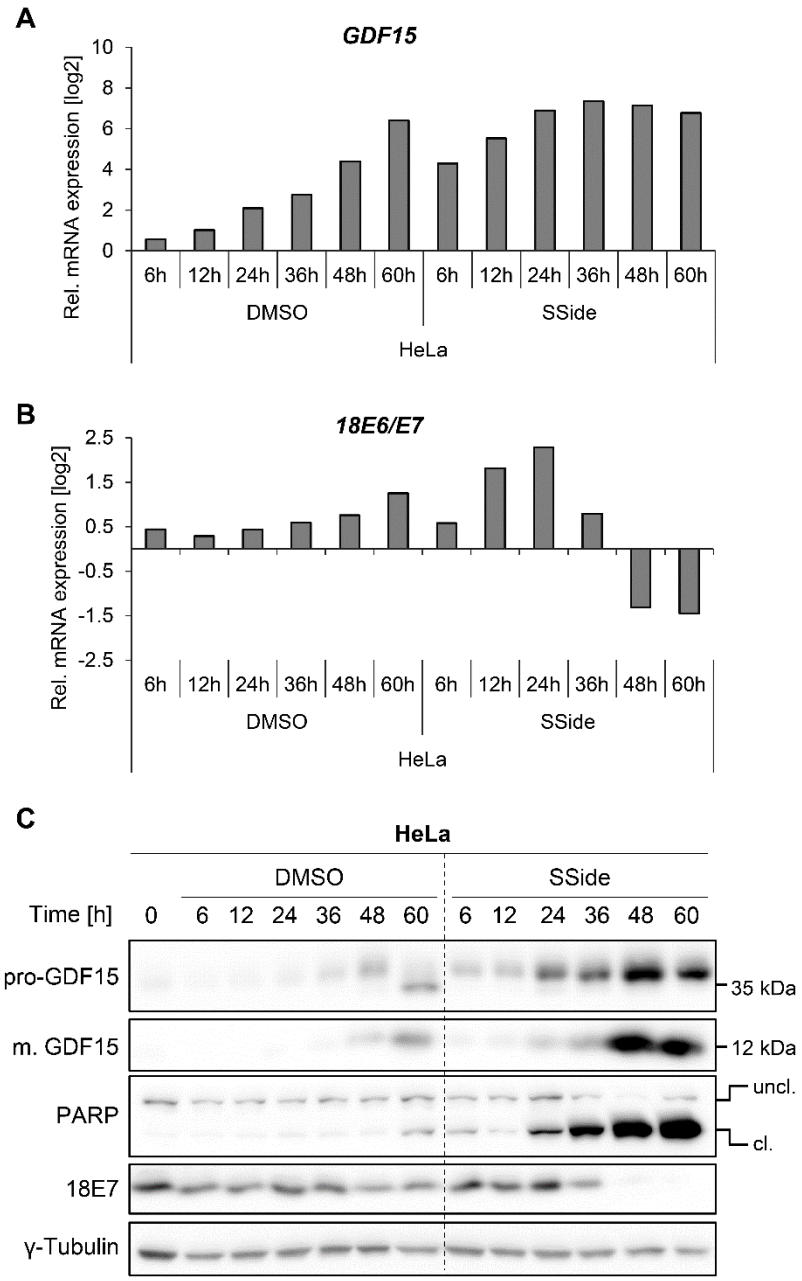

Figure 27 Time-dependent regulation of GDF15, E7, and PARP cleavage in HeLa cells in SSide experiments. Either DMSO (solvent control) or 50 µM SSide was added to HeLa cells cultivated in FCS-free medium. Cells were harvested at time point zero or 6h, 12h, 24h, 36h, 48h, and 60h after SSide treatment. Representative mRNA and protein analyses are shown out of two independent experiments. (**A, B),** qRT-PCR analyses determining relative transcript levels of *GDF15* (A) and HPV18 *E6/E7* (B). Depicted is the log2 of the expression relative to time point zero. (**C**) Immunoblot analyses of pro-GDF15, mature (m.) GDF15, PARP, and E7 expression. Uncleaved (uncl.), cleaved (cl.). γ-Tubulin, loading control.

In summary, SSide upregulates intracellular GDF15 expression in cervical cancer cells, which associates with the induction of apoptosis. This implies that intake of NSAIDs can have GDF15-mediated chemopreventive effects against cervical cancer cells. The regulation of E6/E7 levels in this experimental setup is time-dependent and could be negatively affected by two different factors: at late time points, E6/E7 expression seems to be downregulated by SSide treatment and by prolonged FCS-free cultivation. GDF15 amounts correlate with increased CHOP and p53 expression in SSide-treated cervical cancer cells, suggesting that the two transcription factors might be involved in the upregulation of GDF15 after SSide treatment.

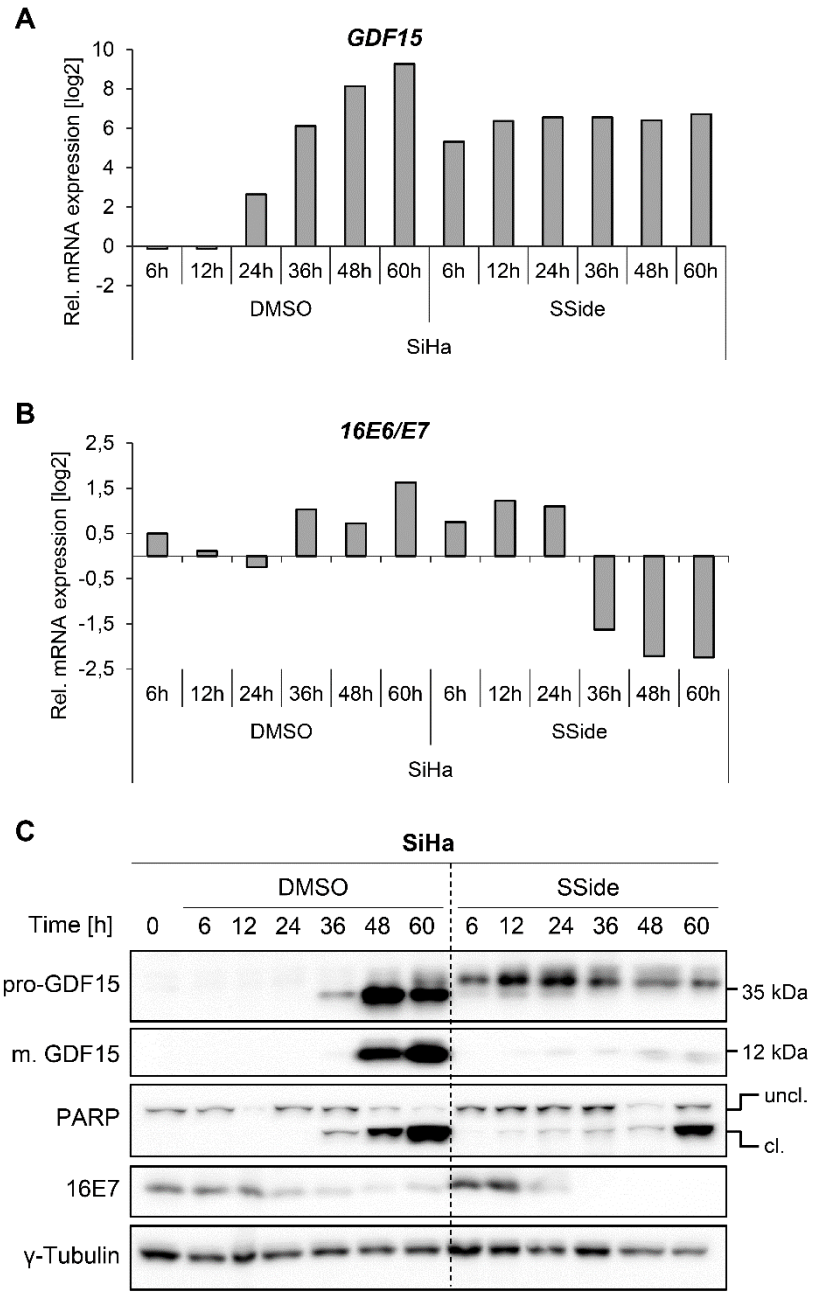

Figure 28 Time-dependent regulation of GDF15, E7, and PARP cleavage in SiHa cells in SSide experiments. Either DMSO (solvent control) or 50 µM SSide was added to SiHa cells cultivated in FCS-free medium. Cells were harvested at time point zero or 6h, 12h, 24h, 36h, 48h, and 60h after SSide treatment. Representative mRNA and protein analyses are shown out of two independent experiments. (**A, B),** qRT-PCR analyses determining relative transcript levels of *GDF15* (A) and HPV16 *E6/E7* (B). Depicted is the log2 of the expression relative to time point zero. (**C**) Immunoblot analyses of pro-GDF15, mature (m.) GDF15, PARP, and E7 expression. Uncleaved (uncl.), cleaved (cl.). γ-Tubulin, loading control.

2.3.2.2. P53 contributes to the upregulation of GDF15 after SSide treatment

To analyze whether CHOP and/or p53 play a role in the stimulation of GDF15 by SSide, *CHOP* or *TP53* mRNA levels were downregulated by RNAi in SSide-treated HeLa cells. Protein and mRNA expression analyses were carried out by immunoblotting and qRT-PCR, respectively. Firstly, the role of CHOP was investigated. CHOP was upregulated on mRNA (Figure 29A) and protein level (Figure 29D) after adding SSide to HeLa cells. Notably, silencing of CHOP did not affect the SSide-induced increase of *GDF15* transcripts (Figure 29B) and protein (Figure 29D) levels. CHOP downregulation also had no or a limited negative impact on PARP

cleavage (Figure 29D) or p53 expression (Figure 29C and D), respectively. This suggests that CHOP neither takes part in the upregulation of GDF15 nor in the induction of apoptosis by SSide treatment, but other pro-apoptotic factors are involved.

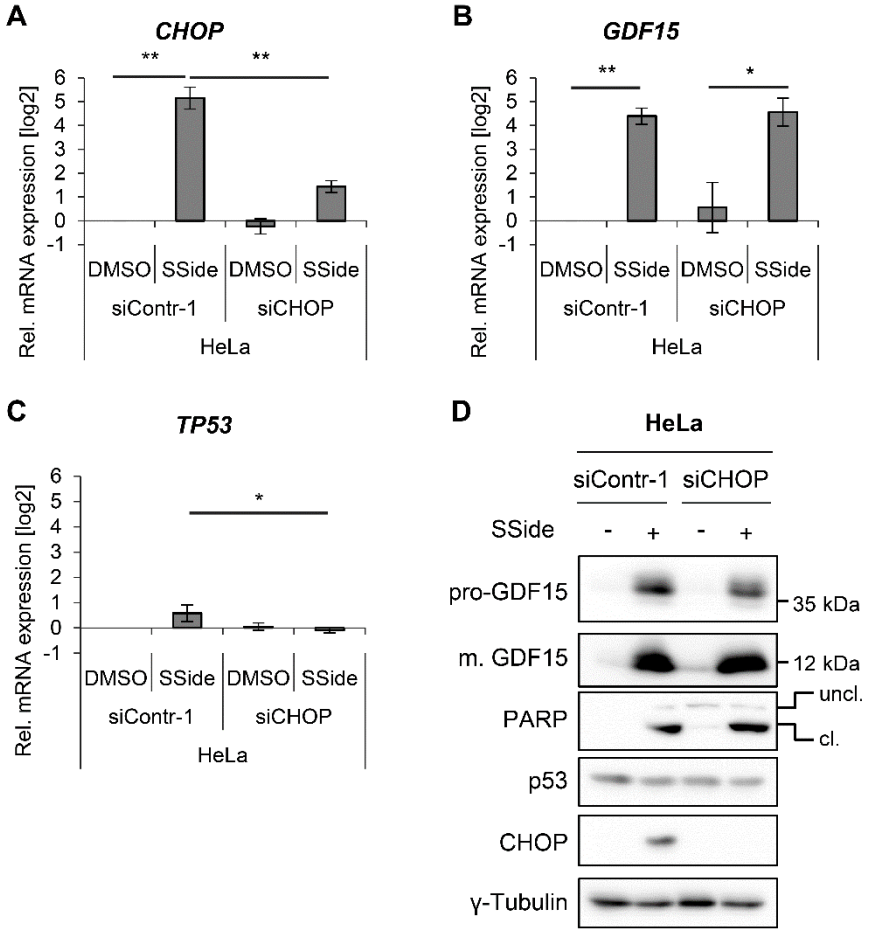

Figure 29 Activation of GDF15 expression by SSide is CHOP-independent. Firstly, HeLa cells were transfected either with a control siRNA (siContr-1) or with an siRNA pool targeting *CHOP* mRNA (siCHOP). Afterwards cells were treated with DMSO as solvent control or with 50 µM SSide in FCS-free medium 24h before harvest. (**A-C**) qRT-PCR analyses determining relative expression levels of *CHOP* (A), *GDF15* (B), and *TP53* mRNA (C). Depicted is the log2 of mean expression levels relative to siContr-1-transfected and DMSO-treated cells. Bars represent standard deviations. Asterisks indicate statistically significant differences between samples connected by crosslines as determined by two-sided *t*-test. *p ≤ 0.05, **p ≤ 0.01. (**D**) Immunoblot analyses of pro-GDF15, mature (m.) GDF15, PARP, p53, and CHOP expression. Uncleaved (uncl.), cleaved (cl.). γ-Tubulin, loading control.

Secondly, the role of p53 was examined. To this end, SSide was added to HeLa cells expressing p53 and to HeLa *"p53 null"* cells, which raised PARP cleavage and GDF15 expression in both cell lines (Figure 30A). However, the increase in GDF15 amounts was lower in HeLa *"p53 null"* than in parental HeLa cells (Figure 30A), suggesting a contribution of p53 to the SSide-induced upregulation of GDF15 expression in HeLa cells.

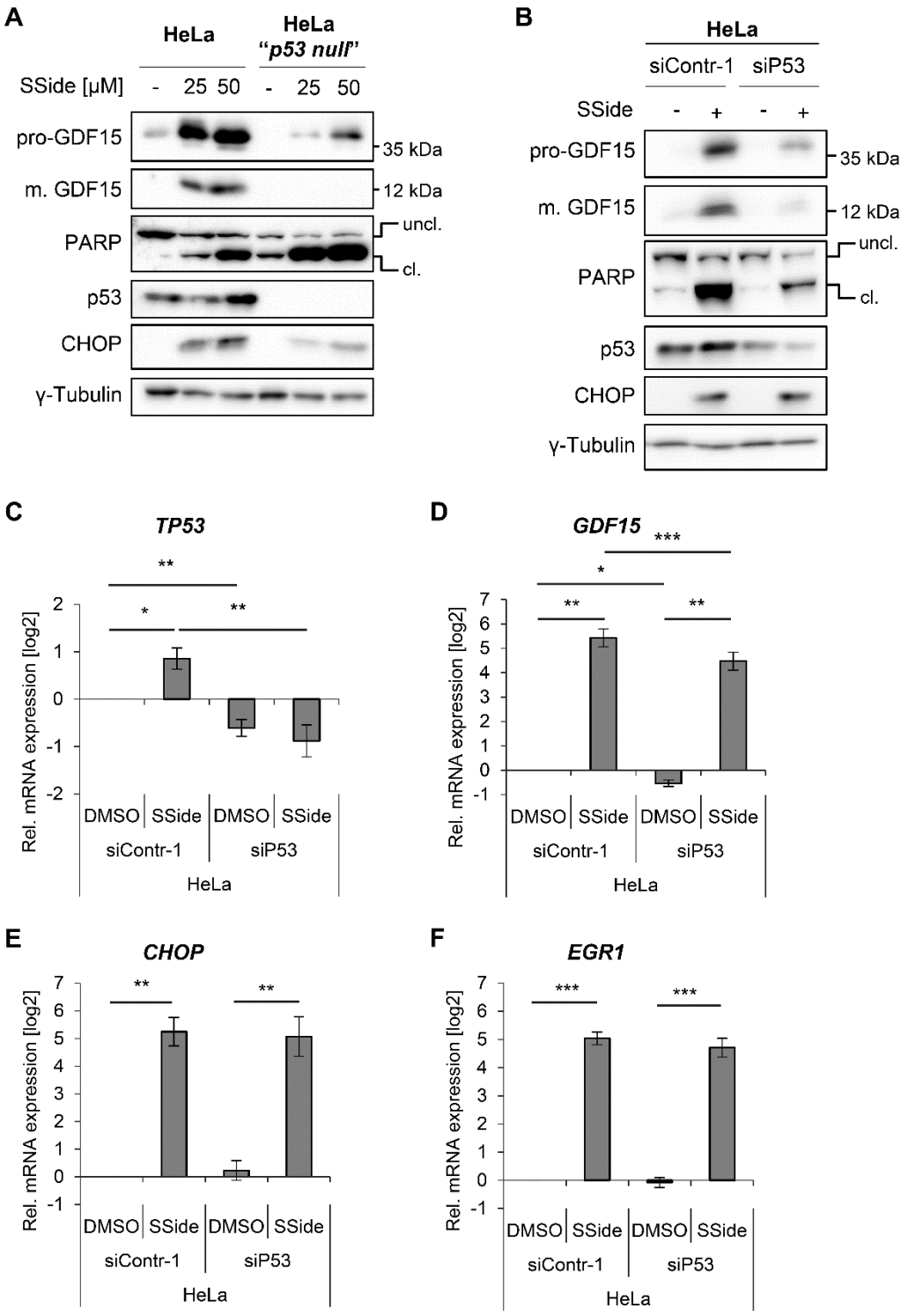

Figure 30 P53 contributes to the SSide-induced upregulation of GDF15. (**A**) HeLa and HeLa *"p53 null"* cells were treated with DMSO (solvent control) or SSide for 24h in FCS-free medium. Immunoblot analyses of pro-GDF15, mature (m.) GDF15, PARP, p53, and CHOP expression. Uncleaved (uncl.), cleaved (cl.). γ-Tubulin, loading control. (**B-F**) HeLa cells were transfected with either control siRNA (siContr-1) or siRNA targeting *TP53* mRNA and treated with DMSO or 50 µM SSide 24h prior to harvest. (B) Immunoblot analyses of pro-GDF15, mature (m.) GDF15, PARP, p53, and CHOP expression. Uncleaved (uncl.), cleaved (cl.). γ-Tubulin, loading control. (C-F) qRT-PCR analyses determining relative expression of *TP53* (C), *GDF15* (D), *CHOP* (E), and *EGR1* mRNA (F). Depicted is the log2 of mean expression levels relative to siContr-1-transfected and

DMSO-treated cells. Bars represent standard deviations. Asterisks indicate statistically significant differences between samples connected by crosslines as determined by two-sided *t*-test. *p ≤ 0.05, **p ≤ 0.01, ***p ≤ 0.001.

In a further approach, HeLa cells were transfected with either a control siRNA or an siRNA targeting *TP53* mRNA and subsequently treated with SSide. The activation of GDF15 expression by SSide was reduced after p53 knockdown (Figure 30B). Interestingly, decreased levels of p53 and GDF15 correlated with reduced PARP cleavage in HeLa cells after adding SSide. On transcriptional level, SSide stimulated slightly *TP53* (Figure 30C) and strongly *GDF15* (Figure 30D) mRNA expression in HeLa cells. On average, silencing of p53 attenuated the activation of *GDF15* mRNA levels by a factor of 2 (Figure 30D). The divergence between GDF15 protein (Figure 30B) and mRNA levels (Figure 30D) indicates that p53 could additionally stimulate GDF15 expression on protein level.

Whereas CHOP levels were similarly upregulated by SSide after transient p53 knockdown (Figure 30B and E), HeLa *"p53 null"* cells showed lower CHOP levels than parental HeLa cells (Figure 30A). This divergence could results from a lower cell number of HeLa *"p53 null"* cells after cultivation in FCS-free medium, which is linked to reduced CHOP expression (Figure 9B and E).

In addition, the role of the transcription factor EGR1 for the response of the *GDF15* gene towards SSide was investigated. This is based on studies of Baek *et al*., who identified binding sites for EGR1 in the *GDF15* promoter and reported that increased EGR1 amounts mediated the stimulation of GDF15 expression by SSide in HCT-116.[80] Indeed, *EGR1* mRNA levels were also elevated after treating HeLa cells with SSide (Figure 30F). This effect was not affected by silencing of *TP53*.

Altogether, these results suggest that p53 contributes to the SSide-induced upregulation of GDF15 expression in cervical cancer cells, while it is independent from CHOP. Additional factors could be involved such as EGR1, which is also increased by SSide treatment. Whether EGR1 is involved in GDF15 regulation of HPV-positive cells, awaits further exploration.

2.3.2.3. Knockout of *GDF15* protects HeLa cells against SSide treatment

The next interesting point is whether the downregulation of GDF15 by HPV E6 protects cervical cancer cells towards NSAID-induced apoptosis. A first hint in this direction was that GDF15 upregulation correlated with PARP cleavage after SSide treatment (Figure 26A-C). To this end, parental HeLa and three HeLa *GDF15* KO clones were treated with SSide and apoptosis rates were compared by three different methods.

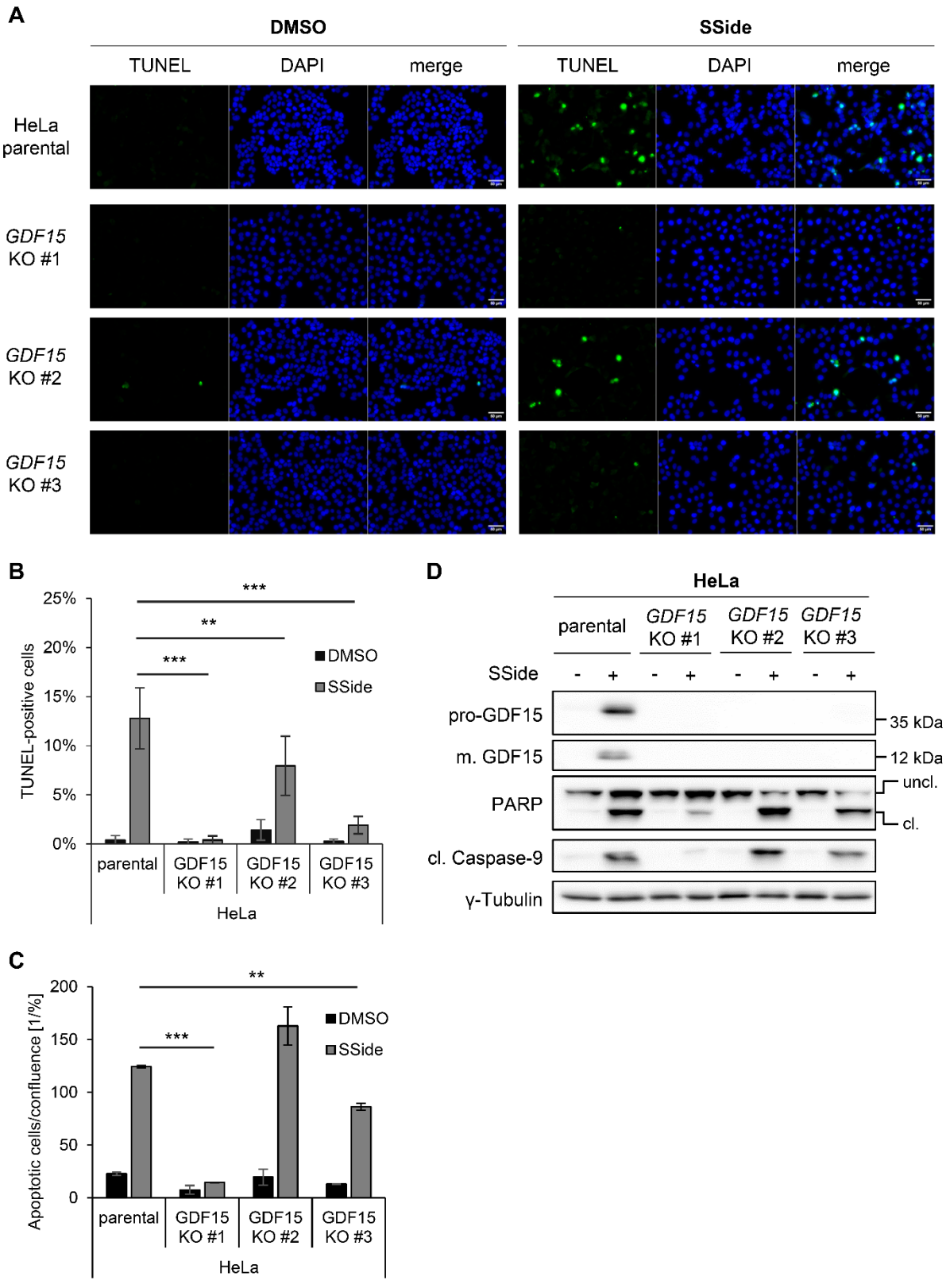

Figure 31 Downregulation of GDF15 can protect HeLa cells against SSide-induced apoptosis. Parental HeLa cells or HeLa *GDF15* KO clones #1-3 were treated with DMSO (solvent control) or with 50 µM SSide for 20h (A-C) or 36h (D) in FCS-free medium. (**A**) Representative images after TUNEL and DAPI staining (apoptotic cells: green; cell nuclei: blue). Scale bar: 50 µM. **(B**) Rel. quantification of TUNEL-positive cells on total cell number. Shown are means of at least five images per sample

gained from a representative replicate. Bars represent standard deviations. Asterisks indicate statistically significant differences between samples connected by crosslines as determined by two-sided *t*-test. **p ≤ 0.01, ***p ≤ 0.001. (**C**) Live cell imaging assay detecting activated Caspase-3/7 (IncuCyte). Apoptotic cells as determined by positive staining with IncuCyte Caspase-3/7 Green Reagent were normalized on cell confluence. Shown are means of two independent replicates at the time point where the number of green cells was half-maximal in the SSide-treated parental HeLa cells. Bars represent standard deviations. Asterisks indicate statistically significant differences between samples connected by crosslines as determined by two-sided *t*-test. **p ≤ 0.01, ***p ≤ 0.001. (**D**) Immunoblot analyses of pro-GDF15, mature (m.) GDF15, PARP, and cleaved Caspase-9 expression. Uncleaved (uncl.), cleaved (cl.). γ-Tubulin, loading control.

Comparison of parental HeLa with HeLa *GDF15* KO clones #1 and #3 indicates that HeLa cells are protected by *GDF15* knockout against SSide-induced apoptosis: HeLa *GDF15* KO clones #1 and #3 showed a lower percentage of TUNEL-positive (Figure 31A and B) or activated Caspase-3/7-stained cells (Figure 31C) after SSide treatment. Additionally, *GDF15* KO clone #1 presented less SSide-induced PARP and Caspase-9 cleavage in comparison to parental HeLa cells (Figure 31D). HeLa *GDF15* KO clone #2, however, behaved differently towards SSide treatment than the other two *GDF15* KO clones. Although, apoptosis rates of *GDF15* KO clone #2 were lower in TUNEL assays (Figure 31A and B), increased activity of Caspase-3/7 (Figure 31C) and similar levels of cleaved PARP and Caspase-9 (Figure 31D) were found in *GDF15* KO clone #2 compared to GDF15-expressing HeLa cells. This indicates that HeLa *GDF15* KO clone #2 has a similar apoptotic response towards SSide as parental HeLa cells.

Considering all results, the knockout of *GDF15* protects two out of three HeLa clones against SSide-induced apoptosis. This observation would be consistent with data from other tumor entities indicating that GDF15 is an important mediator in the pro-apoptotic response of cancer cells towards NSAID treatment.[62,153,175,176]

2.3.3. Downregulation of GDF15 expression can protect cervical cancer cells against cisplatin treatment

In the treatment of cervical carcinoma, chemotherapy with cisplatin plays a major role besides surgery and radiotherapy. It has been reported that GDF15 expression was upregulated after γ-irradiation and cisplatin treatment of human breast cancer cell lines.[123] Moreover, cisplatin is known to activate ER stress pathways.[166] Therefore, it is of clinical interest to analyze whether the repression of GDF15 can increase the resistance of HPV-positive cervical cancer cells against chemotherapy with cisplatin.

2.3.3.1. Induction of GDF15 levels by cisplatin is p53-dependent

Firstly, GDF15 expression after cisplatin treatment was studied in cervical cancer cells by immunoblotting. Secondly, it was investigated whether p53 and/or CHOP are mechanistically involved by CHOP knockdown experiment in cisplatin-treated HeLa and HeLa *"p53 null"* cells. Transcript levels were determined by qRT-PCR analyses.

GDF15 expression was strongly upregulated by cisplatin treatment of HeLa (Figure 32A) and MRI-H186 cells (Figure 32B), which correlated with an induction of PARP and Caspase-9 cleavage, indicating apoptosis. Treatment of HeLa cells with cisplatin also raised levels of secreted GDF15 as detected by immunoblotting of cell culture supernatants (Figure 32C). Especially the N-glycosylated form of GDF15 was detected after treatment (Figure 32). Furthermore, cisplatin repressed E7 levels, while it activated p53 expression and generated ER stress in both cell lines as indicated by increased BiP expression (Figure 32A and B).

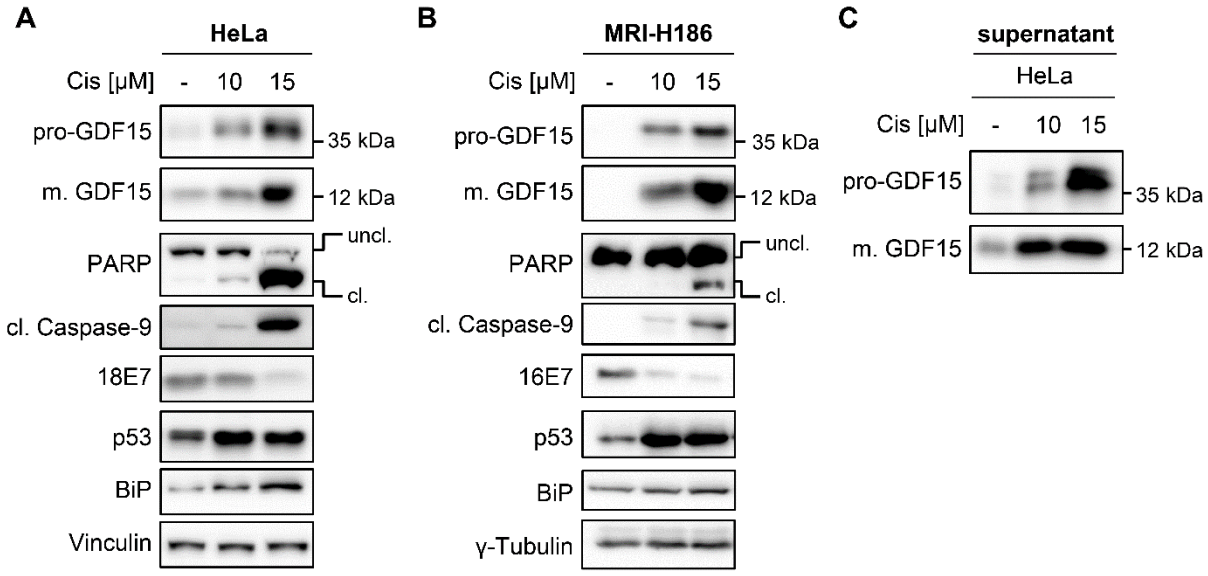

Figure 32 Cisplatin upregulates GDF15 levels in HeLa and MRI-H186 cells. Cells were treated with 10 µM or 15 µM cisplatin (Cis). Protein lysates and cell culture supernatant were collected 24h (HeLa) or 20h (MRI-H186) later. (**A, B**) Immunoblot analyses of pro-GDF15, mature (m.) GDF15, PARP, cleaved Caspase-9, E7, p53, and BiP expression in cell lysates of HeLa (A) and MRI-H186 cells (B). Uncleaved (uncl.), cleaved (cl.). Vinculin and γ-Tubulin are loading controls. (**B**) Immunoblot analysis of cell culture supernatants from HeLa cells detecting secreted pro-GDF15 and mature (m.) GDF15 levels. Loading volumes were normalized on amounts of total intracellular protein.

Since CHOP mediated the upregulation of GDF15 levels after TM- or TG-induced ER stress (Figure 23A and C), CHOP could have similar functions in the response towards cisplatin treatment. In control-transfected HeLa cells, CHOP mRNA (Figure 33A) and protein (Figure 33D) expression levels were downregulated by cisplatin. Silencing of CHOP did not impair the upregulation of *GDF15* mRNA (Figure 33B) and protein levels nor PARP and Caspase-9 cleavage (Figure 33D) in cisplatin-treated cells. Whereas the CHOP knockdown did not alter

TP53 mRNA expression (Figure 33C), it lowered the increase of p53 protein levels after cisplatin treatment of HeLa cells (Figure 33D).

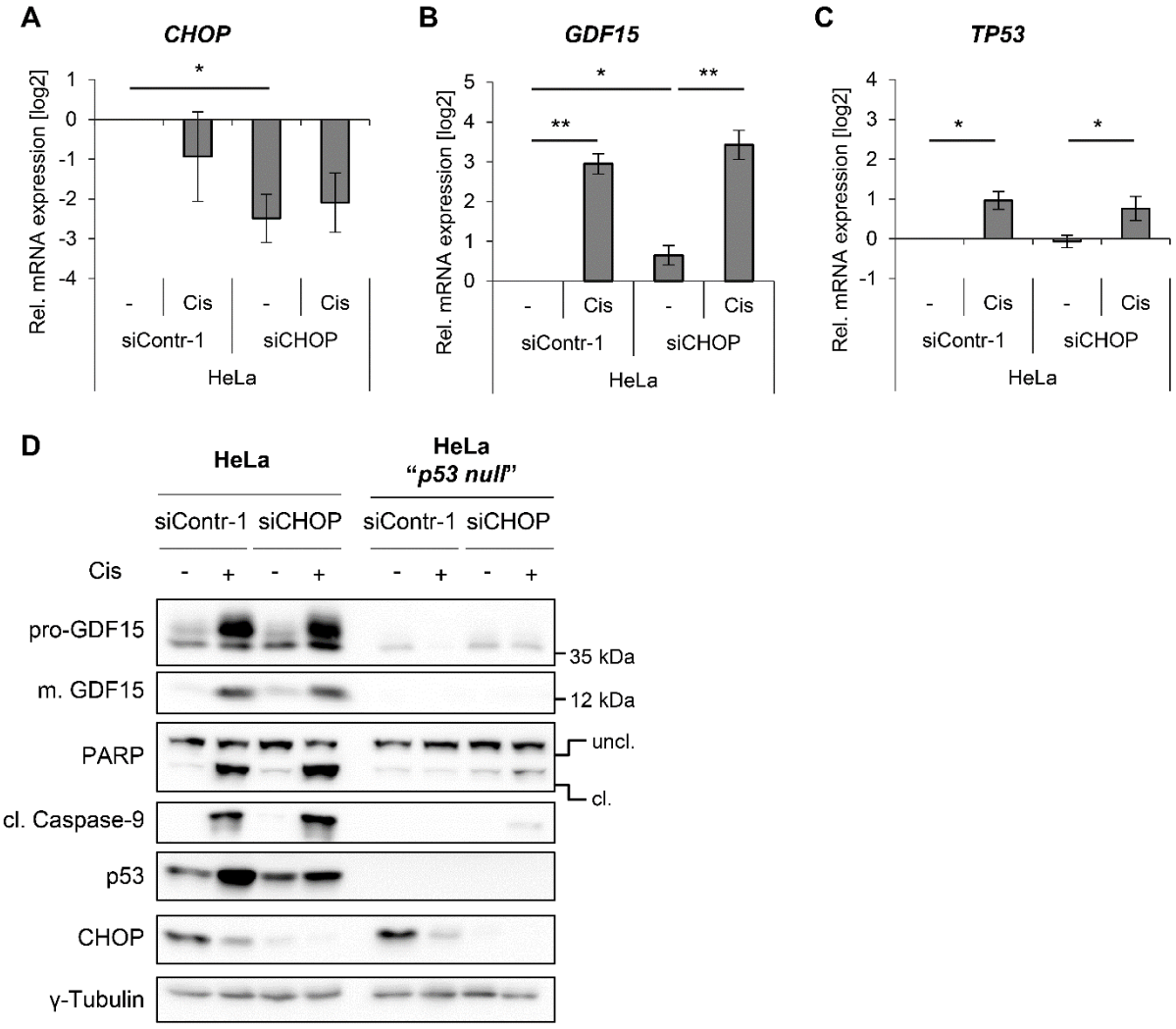

Figure 33 P53 mediates the upregulation of GDF15 levels in cisplatin-treated HeLa cells. HeLa or HeLa *"p53 null"* cells were transfected either with control siRNA (siContr-1) or with an siRNA pool targeting *CHOP* mRNA expression (siCHOP) and were treated with 10 µM cisplatin 24h before harvest. (**A-C**) qRT-PCR analyses determining relative expression of *CHOP* (A), *GDF15* (B), and *TP53* mRNA (C) in HeLa cells. Depicted is the log2 of mean expression levels relative to untreated, siContr-1-transfected cells. Bars represent standard deviations. Asterisks indicate statistically significant differences between samples connected by crosslines as determined by two-sided *t*-test. *p ≤ 0.05, **p ≤ 0.01. (D) Immunoblot analyses of pro-GDF15, mature (m.) GDF15, PARP, cleaved Caspase-9, p53, and CHOP expression in HeLa and HeLa *"p53 null"* cells. Uncleaved (uncl.), cleaved (cl.). γ-Tubulin, loading control.

To further analyze the function of p53, HeLa *"p53 null"* cells were also treated with cisplatin. No appreciable cleavage of PARP and Caspase-9 was observed and the stimulation of GDF15 levels by cisplatin was completely suppressed in cisplatin-treated HeLa *"p53 null"* (Figure 33D). These findings provide evidence that the upregulation of GDF15 expression by cisplatin treatment is critically dependent on p53. Moreover, the increasing GDF15 levels could be

involved in cisplatin-induced apoptosis of HeLa cells, since PARP and Caspase-9 cleavage correlated with GDF15 expression.

2.3.3.2. Transient silencing of GDF15 expression affects the sensitivity of cervical cancer cells against cisplatin treatment

To investigate the functional role of GDF15 for cisplatin-induced apoptosis, GDF15 expression was transiently suppressed in cisplatin-treated cervical cancer cells lines and apoptosis rates were measured.

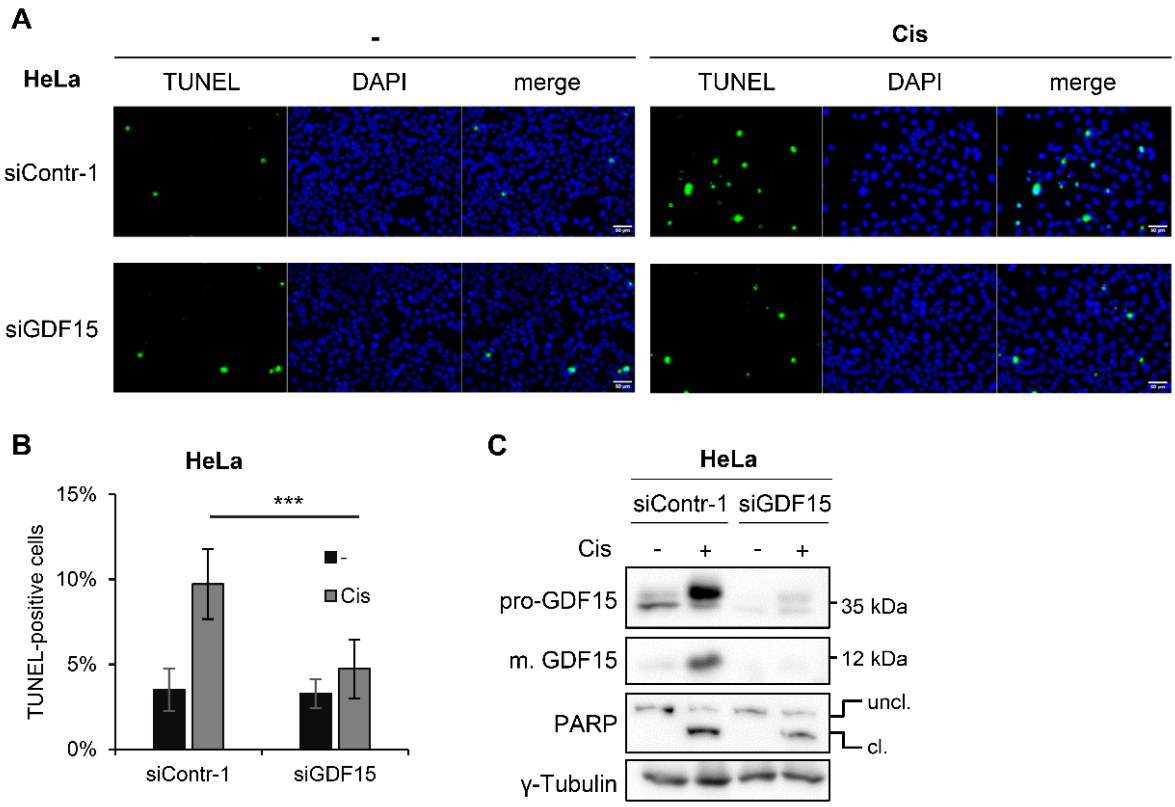

Figure 34 Transient repression of GDF15 levels reduces cisplatin-induced apoptosis of HeLa cells. HeLa cells were transfected either with control siRNA (siContr-1) or with an siRNA pool targeting *GDF15* mRNA (siGDF15) and were treated with 15 µM cisplatin (Cis) for 20h. (**A**) Representative images after TUNEL and DAPI staining (apoptotic cells: green; cell nuclei: blue). Scale bar: 50 µM. **(B**) Rel. quantification of TUNEL-positive cells on total cell number. Shown are means of at least five images per sample from a representative replicate. Bars represent standard deviations. Asterisks indicate statistically significant differences between samples connected by a crossline as determined by two-sided *t*-test. ***p ≤ 0.001. (**C**) Immunoblot analyses of pro-GDF15, mature (m.) GDF15, and PARP expression. Uncleaved (uncl.), cleaved (cl.). γ-Tubulin, loading control.

In HeLa cells, GDF15 knockdown by RNAi reduced the number of TUNEL-positive cells (Figure 34A and B) and PARP cleavage (Figure 34C) after cisplatin treatment. These results support the notion that GDF15 downregulation protects HeLa cells against cisplatin-stimulated apoptosis.

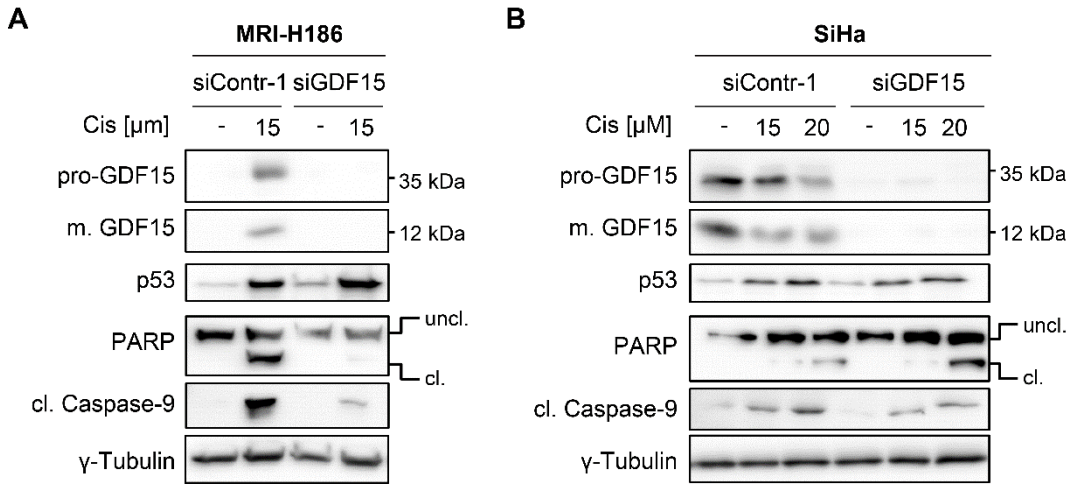

Figure 35 GDF15 knockdown has divergent effects on the response of MRI-H186 and SiHa cells towards cisplatin treatment. Cells were transfected with either a control siRNA (siContr-1) or an siRNA pool targeting *GDF15* mRNA (siGDF15). Subsequently, they were treated with 15 µM or 20 µM cisplatin (Cis) for 20h (MRI-H186) or 28h (SiHa). Immunoblot analyses of pro-GDF15, mature (m.) GDF15, p53, PARP, and cleaved Caspase-9 expression. Uncleaved (uncl.), cleaved (cl.). γ-Tubulin, loading control.

Similar to HeLa cells, GDF15 and apoptosis levels were strongly increased in MRI-H186 cells after adding 15 µM cisplatin, as indicated by cleaved PARP and Caspase-9 (Figure 35A). Repression of GDF15 during cisplatin treatment also decreased cleavage of PARP and Caspase-9 in these cells (Figure 35A). In contrast, cisplatin treatment, however, did not induce GDF15 expression in SiHa cells, although p53 levels were still upregulated by the treatment (Figure 35B). Another difference was that cisplatin promoted the N-glycosylation of pro-GDF15 in only half of the analyses of SiHa cells. GDF15 downregulation hardly affected Caspase-9 cleavage and, in some experiments, even increased cleaved PARP levels in cisplatin-treated SiHa cells (Figure 35B).

Thus, for both HPV18-positive HeLa and HPV-16-positive MRI-H186 cells, GDF15 appears to be a major mediator of cisplatin-induced apoptosis. However, the data obtained for SiHa cells suggest that this regulatory principle is not necessarily shared by all HPV-positive cancer cells.

2.3.3.3. *GDF15* KO protects HeLa cells against cisplatin treatment

To further corroborate the decisive role of GDF15 for cisplatin-induced apoptosis in cervical cancer cells, HeLa cells were compared with HeLa *GDF15* KO cells after cisplatin treatment. Consistent with findings from transient transfection experiments (Figure 34), the knockout of *GDF15* protected HeLa cells against cisplatin treatment. The number of TUNEL-positive cells after cisplatin treatment was strongly decreased in HeLa *GDF15* KO clones #1-3 in comparison to parental HeLa cells (Figure 36A and B). All three *GDF15* KO clones also presented lower

levels of PARP and Caspase-9 cleavage (Figure 36C) and reduced apoptosis rates in live cell imaging experiments visualizing Caspase activation (Figure 36D) after cisplatin treatment.

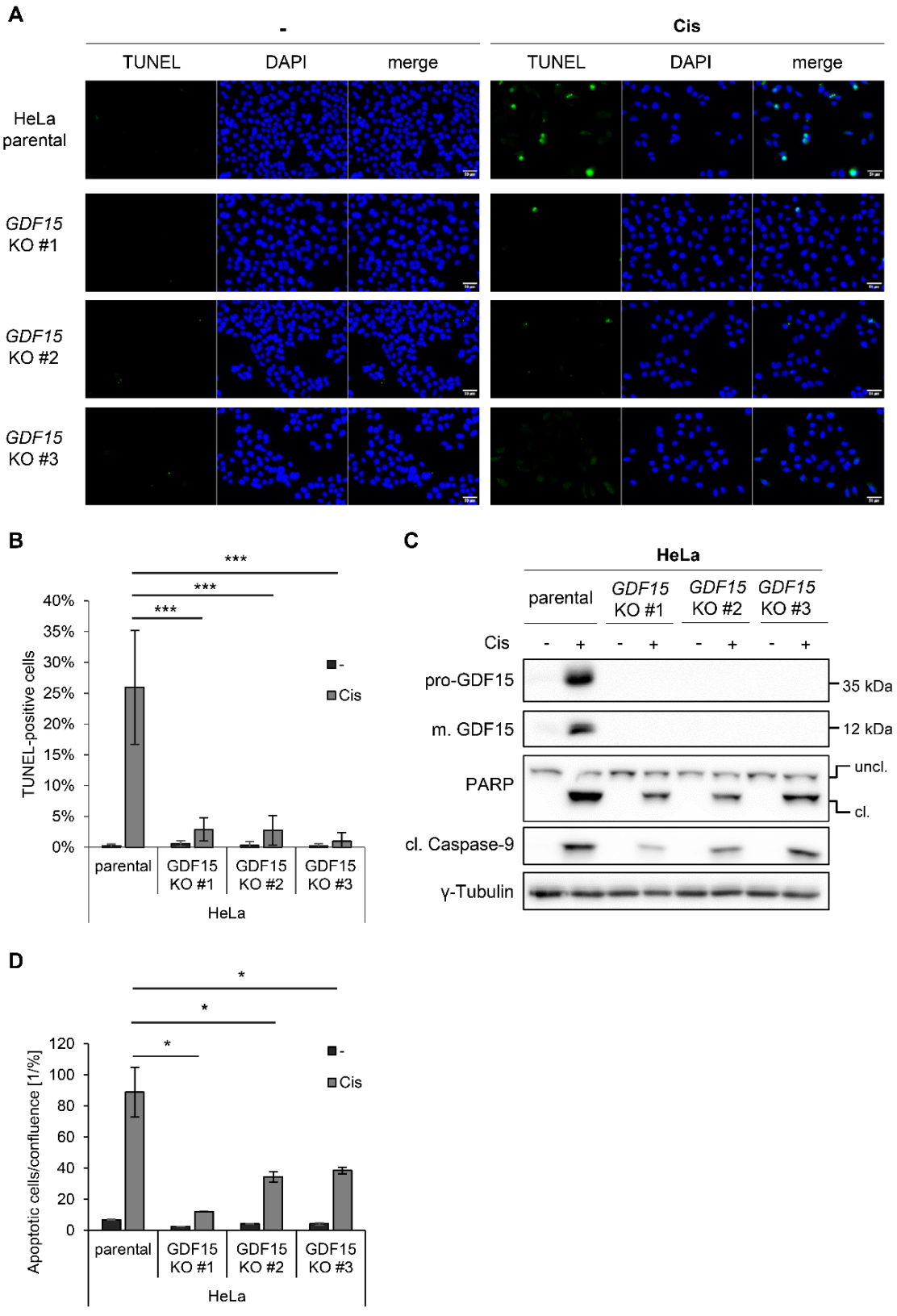

Figure 36 Knockout of *GDF15* protects HeLa cells against cisplatin-induced apoptosis. Parental HeLa or HeLa *GDF15* KO clones #1-3 were treated with 15 µM cisplatin (Cis) for 20h (A, B, and D) or

for 16h (C). (**A**) Representative images after TUNEL and DAPI staining (apoptotic cells: green; cell nuclei: blue). Scale bar: 50 µM. **(B**) Rel. quantification of TUNEL-positive cells on total cell number. Shown are means of at least five images per sample from a representative replicate. Bars represent standard deviations. Asterisks indicate statistically significant differences between samples connected by crosslines as determined by two-sided *t*-test. ***p ≤ 0.001. (**C**) Immunoblot analyses of pro-GDF15, mature (m.) GDF15, PARP, and cleaved Caspase-9 expression. Uncleaved (uncl.), cleaved (cl.). γ-Tubulin, loading control. (**D**) Live cell imaging assay detecting activated Caspase-3/7 (IncuCyte). Apoptotic cells as determined by positive staining with IncuCyte Caspase-3/7 Green Reagent were normalized on cell confluence. Shown are means of two independent replicates at the time point where the number of green cells was half-maximal in the cisplatin-treated parental HeLa cell line. Bars represent standard deviations. Asterisks indicate statistically significant differences between samples connected by crosslines as determined by two-sided *t*-test. *p ≤ 0.05.

Overall, these data show that GDF15 can be a major promoter of the pro-apoptotic effects in cisplatin-treated HPV-positive cancer cells. The ability of the viral E6 oncoprotein to reduce GDF15 expression thus contributes to the chemotherapeutic resistance of HPV-positive cancer cells.

Chapter 3

Discussion

3. Discussion

HPV-linked cancer cells rely on the *E6*/*E7* expression of high-risk HPV types in order to fulfil the six hallmarks of cancer: sustained proliferation, growth suppressor evasion, tissue invasion and metastasis, infinite replicative potential, neo-angiogenesis, and resistance against cell death.[177] To this end, the viral oncoproteins dysregulate numerous host cell pathways, which have not yet been completely illuminated. The identification of novel target genes and characterization of phenotypic consequences can contribute to a better understanding of cervical carcinogenesis. The gained insights may reveal new strategies to prevent and treat cervical carcinomas. The present thesis exhibited that the stress response gene *GDF15* is downregulated by oncogenic HPVs. Key regulators of basal and stress-activated GDF15 expression in cervical cancer cells were identified. It was also revealed that HPV-positive cervical cancer cells are more resistant towards apoptotic stress induced by different drugs via *GDF15* repression.

3.1. GDF15 expression in cervical cancer cells

3.1.1. *GDF15* as a novel target gene of oncogenic HPVs

E6/*E7* knockdown experiments showed that GDF15 was strongly upregulated both at the mRNA and protein level after repressing E6 or E6/E7 in HPV16- and HPV18 positive cancer cell lines as well as an HPV16-immortalized keratinocyte cell line. Moreover, levels of secreted GDF15 were also elevated after silencing E6 or E6/E7. These results imply that E6 represses GDF15 expression in HPV-positive cells. This hypothesis is in line with the transcriptome data from Kuner *et al*.[60] and is further supported by following microarray analyses, which used different cell lines and/or had alternative approaches to alter E6/E7 expression. For instance, Kelley and colleagues reported that *GDF15* transcript levels were upregulated after silencing E6 in HeLa, Caski, or SiHa cells.[178] Additionally, *GDF15* mRNA expression was increased after re-introducing HPV18 E2 into HeLa cells, which also downregulates E6/E7 expression.[179] *Vice versa*, transfection of HPV16 *E6/E7* DNA into foreskin led to decreased *GDF15* transcript levels.[180] Remarkably, mere expression of HPV16 E6 diminished *GDF15* mRNA levels in cervical keratinocytes, whereas HPV16 E7 did not appreciably modulate them,[181] which further corroborates that GDF15 expression is inhibited by E6 and not by E7.

Mechanistically, the increase in GDF15 levels after E6 knockdown observed in the present studies was likely dependent on the reconstitution of p53 because the effect on GDF15 expression was abolished in HeLa *"p53 null"* cells. The role of p53 as a key transcriptional regulator of GDF15 expression was further supported by the result that silencing of p53 reduced basal GDF15 mRNA and protein levels in HPV-positive cancer cells. Interestingly,

downregulation of E6AP by RNAi also upregulated *GDF15* expression in HPV18- and HPV16-positive cervical cancer cell lines.[178] This report complements the findings of the present work because E6 inhibits p53 by recruiting the ubiquitin ligase E6AP to p53, which is subsequently marked for proteasomal degradation.[42] Altogether, these results indicate that E6 represses GDF15 expression by mediating the degradation of its transcription activator p53.

Since CHOP was previously identified as another positive key regulator of GDF15 expression apart from p53,[77] the effects of CHOP were also analyzed in more detail. In the present work, it was found that CHOP does not function as a transcriptional activator of basal GDF15 expression in cervical cancer cells. GDF15 levels were either not appreciably affected or slightly increased (< twofold) by CHOP silencing in the absence of stress. In order to negatively affect basal GDF15 expression, CHOP might inhibit C/EBPβ,[135,183] which is another transcription activator of the *GDF15* promoter.[79]

Interestingly, the performed E6/E7 knockdown experiments of this thesis suggest that *CHOP* itself may represent a hitherto unreported target gene for E6/E7. After silencing E6/E7 (and to some extent E6 alone), CHOP mRNA and protein expression was downregulated in HPV-positive cell lines. These observations indicate that E6/E7 induce the expression of CHOP. Mechanistically, the HPV oncoproteins possibly stimulate UPR signaling pathways and thereby CHOP levels as reported for other oncoproteins. Expression of H-ras G12V or K-ras G12D mutant, for example, activated CHOP expression via PERK signaling in human melanocytes, rat fibroblasts, or murine lung cell.[183,184] Additionally, E6/E7 could increase CHOP expression on the protein level by blocking the enzymatic activity of p300, since acetylation of CHOP by p300 promotes its proteasomal degradation.[185–187]

Unexpectedly, the present work revealed that GDF15 mRNA and protein levels were decreased after E6/E7 knockdown in HeLa *"p53 null"* cells, pointing to a positive effect of E6/E7 on GDF15 expression in this particular cellular background. A possible explanation for this observation is that CHOP compensates for the missing p53 expression and therefore has an activating impact on GDF15 levels in HeLa *"p53 null"*. In summary, these findings point out that CHOP has a subordinate role to p53 in regulating basal GDF15 expression of HPV-positive cancer cells. *Vice versa,* GDF15 probably does not influence the expression of the HPV oncoproteins, p53, or CHOP as analyzed by GDF15 overexpression, knockdown, and knockout experiments.

Interestingly, cervical cancer cells exhibited a cell line-dependent expression pattern of GDF15 pro-forms. The major levels of pro-GDF15 in MRI-H186 cells were N-glycosylated whereas the non-glycosylated pro-form was predominant in SiHa cells. HeLa cells showed both pro-GDF15 forms, but the knockdown of E6/E7 caused a shift towards the N-glycosylated pro-GDF15 form. This indicates that E7 or E6/E7 might inhibit the N-glycosylation of pro-GDF15 in HeLa cells. The band pattern of extracellular pro-GDF15 featured additional bands, which suggests that

pro-GDF15 is further modified during the secretion process or extracellularly. A potential mechanism for this effect could be that complex N-linked oligosaccharide chain of pro-GDF15 are altered by glycosyltransferases or glycosidases while passing the Golgi apparatus during secretion.[91,188] Pro-GDF15 might alternatively represent a target for extracellular proteases like matrix metalloproteinases as it was shown for mature GDF15 by Abd El-Aziz.[189]

To sum up, these results support the notion that GDF15 expression is repressed in HPV-positive cells, predominantly via E6-mediated degradation of p53.

3.1.2. Glucose deprivation upregulates GDF15 expression via p53 and CHOP

In this thesis, increased GDF15 mRNA and protein levels were also detected under cell culture conditions in which nutrient supply was depleted in cervical cancer cells, e.g. after prolonged cell cultivation. In closer analyses of medium components, glucose deprivation strongly upregulated *GDF15* expression, while the lack of FCS barely affected it. In support of the former findings, the literature reveals that glucose deprivation is very common in tumor tissues and also induces GDF15 expression in various other cell types.[74,190,191] The supply of oxygen and essential amino acids like lysine or methionine can be limiting for the proliferation of cancer cells as well.[192–194] Both hypoxia and lysine or methionine-deficient diets have also been reported to induce GDF15 expression.[71,74,195]

CHOP knockdown experiments performed in this thesis suggest that the rise in GDF15 levels after glucose deprivation is due to increased CHOP expression in cervical cancer cells. Previously, it was shown by using rat fibroblasts or HeLa cells that ER stress pathways mediate this CHOP upregulation.[184,196] P53 silencing studies of the present work strongly imply that p53 increases GDF15 levels after glucose deprivation besides CHOP. However, p53 levels were not appreciably modulated after glucose deprivation in cervical cancer cells, pointing out that alterations in p53 activity could account for this result instead of increased p53 expression levels. In line with this, Kelly and colleagues have reported that p53 stimulates GDF15 expression in prostate cancer cells in relation to their cell density.[122] In addition, activating posttranslational modifications of p53 have been shown to be important in this context, since restricted glucose supply arrested the cell cycle of lung cancer cells upon the phosphorylation of p53 at Ser15.[197] Glucose deprivation also promoted the phosphorylation of the Ser46 residue in p53 in osteosarcoma cells, leading to their cell death.[198] *Vice versa*, high glucose level inhibited this p53 phosphorylation in colorectal and lung cancer cells.[199]

In summary, glucose deprivation can increase CHOP expression and p53 activity and thereby upregulates GDF15 levels in HPV-positive cancer cells.

3.1.3. Regulation of intra- and extracellular GDF15 levels by TM- or TG-induced ER stress

Some chemotherapeutic drugs like TM or TG can generate unresolvable, excessive ER stress, which leads to the induction of apoptosis.[131] As previously shown for a spectrum of different tumor cell lines and murine hepatocytes,[74,77,200] both GDF15 mRNA and protein levels were found in the present study to be upregulated by TM or TG treatment in HeLa or SiHa cells. There is strong evidence in cancer and non-cancerous cells from human or murine origin that ER stress induces GDF15 expression via CHOP, which can be inhibited by interrupting the PERK signaling pathway at different regulatory interfaces upstream of CHOP.[74,77,78,111,195,200] Accordingly, CHOP knockdown studies of this thesis revealed that increasing CHOP levels led to the raised GDF15 protein levels in TM- or TG-treated HeLa cells. Notably, CHOP silencing by RNAi decreased *GDF15* mRNA levels only after exposure to TG, but not after adding TM. This discrepancy between mRNA and protein levels suggests that CHOP may affect GDF15 expression by additional means than by directly regulating transcription, potentially dependent on the nature of the stress-inducing agent. From the literature, CHOP is known to promote protein synthesis in general after ER stress by transcriptional activation of *GADD34* (growth arrest and DNA damage-inducible protein 34) and subsequent dephosphorylation of eIF2α.[201,202] As another feasible mechanism, CHOP might increase GDF15 translation specifically by inhibiting the expression of microRNAs (miRs) which target *GDF15* mRNA. For example, CHOP was shown to modulate rhodopsin expression during ER stress via miR-708.[203] It is also known that GDF15 translation can be regulated by miRs since miR-132, miR-873, and miR-1233 have been identified to downregulate GDF15 protein expression.[204,205] This thesis shows that the levels of p53 were elevated after prolonged TM or TG treatment of cervical cancer cells, as the literature reported for other cell types as well.[195,206,207] However, p53 might not be essential for this increase in GDF15 expression because ER stress also raised GDF15 levels in colorectal and cervical cancer cells expressing no or extremely low levels of p53, respectively. The literature supports these findings of the present study. For example, TM stimulated p53 expression via NF-κB (nuclear factor "kappa-light-chain-enhancer" of activated B-cells) signaling in breast cancer cells.[207] Similarly to TG and TM treatment, a methionine-choline-deficient diet can increase ER stress, p53, and GDF15 levels in mice, whereas inhibition of p53 did not significantly affect the induction of GDF15 in this model system.[195]

Interestingly, both TM and TG reduced the amounts of secreted GDF15, while they raise intracellular GDF15 mRNA and protein levels in the present study. This indicates that TM and TG disturb GDF15 secretion. TM may partly inhibit GDF15 secretion, since it blocks the first step of N-glycosylation. In line with this hypothesis lower amounts of the GDF15

N-glycosylation mutant N70A could be detected extracellularly in comparison to GDF15 wildtype despite being equally expressed. In further support of this notion, Fairlie and colleagues found another GDF15 N-glycosylation mutant (N70S) to be secreted less.[88] These results imply that N-glycosylation is in fact not essential for, but promotes the secretion of GDF15.

Altogether, these results indicate that ER stress signaling mediates the TM- or TG-induced upregulation of GDF15 protein expression in cervical as well as in other cancer cells via CHOP. Furthermore, GDF15 secretion can be promoted by N-glycosylating of its propeptide part.

3.1.4. P53 is involved in the upregulation of GDF15 by SSide

NSAIDs are also known to stimulate pro-apoptotic ER stress signaling pathways.[138,139] In cervical cancer cells, the NSAIDs sulindac, aspirin, and celecoxib have been described to cause apoptosis.[173,208–217] The present work reveals that the active metabolite of sulindac, SSide, also induces PARP cleavage as well as GDF15 mRNA and protein levels in HPV18- and HPV16-positive cancer cells, even though amounts of secreted GDF15 were not altered by the treatment. Other researchers showed that SSide strongly activates GDF15 expression and apoptosis in colorectal and ovarian cancer cells as well.[62,176,218] Importantly, the present thesis exhibits that the downregulation of p53 decreased GDF15 induction in SSide-treated HeLa cells, indicating a key role for p53 in this context. In contrast, CHOP seemed not to be involved in the upregulation of GDF15 expression as indicated by knockdown experiments, although SSide treatment increased CHOP amounts in cervical cancer cells. These findings are supported by the literature because p53 is also described to mediate GDF15 expression and apoptosis after diclofenac treatment of oral cavity and breast cancer cells.[219,220]

The significance of p53 for the rise of GDF15 levels after SSide treatment does, however, not exclude that additional factors could be involved. Possible candidates include the UPR signaling molecule ATF3, which can promote the transactivation activity of C/EBPβ on the *GDF15* promoter.[79] EGR1 represents another potentially interesting transcription factor in this context because EGR1 stimulated the *GDF15* promoter in SSide-treated colorectal cancer cells.[80] In experiments of this thesis, *EGR1* mRNA levels were also upregulated by SSide in cervical cancer cells. Notably, the mechanisms behind SSide-activated GDF15 expression can be cell type-dependent because different regulatory factors were found to be important in this context for colorectal than for cervical cancer cells. In the literature, PERK signaling and CHOP, but not p53 are reported to increase GDF15 levels in SSide-treated HCT-116 cells.[111,221]

These results indicate that p53 is an important mediator for increased GDF15 expression in SSide-treated cervical cancer cells, whereas CHOP-dependent pathways are not involved.

3.1.5. Cisplatin induces GDF15 expression via p53

Cisplatin is used in the treatment of cervical cancer patients besides surgery or irradiation because cisplatin can induce apoptosis in cancer cells by generating excessive DNA damage and ER stress.[166,222,223] Interestingly, it was found in the present study that cisplatin treatment not only stimulated apoptosis in HeLa and MRI-H186 cells, but also increased GDF15 mRNA as well as intracellular and secreted GDF15 protein levels in a dose-dependent manner. In support of these results, cisplatin treatment also raised GDF15 blood serum levels in mice and humans as well as intracellular GDF15 expression in diverse other cancer cell types.[90,123,224–226] RNAi analyses of the present thesis indicate that p53 mediates this upregulation of GDF15 expression, which is in line with similar findings reported for cisplatin-treated embryonal carcinoma cells.[225] In the present study, CHOP expression was decreased and not involved in cisplatin-induced GDF15 expression, although other studies showed that CHOP expression in HeLa and OV-2008 cells is increased by cisplatin treatment at earlier time points or after drug release.[223,227,228] Since increased BiP levels pointed towards ER stress after cisplatin treatment of cervical cancer cells in the present work, CHOP-independent ER stress signaling could be involved. ATF3 represents a promising candidate here because ATF3 expression was shown both to be upregulated in cisplatin-treated cancer cells and to stimulate *GDF15* expression.[229,230] Additionally, ATF3 can interfere in the E6-mediated degradation of p53 in HPV16-positive cancer cells.[231]

In contrast to CHOP, it is very likely that p53 is essential for the induction of GDF15 and apoptosis levels in cancer cells after cisplatin treatment.

Table 1 P53 and CHOP are key regulators of GDF15 expression in HPV-positive cervical cancer cells ("-": probably not involved; "+": involved; ?: unclear).

Involvement of		p53	CHOP
Regulation of GDF15 expression	after E6 knockdown	+	-
	after E6/E7 knockdown	+	?
	regarding basal levels	+	-
	during glucose deprivation	+	+
	after TM/TG treatment	-	+
	after SSide treatment	+	-
	after cisplatin treatment	+	-

In conclusion, the results of this thesis show that both p53 and CHOP can activate GDF15 expression in HPV-positive cancer cells, but their significance depends on the context. Whereas p53 predominately affects basal GDF15 expression levels, p53 and/or CHOP individually contribute to the induction of GDF15 expression in stress responses (Table 1).

3.2. Phenotypic effects of GDF15 downregulation in HPV-positive cervical cancer cells

Both pro- and anti-tumorigenic functions have been reported for GDF15 (chapter 1.2.3.2). Furthermore, GDF15 can promote apoptosis after treating cancer cells with various anti-tumorigenic drugs.[127] Hence, the effects of GDF15 on proliferation and response to pro-apoptotic drugs were analyzed in cervical cancer cells in order to elucidate possible phenotypic consequences of the HPV-mediated downregulation of GDF15 expression.

3.2.1. Effects of GDF15 on proliferation of cervical cancer cells

The link between GDF15 and the proliferation control of cervical cancer cells turned out to be complex and could be dependent on several factors, such as GDF15 expression levels or the analyzed timescale. In the present work, GDF15 was found to be dispensable for the proliferation of HPV-positive cancer cells in following experiments: transient silencing of GDF15 expression by RNAi had no effect in live cell imaging analyses, and four out of six *GDF15* KO clones did also not differ in their proliferation rate from their parental cells. Accordingly, GDF15 knockdown did not modulate the cell cycle profile of HeLa cells. However, these *in vitro* results do not exclude that GDF15 expression can influence tumor growth of cervical cancer cells *in vivo*. For example, Hegyesi *et al.* showed that GDF15 knockdown by RNAi did not significantly affect the proliferation of the breast cancer cell line LM2 *in vitro*, but distinctly repressed tumor growth *in vivo* after cell injection into nude mice.[232]

Interestingly, ectopic GDF15 overexpression strongly decreased the colony formation capability of cervical and colorectal cancer cells, which indicates that very high GDF15 levels inhibit their proliferation. This effect could be due to the notion that strongly elevated GDF15 levels function pro-apoptotic in cervical cancer cells, as it was observed in the present investigations after TM, SSide, or cisplatin treatment. Likewise, GDF15 overexpression or TM- or SSide-mediated upregulation of GDF15 expression led to the induction of apoptosis in HCT-116 cells.[62,77,233]

Interestingly, not only GDF15 overexpression, but also the knockdown of GDF15 reduced the colony formation capability of HeLa, SiHa, MRI-H186, and HCT-116 cells. This implies that too low or too high GDF15 levels might be detrimental for the cell proliferation of cervical and colorectal cancer cells. These latter observations diverge from the results of live cell imaging experiments in which transient downregulation of GDF15 did not affect proliferation of HeLa and SiHa cells. In this context, it is important to consider that the colony formation capability is dependent on several cellular features and thereby not a mere indicator for proliferation. For example, the reduced colony formation capability could be a result of decreased plating efficiency.

The found difference does likely not stem from using HygB as selection agent in CFAs, since control and GDF15 knockdown cells proliferated similarly in live cell imaging experiments after treatment with sublethal doses of HygB or other genotoxic agents. Alternatively, GDF15 downregulation might reduce proliferation of cervical cancer cells only in the long run because the analyzed timescale was 2-4x longer in CFAs (1.5-3 weeks) than in live cell imaging experiments (5 days). However, this is not supported by the findings that four established *GDF15* KO clones had similar proliferation rates as their parental cell lines.

In contrast to the results of this study, Li *et al.* reported that high GDF15 expression levels promote the proliferation of cervical cancer cells and that GDF15 has pro-tumorigenic actions like activating ERK1/2 and PI3K (phosphatidylinositol-4,5-bisphosphate 3-kinase)/AKT signaling pathways.[234] For their analyses, they used recombinant GDF15 preparations. A major problem with these preparations is that they are potentially contaminated with other bioactive substances,[104] and co-treatment experiments with anti-GDF15 antibodies to assess specificity have not been performed. Further, they blocked endogenous GDF15 expression only in HT-3 cells. However, HT-3 is a cell line which is not a good cell model for cervical cancer cells because HT-3 cells are HPV30-positive and have mutated *TP53* and *RB* genes.[235,236] The prevalence of the "possibly carcinogenic" HPV30 type with 0.2% is very low and both *TP53* and *RB* are typically not mutated in cervical carcinomas.[48,237] In addition, much higher GDF15 levels were detected in HT-3 cells than in HPV16- or HPV18-positive cervical cancer cell lines.[234] In contrast to the work of Li *et al.*, the effects of endogenous GDF15 levels were analyzed in the present thesis by performing experiments with cervical cancer cell lines which show typical features of cervical carcinomas. Here, the used cell lines are either positive for HPV16 or HPV18, which are the most common HPV types in cervical tumors,[48] and have intact *TP53* and *RB* genes.[236]

Summing up the proliferation-related data of this thesis, cervical cancer cells largely do not require GDF15 for proliferation. However, too high and too low GDF15 levels can inhibit the ability of cervical cancer cells to form colonies. This points towards a small corridor for *GDF15* expression in which cervical cancer cells maintain their colony formation capacity.

3.2.2. Downregulation of GDF15 protects cervical cancer cells against stress-induced apoptosis

Since GDF15 is known as a pro-apoptotic stress response protein,[127,140] it was examined in this thesis whether GDF15 repression by E6 may increase the response of cervical cancer cells towards three different anti-proliferative drugs. A limitation of the experimental approaches chosen in the present study is the fact that it is technically difficult to *directly* analyze whether E6 modulates the stress resistance of HPV-positive cells via GDF15

downregulation because of various experimental restrictions. On the one hand, silencing of endogenous E6 expression itself leads to the rapid induction of apoptosis in HPV-positive cancer cells,[29] an effect that would overlap with a possible pro-apoptotic effect of GDF15. On the other hand, E6 could be expressed in HPV-negative cervical cells, however this approach has also several pitfalls to consider. Ectopic expression may not represent physiologically relevant E6 protein levels. Further, the cellular response to E6 expression could be affected by differences in the cellular background. Primary cervical keratinocytes, for example, miss the additional genetic alterations which are necessary for HPV-linked carcinogenesis. Alternatively, E6 could be expressed in the cell line C33A, which is widely used as a rare example for HPV-negative cervical cancer cells. However, C33A cells express the p53 mutant R273C,[236] which shows an altered DNA binding behavior[238] and thereby probably regulates GDF15 expression differently than the wildtype p53.

The results of this study, however, provide strong evidence that GDF15 plays an important role for the apoptosis regulation in HPV-positive cancer cells. It was found that elevated GDF15 levels were associated with PARP cleavage in cervical cancer cells after TM or TG treatment. This is in line with similar findings in colorectal cancer cells.[77] In addition, the present works showed that the knockout of *GDF15* decreases apoptosis rates after TM treatment in HeLa cells as indicated by the reduction of different apoptosis markers (DNA double stand breaks, cleaved PARP, and cleaved Caspase-9). This result also suggests that N-glycosylation of pro-GDF15 is not essential for the pro-apoptotic function of GDF15, since it is inhibited by TM.

As previously observed for colorectal cancer cells,[62,111] the present work exhibited that the downregulation of GDF15 levels can also attenuate the activation of apoptosis in SSide-treated cervical cancer cells. Two out of three HeLa *GDF15* KO clones showed lower apoptosis rates compared to parental HeLa cells in TUNEL, immunoblot, and live cell imaging analyses. It is unclear why HeLa *GDF15* KO clone #2 responded differently from clone #1 and clone #3 but similarly to parental cells. For example, clone #2 did not show altered p53 levels, reduced proliferation, or changed cell morphology in live cell imaging assays. The divergent behavior of clone #2 may be an effect of clonal variation and, interestingly, seems to be specific for SSide treatment because it was not observed after TM or cisplatin treatment.

Remarkably, SSide treatment in this study diminished *E6/E7* mRNA and E7 protein expression. Prolonged cultivation in FCS-free medium also reduced E7 expression, but – in comparison to SSide – at later time points and only on the protein level. This is further substantiated by results of another research group which show that sulindac also strongly decreased *E6/E7* mRNA and E7 protein expression in HeLa cells.[173] These findings indicate that regular sulindac intake has the potential to prevent or reduce cervical neoplasia formation because E6/E7 expression is an essential driving force in the cervical carcinogenesis.[35,36]

Regarding clinical aspects, it is particularly interesting that GDF15 downregulation in cervical cancer cells can also lead to a higher resistance against cisplatin-mediated apoptosis. According, experiments of the present thesis revealed that HeLa *GDF15* KO clones had lower apoptosis levels than parental HeLa cells after cisplatin treatment. Transient downregulation of GDF15 levels by RNAi decreased cisplatin-induced apoptosis in HeLa and MRI-H186 cells as well. However, findings in cisplatin-treated SiHa cells point towards some heterogeneity between cervical cancer cells regarding the regulation and function of GDF15 in this context. In cisplatin-treated SiHa cells, GDF15 expression was not upregulated despite increasing p53 levels and did not promote apoptosis, at least under the chosen experimental conditions. The divergent cellular response is apparently not due to different histological origins (squamous cell carcinoma MRI-H186 and SiHa cells vs. adenocarcinoma HeLa cells) or HPV types (HPV16-positive MRI-H186 and SiHa cells vs. HPV18-positive HeLa cells). Notably, SiHa cells seemed to be generally more resistant towards cisplatin treatment because similar cisplatin concentrations induced less PARP cleavage in SiHa cells than in HeLa and MRI-H186 cells. In line with this hypothesis, the reported IC50 (half maximal inhibitory concentration) value of cisplatin for 24h treatment is 5-6x higher in SiHa cells (38 µM) than in HeLa or C33A cells.[239]
Very little is known about the mechanisms downstream of GDF15 which lead to the induction of apoptosis. GDF15 secretion seems not to be essential for mediating its pro-apoptotic effects since it was differently affected by the tested drugs. TM, TG, and SSide led to reduced and cisplatin to increased GDF15 levels in the supernatant of treated cells. Notably, the subcellular localization of GDF15 could be important for its function because GDF15 co-localized with mitochondria after GL-V9 treatment and induced apoptosis by lowering the MMP.[86] Accordingly, GDF15 downregulation during TM, SSide, and cisplatin treatment was observed in this thesis to decrease the cleavage of Caspase-9, which is a key mediator of the intrinsic/mitochondrial apoptotic pathway.[240]
In summary, the results of this study indicate that very high GDF15 levels are detrimental for the proliferation of cervical cancer cells. Moreover, GDF15 mediates the pro-apoptotic response of cervical cancer cells towards different anti-proliferative drugs. These findings suggest that HPV-positive cancer cells are protected against miscellaneous forms of stress by blunting the GDF15-linked apoptotic response through E6 (Figure 37).

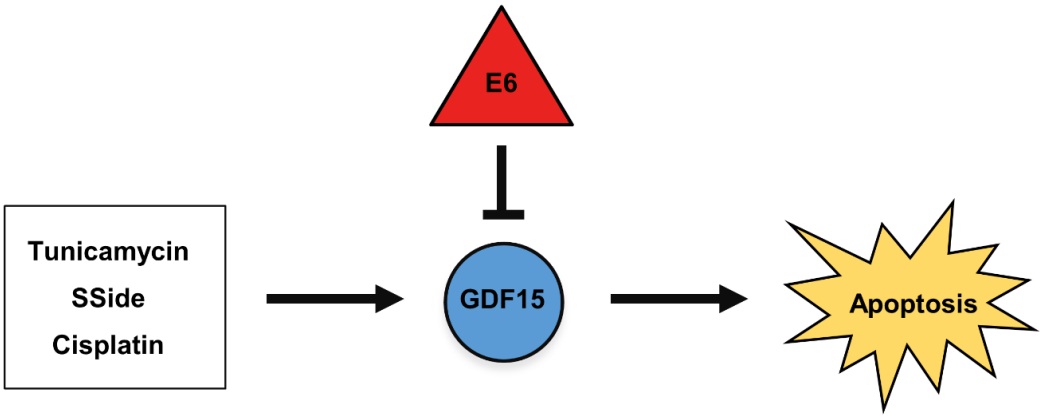

Figure 37 Increased drug resistance of HPV-positive cancer cells. E6 downregulates GDF15 expression in HPV-positive cervical cancer cells and thereby reduces pro-apoptotic effects of tunicamycin, SSide, and cisplatin.

3.3. Implications of GDF15 expression and its inhibition by oncogenic HPVs for prevention and therapy of cervical carcinomas

Remarkably, GDF15 levels are higher in cervical carcinomas than in normal cervical tissues.[180,234] At first, this finding seems counterintuitive in regard to the GDF15 repression by E6 and the potentially anti-tumorigenic function of GDF15, which were observed in this thesis. However, an increased expression in tumors does not necessarily mean that a protein has oncogenic effects. For example, host cells could induce the expression of an anti-proliferative protein to counteract and compensate exceeding pro-proliferative stimuli. The difference in GDF15 expression is in fact rather small (≤ twofold) between cervical cancer and healthy tissue.[234] Notably, the survival data of cervical cancer patients point towards a tumor-suppressive function of GDF15 since patients with high *GDF15* mRNA levels had better survival rates than patients with low levels (Human Protein Atlas available from http://www.proteinatlas.org).[69] For instance, the 5-year survival rate of patients with high *GDF15* expression was almost 10% higher compared to patients with low *GDF15* expression (p = 1.9%). The gap between the survival rates of the two study groups became larger with increasing years. These findings are compatible with the experimental data of this thesis, favoring an anti-tumorigenic function for GDF15 by promoting apoptosis in cervical cancer cells.

Although CHOP expression is induced by E6/E7 and higher in cervical cancer than in CIN3 tissues,[241] CHOP might have anti-tumorigenic functions in cervical carcinomas as well. Similarly to GDF15, higher *CHOP* transcript levels were also associated with better survival rates of cervical cancer patients, although the difference between the 5-year survival rates of the two study groups was not statistically significant (p = 5.3%) (Human Protein Atlas available

from http://www.proteinatlas.org).[69] For a clear pro- or antitumorigenic classification of CHOP, additional experiments are required in order to identify further CHOP functions in cervical cancer cells, beyond increasing GDF15 expression after ER stress and glucose deprivation as observed in this thesis.

Taking the tumor-suppressive effects and the role of GDF15 as a pro-apoptotic stress response protein into account, two opposing driving forces may determine GDF15 levels in cervical carcinomas. On the one hand, it is possible that proliferating tumor cells inevitably induce GDF15 expression because they have high bioenergetic and biosynthetic demands and therefore often face stress caused by limited nutrient supply and misfolded proteins.[242] Accordingly, the present work shows that limited nutrient supply (in form of glucose deprivation) leads to an upregulation of GDF15 levels in cervical cancer cells. Likewise, hypoxia, amino acid deficiencies, and solid stress could increase GDF15 levels because they also represent common stress types in tumor tissues and stimulate GDF15 expression.[71,74,110,192,193,243] On the other hand, however, tumor cells must establish mechanisms to regularly cope with excessive, cellular stress and prevent stress-associated apoptosis in order to survive. In the case of HPV-positive cancer cells, they could blunt apoptotic stress responses via E6-mediated GDF15 repression, thereby keeping GDF15 levels below a threshold which is needed to efficiently induce apoptosis.

The results of this thesis indicate that this also applies to the stress generated by chemotherapeutic drugs, which could contribute to the therapeutic resistance of HPV-positive cancer cells in the clinic. In this regard, a promising therapeutic approach may be the reinforcement of GDF15 expression in cervical tumors towards apoptotic levels. To this end, pro-apoptotic drugs could be combined which increase GDF15 levels synergistically, for example by activating different positive regulators of GDF15 expression, in order to overcome the repression of GDF15 expression by E6. In line with this notion, co-treatment with NSAIDs or TM raised apoptosis rates in diverse cisplatin-treated cancer cells, including HeLa cells.[211,226,244,245] Depletion of glucose or of other nutrients may represent an alternative way to reinforce apoptotic GDF15 levels in cervical carcinomas during chemotherapy because experiments of the present work show that glucose deprivation can strongly upregulate GDF15 expression. This is further supported by the report that fasting or fasting-mimicking diets, which inter alia decrease glucose or amino acid levels in the blood, sensitize different cancer cell types towards chemotherapy.[246]

In the present thesis, pro-apoptotic effects of GDF15 were observed in HeLa and MRI-H186 cells after using cisplatin at concentrations (10-20 µM) which correspond to the concentrations found in the blood of treated cancer patients (8-18 µM).[226,247,248] However, SiHa cells were more resistant towards cisplatin because they showed only low apoptosis levels in treatment experiments performed in this work. Interestingly, SiHa cells also failed to appreciably increase

GDF15 expression in this context. In the therapy of cervical cancer patients, resistance mechanisms also represent one of the major drawbacks of cisplatin chemotherapy. Apart from elevated DNA repair and increased export/decreased import of cisplatin,[56] high glucose concentrations have, notably, been shown to impair cisplatin-mediated cell death.[199] In cisplatin-treated A459 lung and OV-2008 ovarian cancer cells, high glucose levels mediated dephosphorylation of p53 at Ser46 and thereby reduced the transcriptional activation of diverse pro-apoptotic p53 target genes.[199] In the present thesis, it was found that high glucose levels decreased GDF15 expression in cervical cancer cells, which thus might contribute to the inhibition of cisplatin-induced apoptosis in this context.

Remarkably, there are also links reported between cisplatin resistance and impairment of ER stress signaling, which was observed in this thesis to mediate GDF15 upregulation after glucose deprivation and TM/TG treatment. For instance, cisplatin was able to induce lethal ER stress pathways in cisplatin-sensitive ovarian or pleural mesothelioma cancer cells, but not in their cisplatin-resistant counterparts.[249,250] ER stress can also be attenuated by diverse pro-survival proteins like the chaperon BiP, the pro-autophagic protein p62, or the vesicle protein NAPA (N-ethylmaleimide-sensitive factor attachment protein alpha).[222] Increased expression of these survival proteins has been shown to reduce cisplatin sensitivity in different cancer cell types.[222]

Using an additional, ER stress-inducing drug might therefore enhance the anti-tumorigenic effect of cisplatin. For co-treatment with cisplatin, TM and TG cannot be applied in cervical cancer patients because both agents also generate cytotoxic effects in non-cancerous cells. In animal experiments, they were found to damage endothelial and liver cells in particular.[251–253] However, mipsagargin, a prodrug of TG, is currently under investigations in clinical trials for the treatment of hepatocellular cancer because mipsagargin is specifically processed and activated at tumor sites.[251] Alternatively, fucoidan, tocotrienols, and curcumin were reported to activate ER stress pathways, CHOP expression, and apoptosis in cervical cancer cells.[254–256] Whether CHOP and GDF15, however, are involved in the induction of apoptosis by those drugs awaits further exploration.

Since NSAIDs upregulate GDF15 expression as reported in this thesis and in the literature,[127] GDF15 may not only play a role for cancer treatment, but also for cancer prevention. There are many studies in which NSAID intake decreases the incidence of diverse cancer types, in particular of colorectal, gastric, and esophageal cancer.[257,258] Importantly, regular intake of aspirin or non-aspirin NSAIDs like celecoxib can also lead to the regression of CINs and reduce the formation of cervical carcinomas.[170,171,259] For example, frequent users of aspirin in a case-control study showed half the risk of developing cervical cancer compared to the control group.[171] This is in line with the finding of this thesis that GDF15 upregulation by SSide treatment can lead to the elimination of HPV-positive cancer cells. Although E6 might limit

NSAIDs-related effects by inhibiting GDF15 expression, prolonged SSide treatment downregulated *E6/E7* expression, which was accompanied by the induction of apoptosis.
In summary, increased GDF15 levels could be beneficial both for cervical cancer prevention via intake of NSAIDs and for cisplatin-based chemotherapy of cervical carcinomas. However, E6 interferes in the pro-apoptotic effects of these drugs by downregulating GDF15. The combination of cisplatin with special diets, NSAIDs, or ER stress-inducing drugs might be a promising strategy to overcome GDF15 repression by oncogenic HPVS, thereby raising the chemosensitivity of cervical cancer cells.

3.4. Conclusions

This study identifies *GDF15* as a novel cellular target gene of oncogenic HPVs. E6 represses GDF15 via the downregulation of p53 and thereby protects cervical cancer cells against pro-apoptotic stimuli like nutrient deprivation or ER stress (see model in Figure 38).

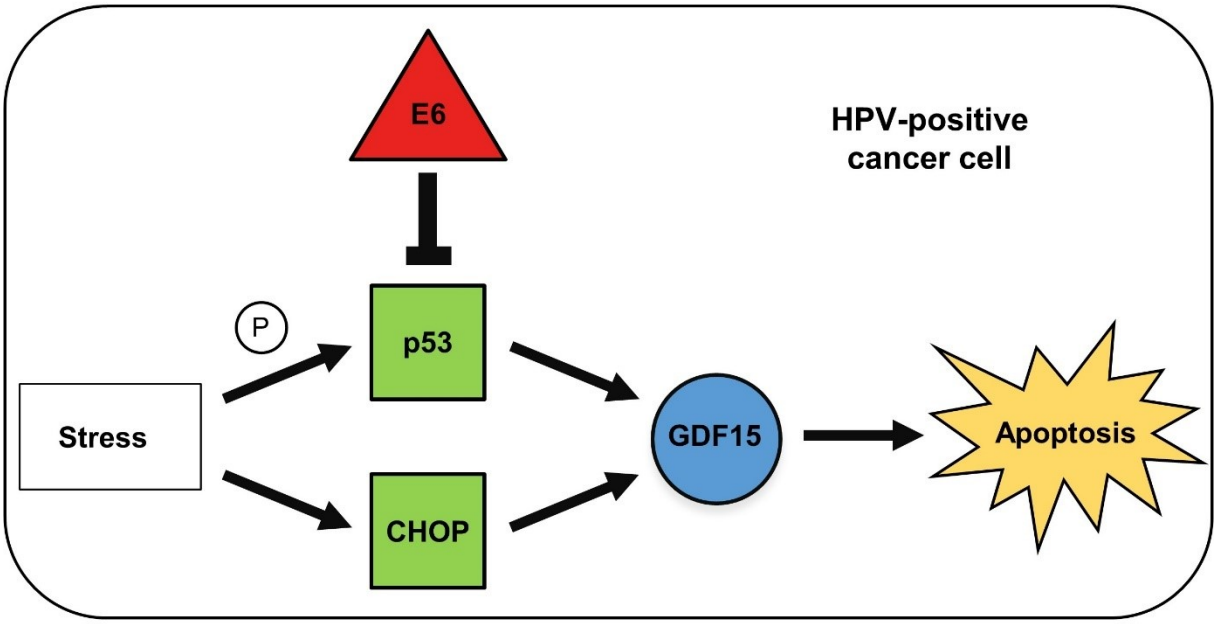

Figure 38 Schematic regulation of GDF15 expression in HPV-positive cervical tumor cells. Highly proliferating cervical cancer cells often suffer from stress, which can be induced inter alia by glucose deprivation, ER stress, or anti-tumorigenic drugs. The different stress factors individually upregulate GDF15 expression via CHOP and/or p53. However, E6 mediates the degradation of p53 in cervical cancer cells and thereby strongly counteracts the induction of GDF15 expression and apoptosis after stress.

CHOP and p53 represent key activators of GDF15 expression in response to different forms of cell stress. These findings may also be clinically relevant because GDF15 inhibition by oncogenic HPVs could increase the resistance of HPV-cancer cells against cancer-preventive effects of NSAIDs as well as against chemotherapy. Relieving GDF15 repression, e.g., by combining chemotherapy with other GDF15-inducing agents, may therefore represent a

promising strategy to improve current treatment regimens employed for the therapy of HPV-positive cancers.

Chapter 4

Material and Methods

4. Material and Methods

4.1. Reagents and material

Molecular biology grade reagents were applied where possible. Buffers and solutions were prepared with Millipore water if not stated otherwise. All standard material and reagents for buffers and media were supplied by Abcam (Cambridge, United Kingdom), Addgene (Cambridge, MA, USA), Agilent Technologies (Santa Clara, CA, USA), AppliChem (Darmstadt, Germany), Applied Biosystems (Foster City, CA, USA), Arbor Vita Corporation (Fremont, CA, USA), BD Biosciences (Heidelberg, Germany), Becton Dickinson (BD, Franklin Lakes, NJ, USA), Bio-Rad (Hercules, CA, USA), Carl Roth (Karlsruhe, Germany), Cayman Chemical (Ann Arbor, MI, USA), Cell Signaling (Cambridge, United Kingdom), Corning (Corning, NY, USA), Dharmacon (Lafayette, CO, USA), Enzo Life Sciences (Lörrach, Germany), Eppendorf (Hamburg, Germany), Essen Bioscience (Göttingen, Germany), Eurofins Scientific (Luxemburg, Luxemburg), Eurogentec (Lüttich, Belgium), GE Healthcare (Chicago, IL, USA), Greiner Bio-One (Kremsmünster, Österreich), Jackson ImmunoResearch Laboratories (West Grove, PA, USA), Merck (Darmstadt, Germany), New England Biolabs (NEB, Frankfurt, Germany), Promega (Madison, WI, USA), QIAGEN (Venlo, Netherlands), Roche Applied Science (Penzberg, Germany), Santa Cruz Biotechnology (Dallas, TX, USA), Sigma-Aldrich (St. Louis, MO, USA), Thermo Fisher Scientific (Waltham, MA, USA), Vector Laboratories (Burlingame, CA, USA) and VWR International (Radnor, PA, USA). Manufactures of specific reagents are named in the text.

4.2. Cell-based methods and assays

4.2.1. Human cell lines and cultivation

All cell lines used in this thesis are listed in Table 2 with their origin, HPV status and culture medium (Gibco, Thermo Fisher Scientific). As standard, human cells were cultivated in medium containing 5.5 mM glucose and supplemented with 10% fetal calf serum (FCS, Gibco, Life Technologies), 100 U/ml penicillin, 0.1 mg/ml streptomycin and 2 mM L-glutamine ("PSG", all from Sigma-Aldrich). All cells were incubated in a humidified atmosphere at 37 °C, 5% CO_2 and 21% O_2. Selection agents were omitted from the media during experiments.

The cell line HCT-116 $p53^{-/-}$, in which *TP53* is partially deleted, was generated by the Vogelstein lab.[260] HeLa *"p53 null"* cells stably express a shRNA targeting *TP53* mRNA and hence repress p53 expression efficiently.[156] HeLa mCherry H2B and SiHa mCherry H2B cells are expressing the nuclear fluorophore H2B_mCherry (Binder Lab, DKFZ Heidelberg, Germany). HPKII cells are derived from a human foreskin keratinocyte that was immortalized by transfecting HPV16 DNA.[23]

Routinely, stock cultures were supplied with fresh medium or - in case of confluence – were split every 3-4 days. After washing with phosphate-buffered saline (PBS; 137 mM NaCl, 2.7 mM KCl, 4.3 mM Na_2HPO_4, 1.4 mM KH_2PO_4, pH 7.4) cells were detached with 0.25% Trypsin-EDTA (Gibco, Thermo Fisher Scientific).

For seeding, cells were trypsinized and viable cells were counted after staining with Trypan Blue Stain 0.4% (Thermo Fisher Scientific) using the Countess™ Automated Cell Counter (Invitrogen). Seeding cell numbers ranged from 3-12 *10^5 cells for a 6 cm dish (3 ml medium) and 1,000-6,000 cells per well for a 96-well plate (100-200 µl medium/well).

Table 2 Human cell lines and corresponding medium

Cell line	Origin	HPV status	Medium
HCT-116	Colorectal carcinoma	-	McCoy's 5A
HCT-116 $p53^{-/-}$	Colorectal carcinoma	-	McCoy's 5A
HeLa	Cervical adenocarcinoma	HPV18	DMEM
HeLa *"p53 null"*	Cervical adenocarcinoma	HPV18	DMEM + 0.7 mg/ml G418
HeLa mCherry H2B	Cervical adenocarcinoma	HPV18	DMEM + 1 µg/ml puromycin
HPKII	HPV-immortalized foreskin keratinocyte	HPV16	DMEM
MRI-H186	Cervical squamous cell carcinoma	HPV16	RPMI-1640
SiHa	Cervical squamous cell carcinoma	HPV16	DMEM
SiHa mCherry H2B	Cervical squamous cell carcinoma	HPV16	DMEM + 1 µg/ml puromycin

4.2.2. Cryopreservation and thawing of cells

For cryopreservation, cells were trypsinized, pelleted by centrifugation at 140x *g* for 3 min and resuspended in medium supplemented with 30% FCS and 10% DMSO and aliquoted into cryotubes. The cryotubes were set into a freezing container (Nalgene, Thermo Fisher Scientific), filled with isopropanol and slowly frozen at -80 °C. After several days, the cryotubes were transferred into liquid nitrogen for long-term storage.

For rapid thawing, a frozen cell aliquot was warmed up in a 37 °C warm water bath, pelleted by centrifugation at 140x *g* for 3 min and resuspended in fresh medium to remove DMSO residuals before seeding the cells into a culture flask. The next day, medium was renewed.

4.2.3. Transfection of nucleic acids

4.2.3.1. Plasmid transfection using calcium phosphate coprecipitation

Calcium phosphate transfection as described by Chen and Okoyama[261] was used as standard method to transfect plasmids. A list of used plasmids can be found in the appendix (Table 14).

Cells were seeded into 6 cm dishes to reach 20% confluence the following day. Because temperature and pH value are important for successful transfection, $CaCl_2$ solution (0.25 M) and BES buffer (50 mM BES, 280 mM NaCl, 1.5 mM Na_2HPO_4, pH 6.95) were prewarmed to room temperature (RT). Afterwards, 0.1-6.5 µg plasmid DNA was replenished with pBluescript II vector (pBS, Stratagene, Heidelberg, Germany) to a final mass of 6-6.5 µg DNA per dish. Firstly, 150 µl $CaCl_2$ solution and then 150 µl BES buffer were added to the DNA and were gently mixed by inversion. After incubation for 15 min at RT, the transfection mix was added dropwise onto cells cultivated in 3 ml DMEM. Cells were kept at 35 °C and 3% CO_2 for 16-18h in a humidified atmosphere. Having washed twice with PBS, cells were further cultivated in their standard medium for 24h in case of protein overexpression or for 48h in case of shRNA expression.

4.2.3.2. Plasmid transfection using FuGENE Transfection Reagent

Cells were seeded into 6 cm dishes for 30-40% confluence the following day. Opti-MEM I Reduced Serum Media (Gibco, Thermo Fisher Scientific) and FuGENE HD Transfection Reagent (Promega) were prewarmed to RT. Firstly, 100 µl Opti-MEM were mixed with 0.1-2 µg plasmid DNA, which was adjusted to a final mass of 2 µg DNA with pBS. Then, 7 µl FuGENE HD was added and the transfection mix was vortexed briefly. During incubation of the transfection mix for 5-15 min at RT, the medium of the dishes was replaced by 2 ml PSG-free medium supplemented with 10% FCS. Afterwards the transfection mix was added dropwise onto the cells. The medium was exchanged to 3 ml standard medium 24h post transfection and cells were further cultivated until harvest.

4.2.3.3. Transfection of siRNAs using DharmaFECT Transfection Reagent

DharmaFECT (DF) Transfection Reagents (Dharmacon) were applied for transfection of synthetic siRNAs (*Silencer* Select siRNA, Ambion, Thermo Fisher Scientific). Type and volume of DF Reagent were optimized for best transfection efficiency in each cell line. The used type and volume are listed in Table 3.

Cells were seeded into 6 cm dishes for 30-40% confluence the following day. A DF master mix was prepared by adding 194-196 µl Opti-MEM to 4-6 µl DF Reagent for a final volume of 200 µl per dish. The DF master mix was inverted and incubated for 5 min at RT. In parallel, 2 µl siRNA (pool) (10 µM, Ambion Silencer Select, Thermo Fisher Scientific) and 198 µl Opti-MEM were mixed per dish for a final siRNA concentration of 10 nM.

An exception was the double knockdown experiment in Figure 12. Here, 20 nM siP53 and/or 20 nM siRNA pool targeting CHOP were applied as indicated in the legend of the figure. Each sample was filled up with siContr-1 to a final siRNA concentration of 40 nM if needed.

Table 3 Assignment of cell lines to DharmaFECT Transfection Reagents

Cell line	DharmaFECT Reagent	Volume per	
		6 cm dish	well (96-well plate)
HeLa	DF Reagent I	6 µl	-
HeLa *"p53 null"*	DF Reagent I	4 µl	-
HeLa mCherry H2B	DF Reagent I	-	0.4 µl
HPKII	DF Reagent III	4 µl	-
MRI-H186	DF Reagent I	4 µl	-
SiHa	DF Reagent I	6 µl	-
SiHa mCherry H2B	DF Reagent I	-	0.4 µl

Subsequently, 200 µl DF master mix and 200 µl siRNA mix were combined and incubated for 20 min at RT. Meanwhile, the medium of the dishes was replaced by 1.6 ml PSG-free medium supplemented with 10% FCS. After the incubation, 400 µl transfection mix was added dropwise onto the cells. Medium was exchanged to 3 ml standard medium 24h post transfection.

Table 4 siRNA sequences and pools

Target transcript	Name	Sequence	siRNA pool
-	siContr-1	CAGUCGCGUUUGCGACUGG	-
CHOP	siCHOP.3	AAGAGAAUGAACGGCUCAA	siCHOP
	siCHOP.4	GGCUCAAGCAGGAAAUCGA	
GDF15	siGDF15.1	UCCCAUGGUGCUCAUUCAA	siGDF15
	siGDF15.5	GCUACAAUCCCAUGGUGCU	
HPV16 *E6*	si16E6-1	ACCGUUGUGUGAUUUGUUA	si16E6
	si16E6-2	GGGAUUUAUGCAUAGUAUA	
	si16E6-3	UUAGUGAGUAUAGACAUUA	
HPV16 *E6/E7*	si16E6/E7-1	CCGGACAGAGCCCAUUACA	si16E6/E7
	si16E6/E7-2	CACCUACAUUGCAUGAAUA	
	si16E6/E7-3	CAACUGAUCUCUACUGUUA	
HPV18 *E6*	si18E6-1	GACAUUAUUCAGACUCTGU	si18E6
	si18E6-2	CAGACUCUGUGUAUGGAGA	
	si18E6-3	CUCUGUGUAUGGAGACACA	
HPV18 *E6/E7*	si18E6/E7-1	CCACAACGUCACACAAUGU	si18E6/E7
	si18E6/E7-2	CAGAGAAACACAAGUAUAA	
	si18E6/E7-3	UCCAGCAGCUGUUUCUGAA	
TP53	siP53	GACUCCAGUGGUAAUCUAC	-

For transfections in 96-well-plate-format, 2,500-6,000 cells were seeded per well and volumes of the transfection protocol were adjusted as following. Per well, 10 µl DF master mix (0.4 µl DF reagent and 9.6 µl Opti-MEM) and 10 µl siRNA mix (≙ 0.1 µl of 10 µM siRNA (pool) and 9.9 µl Opti-MEM) were gently mixed and added to 80 µl of PSG-free medium supplemented with 10% FCS. Medium was replaced by 200 µl standard medium 24h after transfection and cells were harvested 72h post transfection if not indicated otherwise.
All used siRNAs are listed in Table 4. As control sample, cells were transfected with siContr-1. The sequence of siContr-1 mismatches to all known human genes in at least four DNA bases. To reduce off-target effects, a pool of 2-3 siRNAs was used at equimolar concentrations where possible.

4.2.4. Expression analyses under different cell culture conditions

To analyze protein and mRNA expression in the course of cell cultivation (see Figure 8), 4-6 *10^5 cells were seeded into 6 cm dishes. The next day, one dish was harvested as reference value for time point zero. The medium of the residual dishes was removed and 3 ml medium with or without 10% FCS was added. Cells were harvested 24h, 48h, and 72h after medium exchange.
For the cell seeding experiments of Figure 9, 3 *10^5, 6 *10^5, or 12 *10^5 cells were seeded into a 6 cm dish. Medium was replaced with fresh medium the following day. Cells were harvested 48h later.
In order to analyze whether glucose levels in the medium affect protein and mRNA expression, 6-7.5 *10^5 cells were seeded into 6 cm dishes. Two days later, medium was replaced by medium containing either 0 mM, 5.5 mM, or 25 mM glucose. Cells were either harvested 24h or 48h later.

4.2.5. Treatment with chemical compounds

Two days after seeding or 24h post transfection, cells were supplied with fresh medium and treated with drugs if not stated otherwise. The equivalent volume of solvent was applied to control cells. Used compounds and their solvents are listed in Table 5.
For sulindac sulfide (SSide) treatment, a pre-mix with SSide in FCS-free medium was freshly prepared. Cells were washed with PBS prior to addition of the SSide solution in order to avoid binding of SSide to serum albumin.

Table 5 Chemical compounds

Compound	Abbreviation	Supplier	Solvent	Final concentration
Camptothecin	CPT	Cayman Chemical	Medium	10-30 nM
Cisplatin	Cis	EMD Millipore	0.9% NaCl	0.75-20 µM
Doxorubicin	Doxo	Enzo Life Sciences	H_2O	30-60 nM
Hygromycin B	HygB	Invitrogen	-	20-250 µg/ml
Sulindac sulfide	SSide	Cayman Chemical	DMSO	1-50 µM
Thapsigargin	TG	Enzo Life Sciences	DMSO	0.5 µM
Tunicamycin	TM	Cayman Chemical	DMSO	1-5 µM

4.2.6. *GDF15* knockout and generation of single cell clones (CRISPR/Cas9)

Cloning of CRISPR/Cas9 plasmids and background information on the technique are described in chapter 4.3.5.3. Transfection with Fudgene HD was used to transfer CRISPR/Cas9 plasmids into cervical cancer cells. To select successfully transfected cells, culture medium was replaced by medium supplemented with 1 µg/ml puromycin 36-40h post transfection. Cells were kept under selection until all cells of a mock-transfected plated died (about 3-4 days later). Selected cells were split, serially diluted, seeded into 96-well plates, and further cultivated in standard medium. Single cell clones were identified using light microscopy. The knockout was evaluated by detecting target protein expression using immunoblot analyses. Clones with a successful knockout of the target gene were cryopreserved (see section 4.2.2) in an early passage.

4.2.7. Cell cycle analysis

Flow cytometry was used to analyze cell cycle distribution after DNA staining with propidium iodide (PI). For that reason, cells were harvested by trypsination after washing with PBS. Cells were pelleted by centrifugation at 1,000x *g* for 5 min, washed with pre-cooled PBS and resuspended in 300 µl cold PBS. After cells were fixed by adding 900 µl ice-cold ethanol during vortexing, they were kept at -20 °C overnight for permeabilization. To remove residual ethanol, cells were pelleted by centrifugation and resuspended in 925 µl cold PBS. Subsequently, 25 µl 1 mg/ml PI solution and 50 µl 10 mg/ml RNAse were added for a final concentration of 25 µg/ml and 0.5 mg/ml, respectively. The staining mix was incubated in the dark at RT for 30 min. The cell suspension was filtered through gaze and cell cycle distribution was analyzed by flow cytometry using the BD LSRFortessa cell analyzer and the BD FACS Diva software version v8.0.1 (BD). The Watson model[159] was applied to quantify cells in the different cell cycle phases. Illustrations were generated with the FlowJo software version 10 (BD).

4.2.8. Live cell imaging (IncuCyte system)

4.2.8.1. Cell proliferation analysis

To analyze cellular proliferation in real-time, 1,000-5,000 cells per well were seeded into 96-well plates. Confluence or – in case of labeled cells – fluorophore counts were measured every six hours for several days with the IncuCyte S3 system (Essen BioScience). Following standard settings were applied: 10x magnification, 4 images/well, phase and red (400 ms). As required, the analysis of proliferation was started 15 min after settlement, transfection and/or treatment of cells using the IncuCyte S3 2019A software (Essen BioScience).

4.2.8.2. Activated Caspase-3/7 assay

Another possibility to detect the induction of apoptosis over time is the use of a cell membrane-permeable dye, which is cleaved during apoptosis by activated Caspase-3 or Caspase-7. After this activation, the released fluorophore is able to intercalate into nuclear DNA in order to stain apoptotic cells during live cell imaging.
For the Caspase-3/7 assay, 4,000 cells per well were seeded into a 96-well plate. Two days later, cultivation medium was freshly prepared by adding the drug of interest or the solvent control, and the inactivated, green dye (IncuCyte Caspase-3/7 Reagents for Apoptosis #4440, Essen Bioscience) in a ratio of 1:1000 (final concentration of dye: 5 µM). After removal of old culture medium, 100 µl Caspase-3/7 assay master mix was added into a well. To exclude potential toxicity of the dye, control cells were also treated with the drug of interest or the solvent control without adding the green dye to the medium. Confluence and green fluorophore counts were measured every 2h for about 5 days with the IncuCyte S3 system and analyzed using the IncuCyte S3 2019A software. Following settings were applied: 10x magnification, 4 images/well, phase, green (300 ms).

4.2.9. Colony formation assay

Cells were seeded and transfected with episomal pCEP expression vectors (listed in Table 14, appendix) by calcium phosphate transfection (4.2.3.1). Two days post transfection, cells were washed with PBS, trypsinized and re-plated in 6 cm dishes in an adequate ratio dependent on the used cell line, transfection rate, and target gene. The culture medium was supplemented with hygromycin B (SiHa, HeLa and MRI-H186: 250 µg/ml, HCT-116: 150 µg/ml) on the next day. For 1-3 weeks, cells were further cultivated under selection with refreshing medium every 3-4 days until all mocked-transfected cells died on the control plate and colonies were formed. After washing with PBS, colonies were stained with 350 µl crystal violet staining solution (12 mM crystal violet dye, 29 mM NaCl, 3% formaldehyde, 22% EtOH) for 5 min under slow shaking. Excess dye was removed by washing dishes with water. After drying the dishes at

37 °C, they were digitalized with the Epson Perfection 4990 Photo Scanner (Epson, Suwa, Japan).

4.2.10. TUNEL assay

One method used to detect apoptotic cells was the terminal deoxynucleotidyl transferase-mediated dUTP nick end labeling (TUNEL) assay. Hereby, the DNA-specific enzyme terminal deoxynucleotidyl transferase catalyzes polymerization of labeled nucleotides to free 3'-hydroxyl termini. These typically form at single or double strand breaks after cleavage of genomic DNA during apoptosis.

Cells were seeded on coverslips in 6 cm dishes, treated and harvested at time points specified in the text. Following washing in PBS, coverslips were incubated in fixation solution (4% paraformaldehyde in PBS) for 15 min. Afterwards, coverslips were washed twice with PBS and kept in 70% ethanol at -20 °C for storage. Coverslips were washed twice with PBS, incubated in permeabilization solution (0.1% Triton X-100, 0.1% sodium citrate in PBS) at 4 °C for 2 min and washed twice with PBS. For 60-90 min, coverslips were incubated with 25 µl TUNEL staining solution (*In Situ* Cell Death Detection Kit, Fluorescein, Roche Applied Science) in a wet chamber at 37 °C. After several PBS washing steps, coverslips were stained with 4',6-diamidino-2-phenylindole (DAPI, 1 µg/ml in PBS, Roche Applied Science) in the dark for 5 min. Coverslips were subsequently washed: five times with PBS, once with water and once with ethanol. Finally, stained coverslips were air-dried and covered with a small layer of Vectashield Antifade Mounting Medium (Vector laboratories). Then, they were placed on microscope slides and could be stored short-time at 4 °C. Images were generated with the Cell Observer microscope (LED module colibri.2, 20x/0.4 LD PlnN Ph2 DICII objective) from Zeiss (Jena, Germany). Fiji ImageJ 1.52p software was used for image adjustments, representation and quantification. The percentage of TUNEL-positive cells per coverslip was determined as the mean of at least five images using an ImageJ Macro (written by Damir Krunic, Light Microscopy Core Facility, DKFZ).

4.3. DNA-based methods

4.3.1. Transformation of bacteria

A heat-shock-based protocol as described by Hanahan[262] was used for transformation of the *E. coli* strains TG2 and Stbl3. TG2 was used as standard strain, whereas Stbl3 was chosen in the context of lentiviral constructs, e.g., pLentiCRISPRv1.

The bacterial culture was incubated at 37 °C with continuous shaking until the culture reached an $OD_{600\ nm}$ value of 0.3-0.4 (≙ log phase). To generate competent *E. coli* cells, all used buffer and materials were pre-cooled. Firstly, 500 ml Lysogeny Broth (LB; 1% Bacto tryptone,

0.5% yeast extract, 170 mM NaCl, pH 7.0) medium was inoculated with 2 ml of a 20 ml overnight culture (37 °C, LB medium). The culture was put on ice for 20 min to cool down and the cells were harvested by centrifugation at 3,800x *g* for 10 min at 4 °C. The bacteria pellet was resuspended on ice in 20 ml TSS buffer (10% polyethylene glycol 8000, 5% DMSO, 50 mM $MgCl_2$ in LB medium, pH 6.5) and 8 ml glycerin was added. The cell suspension was aliquoted, immediately frozen in liquid nitrogen and stored at -80 °C until use. Finally, transformation efficiency was determined by transforming 50 pg plasmid DNA. Batches of competent cells with a transformation efficiency above 5 $*10^7$ were used for further experiments.

For transformation, an aliquot of competent *E. coli* was thawed on ice. Then 100 µl cell suspension was gently mixed with DNA and incubated for 30 min on ice. Afterwards, cells were heat-shocked in a 42 °C warm water bath for 60 s and immediately incubated on ice for 3 min. After addition of 900 µl LB medium, cells were incubated at 37 °C for 20-60 min while shaking. Either 10%, 20%, 50% or all of the gained bacteria were streaked in a volume of 100-200 µl on a LB agar plate (1.5% agar agar for bacteriology (Gerbu, Heidelberg, Germany)) supplemented with the appropriate antibiotic (e.g., 100 µg/ml ampicillin (Amp) or 30 µg/ml kanamycin (both from Sigma-Aldrich)). The LB agar plate was incubated at 37 °C until colonies formed.

4.3.2. Plasmid isolation from bacteria

As needed, plasmids were isolated either from 3 ml bacterial cultures (overnight, LB medium supplemented with the appropriate antibiotic) using the PureLink Quick Plasmid DNA Miniprep Kit (Invitrogen, Thermo Fisher Scientific) for small or from 50 ml cultures applying the PureLink HiPure Plasmid Filter Midiprep Kit (Invitrogen, Thermo Fisher Scientific) for medium amounts of plasmid.

For large-scale purification, plasmids were extracted from 250 ml cultures performing a maxipreparation protocol based on a CsCl-ethidium bromide gradient as described by Sambrook and Russell.[263] Here, cells were pelleted by centrifugation at 3,800x *g* for 10 min, thoroughly resuspended in 10 ml solution I (50 mM glucose, 25 mM Tris, 10 mM EDTA, pH 8.0) and lysed in 20 ml solution II (0.3 M NaOH, 1% sodium dodecyl sulfate (SDS), freshly prepared) at RT for max. 10 min. Lysis was stopped by adding 15 ml solution III (3 M potassium acetate, 11.5% acetic acid, pH 4.8). After incubation for 5 min on ice, cell debris was pelleted by centrifugation at 4,400x *g* and 4 °C for 10 min and the supernatant was transferred into a fresh tube. An equivalent volume of isopropanol was added. The mixture was incubated for 30 min on ice. Precipitated nucleic acids were pelleted by centrifugation at 4,400x *g* and 4 °C for 25 min, resuspended in 4 ml TE buffer (10 mM Tris, 1 mM EDTA, pH 8.0) and mixed with

4 ml 5 M LiCl solution. After incubation for 30 min on ice, RNA was removed by centrifugation at 3,500x *g* and 4 °C for 5 min. The supernatant was transferred into a new tube, and DNA was precipitated by adding 16 ml ethanol, mixing and incubation at -20 °C for 45-60 min. After centrifugation at 4,400x *g* and 4 °C for 25 min, the DNA pellet was resuspended in 4 ml TE.
The CsCl-gradient was prepared at RT by adding 4.4 g CsCl and 120 µl 10 mg/ml ethidium-bromide solution. This solution was transferred into 6 ml PA Ultraclimp tubes (Sorvall, Thermo Fisher Scientific), which were precisely tared, before ultracentrifugation was carried out at 220,000x *g* and 20 °C for 15-16h. Supercoiled plasmid DNA was physically separated from other DNA according to their densities in a CsCl-gradient. Several extraction steps with water-saturated iso-butyl alcohol were performed until all residual ethidium-bromide was removed from the plasmid DNA. Subsequently, the DNA solution was filled up with water to a volume of 10 ml. The DNA was precipitated by addition of 20 ml ethanol, mixing and incubation at -20 °C for 1h. After centrifugation at 4,400x *g* and 4 °C for 25 min, the DNA pellet was resuspended in 4 ml solution IV (0.2 M NaCl in TE) and mixed with 10 ml ethanol. Following precipitation at -20 °C for 1h and centrifugation at 4,400x *g* and 4 °C for 25 min, the DNA pellet was washed with 1 ml 70% ethanol and air-dried. Finally, the purified plasmid DNA was dissolved in an appropriate volume of TE and the DNA concentration was measured with the NanoDrop ND-1000 spectrophotometer (NanoDrop; PEQLAB, VWR International).

4.3.3. Agarose gel electrophoresis and gel purification of DNA fragments

To separate DNA fragments according to their size, horizontal agarose gel electrophoresis was performed. Firstly, 1-2% agarose was dissolved by boiling in 80-120 ml electrophoresis buffer (EP; 40 mM Tris, 5 mM sodium acetate, 1mM EDTA, pH 7.8). When the solution was cooled down to approx. 50-60 °C, the nucleic acid dye peqGREEN (PEQLAB) was added to the agarose solution in a ratio of 1:20,000, mixed, and poured into a gel tray. DNA samples were prepared by adding 6x DNA loading buffer (0.25% bromophenol blue, 0.25% xylene cyanol, 15% Ficoll 400) and loaded on the agarose gel, which had been placed in an electrophoresis chamber (PEQLAB) filled with EP. At least one lane of the gel was loaded with 5 µl SmartLadder (Eurogentec), a DNA size and mass marker. The gel was run at 70-120 V for 30-90 min. Separated DNA fragments were visualized via UV transillumination in a gel documentation system (Intas Science Imaging Instruments, Göttingen, Germany). To extract DNA fragments from the gel for further experiments, the respective gel band(s) was/were cut out, extracted, and purified with the QIAquick Gel Extraction Kit (QIAGEN) according to the manufacturer's protocol.

4.3.4. Precipitation and enzymatic modification of DNA

Restriction enzyme digest (RED)

To cut DNA molecules, restriction endonucleases and their corresponding buffers from NEB were used according to the manufacturer's protocol. For preparative restriction enzyme digests (REDs), 10-20 µg DNA were incubated with 30-60 Units (U) restriction enzyme in a 37 °C warm water bath for 2h or in case of polymerase chain reaction (PCR) amplicons at 37 °C overnight. An exception was the preparative digestion of the pLentiCRISPRv1 vector, which was cut with *Bsm*BI at 55 °C for 1h. In analytical REDs, 0.5-1 µg DNA was digested in a final volume of 20 µl and incubated in a 37 °C warm water bath for 1h before DNA fragments were analyzed for size and mass via gel electrophoresis (4.3.3).

DNA precipitation with ethanol

DNA was precipitated to remove impurities such as proteins or salts or to reduce the volume of the DNA solution for further molecular biological steps, e.g., ligation or (de)phosphorylation. For that, 1x volume DNA solution was mixed with 2.5-3x volume ethanol and 0.1x volume 3 M sodium acetate (pH 5.2) and incubated at -20 °C for 30 min. The DNA was pelleted by centrifugation at 4 °C and 13,000x *g* for 25-30 min and air-dried. As needed, the DNA was dissolved either in water or in TE buffer.

Dephosphorylation of 5' ends

In order to avoid self-ligation of vectors during cloning, digested vectors were dephosphorylated at their 5'-termini. For a total volume of 50 µl, 10-20 µg target DNA was mixed with 50 U Calf Intestinal Alkaline Phosphatase (NEB) in 1x NEBuffer 3 (NEB) and incubated in a 37 °C warm water bath for 60 min.

Phosphorylation of 5' ends

For phosphorylation of 5' termini, 2 µl of oligonucleotides (100 µM) or PCR amplicons were mixed with 1 µl 10x T4 Polynucleotide Kinase Forward Buffer A (Thermo Fisher Scientific), 1 µl T4 Polynucleotide Kinase (10 U/µl, Thermo Fisher Scientific) and 1 µl 10 mM adenosine triphosphate, and filled up with water to a finale volume of 10 µl. The mixture was then incubated at 37 °C for 30 min. After the kinase was heat-inactivated at 70 °C for 10 min in a water bath, the sample was slowly cooled down to 40-50 °C.

Ligation

For a final volume of 20 µl, 3-7x molar excess of the insert was added to 20-100 ng prepared vector and 5 U T4 DNA Ligase (Thermo Fisher Scientific) in 1x T4 DNA Ligase Buffer (Thermo

Fisher Scientific), mixed, and incubated for 1-2h at 21 °C. To inactivate the T4 DNA Ligase, samples were heated to 65 °C for 5 min.

4.3.5. Plasmid cloning strategies

4.3.5.1. Cloning of pSUPER plasmids

In 2002, Brummelkamp *et al.* introduced the pSUPER (suppression of endogenous RNA) vector as a system to express shRNAs in mammalian cells for downregulation of target genes.[264] A small RNA is transcripted under the control of a polymerase-III *H1-RNA* gene promoter and contains a 19-nucleotide-long sequence in sense and antisense orientation which is unique for the targeted mRNA. The palindromic repeats of this sequence are separated by a short spacer. After expression, the shRNA forms a hairpin structure and is further processed into functional siRNAs in mammalian cells.

Table 6 Primer sequences

Name	Sequence	Application	Target
GDF15_HindIII_rev	GATCAAGCTTTCATATGCAGTGG CAGTCTTTGGCTA	Cloning	GDF15
GDF15_KpnI_for	GATCGGTACCACAGCCATGCCCG GGCAAGAACTCAGG	Cloning	GDF15
ACTB_F3	ACAGAGCCTCGCCTTTGCC	qPCR	ACTB
ACTB_R3	CCTCGTCGCCCACATAGGAA	qPCR	ACTB
CHOP_for1	AAGGCACTGAGCGTATCATGT	qPCR	CHOP
CHOP_rev1	GCTTTCAGGTGTGGTGATGTAT	qPCR	CHOP
EGR1_for	AGCCCTACGAGCACCTGAC	qPCR	EGR1
EGR1_rev	GAGTGGTTTGGCTGGGGTAA	qPCR	EGR1
GDF15_F1	ATTCGAACACCGACCTCGTC	qPCR	GDF15
GDF15_R1	CGAGAGATACGCAGGTGCAG	qPCR	GDF15
HPV16E6all_for	CAATGTTTCAGGACCCACAGG	qPCR	16E6/E7
HPV16E6all_rev	CTCACGTCGCAGTAACTGTTG	qPCR	16E6/E7
HPV18E7_for	ATGCATGGACCTAAGGCAAC	qPCR	18E6/E7
HPV18E7_rev	AGGTCGTCTGCTGAGCTTTC	qPCR	18E6/E7
p53_F2	CTGAGGTTGGCTCTGACTGT	qPCR	TP53
p53_R2	CAAAGCTGTTCCGTCCCAGT	qPCR	TP53
CMV_for	CGCAAATGGGCGGTAGGCGTG	Sequencing	pCEP
GDF15_seq_F1	AGGCTGGAATGGTGTCCTCAT	Sequencing	GDF15
GDF15_seq_R1	GATATTCCTACCCAGGGCACAG	Sequencing	GDF15
hU6_for	ACGATACAAGGCTGTTAGAGAGA	Sequencing	pLenti_CRISPR
M13_rev	CAGGAAACAGCTATGAC	Sequencing	pSUPER

To generate pSUPER plasmids, synthetic oligonucleotides with *Bgl*II and *Hind*III compatible ends were ordered from Sigma-Aldrich. For annealing, equimolar amounts of the sense and antisense oligonucleotides were solved in 50 µl 1x TNE buffer (100 mM NaCl, 10 mM Tris

(pH 7.5), 1 mM EDTA). After a short denaturation step at 95 °C for 5 min, the sample was incubated in a 70 °C warm water bath for 10 min and slowly cooled down to 30-40 °C. The pSUPER vector was sequentially digested with *Hind*III and *Bgl*II and ligated with the annealed oligonucleotides (see 4.3.4). *E. coli* TG2 were transformed (see 4.3.1) with the ligation mix and selected with Amp. Successful cloning was validated by analytical double RED with *Eco*R1 and *Hind*III (see 4.3.4) and sequencing with primer M13_rev. Primer and other oligonucleotides used in this thesis were ordered from Sigma-Aldrich. Primer sequences are listed in Table 6. Sequencing services were provided by Eurofins Scientific. Gained sequences were analyzed with the Basic Local Alignment Search Tool provided by the National Center for Biotechnology Information.

The shRNA target sequences encoded by pSUPER constructs are listed in Table 7. The control shRNAs, shContr-1 and shNeg, are characterized by mismatching to all known human genes in at least four DNA bases.

Table 7 Target sequences of shRNAs

Plasmid	Target sequence
pSUPER/pCEP_sh	-
pSUPER/pCEP_shContr-1	CAGUCGCGUUUGCGACUGG
pSUPER/pCEP_shNeg	UACGACCGGUCUAUCGUAG
pSUPER/pCEP_shGDF15.1	UCCCAUGGUGCUCAUUCAA
pSUPER/pCEP_shGDF15.3	CCAAAGACUGCCACUGCAU
pSUPER/pCEP_shGDF15.4	UGCAAGUGACCAUGUGCAU
pSUPER/pCEP_shGDF15.5	GCUACAAUCCCAUGGUGCU

4.3.5.2. Subcloning of pCEP plasmids

Several pCEP plasmids were subcloned from the episomal pCEP4 vector (Thermo Fisher Scientific) for the stable expression of shRNAs in CFAs or the overexpression of proteins in human cells. Hygromycin B is used for the selection of pCEP-transfected human cells.

For the subcloning of pCEP constructs coding for shRNAs, the pCEP4 vector was digested with *Bgl*II and *Xho*I. After the shRNA expression cassette was cut out from the corresponding pSUPER construct with *Bam*HI and *Xho*I, it was ligated with the prepared pCEP backbone. *E. coli* TG2 cells were transformed with the ligation mix and selected with Amp. For validation of cloning, plasmids from formed colonies were analyzed by RED with *Sal*I or by sequencing with primer CMV_for. The shRNA target sequences encoded by pCEP constructs are listed in Table 7. The pCEP_sh vector contains only the empty shRNA expression cassette from pSUPER.

For the overexpression of GDF15, the cDNA of GDF15 wildtype and its N-glycosylation mutant GDF15(N70A) were subcloned from pcDNA3.1/NAG-1[62] and pNAG1GFP_N70A[97], respectively, by PCR. The used PCR primers were designed to introduce a Kozak sequence and a *Kpn*I restriction site into the 5' end and a Hind*III* restriction site into the 3' end of the PCR amplicon. For the PCR mix, 100 ng plasmid DNA, 0.25 µM forward primer (GDF15_KpnI_for), 25 µM reverse primer (GDF15_HindIII_rev), 200 µM of each dNTP, 2.5 U of cloned *Pfu* DNA polymerase AD and 10 µl 10x Cloned *Pfu* Reaction Buffer AD were filled up with water to a final volume of 100 µl. PCR program 1 (listed in Table 8) and the PTC-200 Peltier Thermal Cycler (MJ Research, Bio-Rad Laboratories) were used for amplification. The PCR product and pCEP4 were digested with *Kpn*I and *HindIII* and subsequently ligated. *E. coli* TG2 cells were transformed with the ligation mix and selected with Amp. For verification of successful cloning, analytical REDs with *Rsr*II and sequencing with primer CMV_for were performed.

Table 8 PCR program 1

Step	Temperature	Time	Cycle
Initial denaturation	94 °C	3 min	
Annealing	58 °C	1 min	30x
Elongation	72 °C	1 min	
Denaturation	94 °C	30 s	
Final annealing	58 °C	1 min	
Final elongation	72 °C	10 min	

4.3.5.3. Cloning of pLentiCRISPR plasmids

In order to knockout *GDF15* in cervical cancer cells, the CRISPR (clustered regularly interspaced short palindromic repeats)/Cas9 (CRISPR-associated protein 9) system was used.[265] Cas9 was originally discovered in the bacterial strain *Streptococcus pyogenes* as part of an adapting defense mechanism against phages (reviewed by Horvath and Barrangou).[266] The used pLentiCRISPR_v1 vector (Addgene, USA, plasmid #49535) encodes for both essential components of this technique, the endonuclease Cas9 and a (single) guide RNA ((s)gRNA). At its 5' end, the gRNA contains 20 nucleotides that are complementary to a sequence in the gene of interest that is directly followed by a so-called protospacer adjacent motif (PAM; here NGG). The 3' end of the gRNA forms a hairpin-like structure, which serves as binding site for Cas9 in order to recruit the nuclease to the target gene. At the target site, Cas9 introduces double-strand breaks in the DNA close to the PAM sequence, which are repaired in the transfected cells, inter alia also by error-prone repair mechanisms like the non-

homologous end joining. This can finally lead to permanent alterations in the reading frame and therefore to the knockout of the gene of interest.

The online tool E-CRISP version 5.4 (http://www.e-crisp.org/E-CRISP/, provided by the Boutros lab, DKFZ Heidelberg, Germany) was used to identify suitable gRNA sequences targeting the first exon of *GDF15*. In addition to the directing 20 nucleotides, the sense strand (alias top strand) contained the short sequence CACC at its 5' end and the antisense strand (alias bottom strand) was extended at its 5' end with the motif AAC in order to provide sticky ends for cloning after annealing. Designed oligonucleotides are listed in Table 9.

Table 9 Sequences of top and bottom oligonucleotides for gRNAs targeting *GDF15*

Name of gRNA	Sense	Sequence of oligonucleotide
sgGDF15_1	top	CACCGGACCTGCTAACCAGGCTGC
	bottom	AAACGCAGCCTGGTTAGCAGGTCC
sgGDF15_2	top	CACCTTCGAACACCGACCTCGTCC
	bottom	AAACGGACGAGGTCGGTGTTCGAA
sgGDF15_3	top	CACCGAGTGCAACTCTGAGGGTCC
	bottom	AAACGGACCCTCAGAGTTGCACTC
sgGDF15_4	top	CACCGGCTCGCCTCGGCCAGAGAC
	bottom	AAACGTCTCTGGCCGAGGCGAGCC

For the cloning of the pLentiCRISPR constructs a protocol from Sanjana *et al.* was used.[267] To this end, the top and bottom oligonucleotides for each gRNA were denatured by heating to 95 °C for 5 min and then annealed by slowly ramping down to 25 °C (5 °C/min) in a thermocycler. The pLentiCRISPRv1 vector was digested with *Bsm*BI and ligated with the annealed insert (4.3.4). *E. coli* Stbl3 cells were transformed with the ligation mix (see 4.3.1) and streaked on LB-Amp agar plates. For validation of successful cloning, plasmids were sequenced with primer hU6_for.

4.4. RNA-based methods

4.4.1. RNA extraction from mammalian cells

The PureLink RNA Mini Kit (Thermo Fisher Scientific) was applied to purify total RNA from mammalian cells according to the manufacturer's protocol. Here, cells were washed with ice-cold PBS. Then, 600 µl RNA lysis buffer was freshly mixed with 6 µl 2-mercaptoethanol per sample and was used to lyse cells of a 6 cm dish or of three wells of a 96-well plate. An additional 15-min-step at RT was conducted with PureLink DNase (Thermo Fisher Scientific) to digest DNA. The concentration of the purified RNA was measured with the NanoDrop. Purified samples were stored at -80 °C.

4.4.2. Reverse transcription

For the transcription of mRNA into cDNA, the ProtoScript First Strand cDNA Synthesis Kit from NEB was used, and incubation steps were conducted in a thermal cycler. In brief, 0.5 µg purified total RNA was mixed with 1 µl Random and Oligo $d(T)_{23}VN$ primer mix (ratio 1:1) and filled up to a volume of 4 µl with RNAse-free water. This RNA-primer solution was incubated at 70 °C for 5 min and afterwards cooled down to 4 °C for removal of secondary RNA structures and efficient annealing of primers. After addition of 1 µl M-MuLV enzyme and 5 µl 2x M-MuLV Reaction Mix, the 10 µl mixture was incubated at 25 °C for 5 min for an initial elongation of in particular random primers and then at 42 °C for 1h for cDNA strand polymerization. After the reverse transcriptase was inactivated by heating to 80 °C for 5 min, the cDNA products were diluted with 40 µl RNAse-free water and were stored at -20 °C.

4.4.3. Quantitative real-time polymerase chain reaction (qRT-PCR)

The amounts of target mRNAs were determined by quantitative real-time polymerase chain reaction (qRT-PCR) by the comparative Ct method.[268] To this end, *ACTB* mRNA expression was used as endogenous control. For statistical analyses, the fold change data were transformed logarithmically. Prior to use, all primers were evaluated for sufficient amplification efficiency (90-110%) by generation of a standard curve running serial dilutions. Additionally, qPCR amplicons of the primer standard curve were tested for the right fragment size in agarose gel electrophoresis. Samples were measured in duplicates and a control sample in which cDNA was replaced with water was included for each primer mix. For each sample, dissociation curves were determined to detect potential unspecific amplification artefacts. The sequences of used qPCR primers can be found in Table 6. The primer sets for HPV16 E6/E7 and HPV18 E6/E7 recognize all three classes of their respective transcripts.

Table 10 PCR program 2 (qRT-PCR)

Stage	Step	Temperature	Time	Cycle	Purpose
1	Initiation	50 °C	2 min	1x	Normalization on internal standard dye ROX
2	Initial denaturation	95 °C	10 min	1x	Removal of secondary structures
3	Denaturation	95 °C	15 s	40x	Quantification of samples
	Elongation	60 °C	1 min		
4	Denaturation	95 °C	15 s	1x	Measuring of dissociation curves
	Elongation	60 °C	1 min		
	Denaturation	95 °C	15 s		
	Elongation	60 °C	15 s		

Firstly, primer master mixes were prepared for each primer set of a qPCR run. To this end, 10 µl 2xSYBR Green PCR Master Mix (Thermo Fisher Scientific), 0.4 µl 5 µM reverse primer and 0.4 µl 5 µM forward primer were mixed with water to a final volume of 18 µl per sample. After the primer master mix was aliquoted into wells of a 96-well plate (MicroAmp Optical 96-Well Reaction Plate, Thermo Fisher Scientific), 2 µl diluted cDNA (see chapter 4.4.2) were added. If the cellular copy number of mRNA was very low, the volume of the diluted cDNA was increased (max. 9.2 µl) by replacing the corresponding volume of water in the 20 µl qPCR mixture. The qPCR plate was sealed with MicroAmp Optical Adhesive Film (Thermo Fisher Scientific) and was run in a 7300 Real Time PCR System (Thermo Fisher Scientific) with PCR program 2 (Table 10).

4.5. Protein-based methods

4.5.1. Protein extraction from mammalian cells

To collect protein extracts for immunoblot analyses, all used buffers were cooled down to 4 °C and steps were carried out on ice if possible. Cultured cells were washed with PBS and harvested by scrapping in 0.5 ml PBS. The cell suspension was transferred into a 1.5 ml reaction tube and centrifuged at 13,000x *g* for 10 s. The cell pellet was either stored at -20 °C or directly resuspended in 30-150 µl CSK1 lysis buffer (300 mM NaCl, 300 mM sucrose, 10 mM Pipes, 1 mM $MgCl_2$, 1 mM EDTA, 0.5% Triton X-100; freshly added: 10% PhosSTOP phosphatase inhibitor cocktail (Roche Diagnostics), 2.5 mM of the serine protease inhibitor Pefabloc (Merck) and 1% P8340 phosphatase inhibitor cocktail (Sigma-Aldrich)). The cells were lysed for 30 min on ice, and the lysate was centrifuged at 13,000x *g* and 4 °C for 5 min to remove cellular debris. Afterwards, the supernatant was transferred into a new 1.5 ml reaction tube. For kinetics, all samples were harvested at the corresponding time points and the cell pellets were frozen at -20 °C. Finally, all collected samples were thawed and purified together.

The Bio-Rad Protein Assay (Bio-Rad) was applied to measure the total protein concentration according to the manufacturer's protocol. The assay is based on the Bradford protein assay,[269] in which the absorbance of the dye Coomassie Brilliant Blue G-250 is shifted when binding to protein under acidic conditions. For spectroscopic analyses of this shift at 595 nm, disposable cuvettes (Sigma-Aldrich) and the BioPhotometer D30 (Eppendorf) were used. The protein concentrations were determined by comparison to values gained from a bovine serum albumin (BSA) standard curve.

In order to remove secondary protein structures and to reduce disulfide bonds, protein lysates were adjusted to the desired concentration (1-5 µg/µl) by adding 4x protein loading buffer (250 mM Tris-HCl (pH 6.8), 40% glycerol, 20% 2-mercaptoethanol, 8% SDS,

0.008% bromophenol blue) and incubated at 96 °C for 5 min for denaturation. The cooled samples were analyzed by immunoblotting and stored at -80 °C.

4.5.2. Collection of cell culture supernatant

For immunoblot analyses of proteins in the cell culture supernatant (CCS), 2 ml CCS of 6 cm dishes were transferred into a reaction tube and were centrifuged at 1,000x *g* and 4 °C for 5 min to remove remaining cells. After moving the supernatant into a new reaction tube, further cell debris was pelleted by centrifugation at 13,000x *g* and 4 °C for 15 min. Then, 1.5 ml supernatant was transferred into a new reaction tube. As needed, 3x volume purified CCS were diluted with 1x volume 4x protein loading buffer, heated at 96 °C for 5 min and stored at -80 °C. Meanwhile, intracellular proteins were extracted from the cultured cells as well and total protein concentration was determined by the Bio-Rad Protein Assay as described above. In order to compare proteins of the CCSs in immunoblot analyses, the loading volumes of the purified CCSs were normalized on amounts of total intracellular protein.

4.5.3. SDS polyacrylamide gel electrophoresis (SDS-PAGE)

For comparison of protein samples, they were separated according to their size by SDS polyacrylamide gel electrophoresis (SDS-PAGE).[270] SDS-PAGE gels were prepared according to the recipe in Table 11 and poured into disposable gel cassettes (NuPAGE empty gel cassettes mini, Thermo Fisher scientific) or in glass plates of the same size, which have been sealed with 1% agarose solution. For storage at 4 °C, polymerized gels were wrapped in paper towels soaked with SDS-PAGE running buffer (19.2 mM glycine, 2.5 mM Tris, 0.1% SDS, pH 8.3).

Table 11 Recipe of SDS-PAGE gel. For the running gel, 3 M Tris-HCl buffer (pH 8.9) and for the stacking gel, 0.47 M Tris-HCl buffer (pH 6.7) were used.

Component	Running gel (12.5%)	Stacking gel (4.6%)
Water	2.85 ml	1 ml
Tris-HCl buffer	0.9 ml	0.6 ml
30% acrylamide/bisacrylamide solution (29:1)	2.75 ml	0.31 ml
10% SDS	68.8 µl	23.4 µl
TEMED	1.7 µl	0.9 µl
10% ammonium persulfate (APS)	88.0 µl	91.7 µl

After fixing gels into an Xcell SureLock Mini-Cell Electrophoresis System (Thermo Fisher Scientific), the chamber was filled with 500 ml SDS-PAGE running buffer. Per lane, equal amounts of prepared protein extracts (10-20 µg) or adjusted volumes of CCS samples were

loaded and were run at 80-120 V for approx. 2h. As size marker, 1-2 µl peqGOLD pre-stained Protein Marker IV (PEQLAB) was loaded at least on one lane per gel.

4.5.4. Western transfer and immunodetection of proteins

Immediately after SDS-PAGE, the separated proteins were transferred onto an Immobilon-P PVDF Membrane (Merck Millipore) by semi-dry electroblotting to increase their accessibility for immunodetection. This procedure is also called Western blot.[271] To this end, the polyvinylidene difluoride (PVDF) membrane was activated by short wetting with methanol followed by incubation in Towbin transfer buffer (19.2 mM glycine, 2.5 mM Tris, 20% methanol, pH 8.3). For each gel, 8 Whatman papers fitting to the gel size were soaked in Towbin transfer buffer. A "Western blot sandwich" was formed by stacking 4 Whatman papers, the activated membrane, the gel and further 4 Whatman papers in the stated order on the anode of the Trans-Blot SD Semi-Dry Electrophoretic Transfer Cell (Bio-Rad). After removal of air bubbles in the "Western blot sandwich", the transfer device was assembled completely and the electroblotting was performed at 20 V for 1h.

Table 12 Primary antibodies

Name	Species	Supplier	#	Dilution
Anti-BiP/GRP78	Mouse	BD	610979	1:3,000
Anti-CHOP (L63F7)	Mouse	Cell Signaling	2895	1:1,000
Anti-cleaved Caspase 9 (Asp330)	Rabbit	Cell Signaling	9501	1:1,000
Anti-cleaved PARP (Asp214) (19F4)	Mouse	Cell Signaling	9546	1:1,000
Anti-GDF15 (EPR19939)	Rabbit	Abcam	ab206414	1:500
Anti-HPV16 E6 (clone 849)	Mouse	Arbor Vita Corporation		1:3,000
Anti-HPV16 E7 (NM2)	Mouse	Kind gift of Müller lab, DKFZ, Heidelberg		1:2,000
Anti-HPV18 E6 (clone 399)	Mouse	Arbor Vita Corporation		1:2,000
Anti-HPV18 E7	Chicken	Kind gift of Zentgraf lab, DKFZ, Heidelberg		1:1,000
Anti-p53 (DO-1)	Mouse	Santa Cruz	sc-126	1:1,000
Anti-Vinculin	Mouse	Santa Cruz	sc-173614	1:4,000
Anti-γ-Tubulin	Mouse	Merck Millipore	CP06	1:5,000

After the blotting, the membrane was incubated in blocking buffer 1 (0.2% Tween-20, 5% milk powder (Gabler-Saliter Milchwerk, Obergünzburg, Germany) and 1% BSA in 1xPBS) or blocking buffer 2 (137 mM NaCl, 20 mM Tris (pH 7.5), 0.2% Tween-20 and 5% BSA) for at

least 1h under gentle shaking in order to block unspecific antibody binding sites of the membrane. For simultaneous detection of proteins with dissimilar sizes, the blot was cut into pieces. The pieces contained proteins in the expected size range of the target protein. The primary antibodies were diluted either in blocking buffer 1 or blocking buffer 2. All used primary antibodies are listed in Table 12.The membrane was incubated with primary antibody solution at 4 °C under gentle shaking overnight.

The blot was washed with PBST (0.2% Tween-20 in PBS) three times for at least 10 min. Afterwards the blot was incubated with the appropriate secondary, horseradish peroxidase (HRP)-coupled antibody under gentle shaking for at least 1h at RT. All used secondary antibodies were diluted in blocking buffer 1 and are listed in Table 12. After three washing steps with PBST, target proteins were detected by enhanced chemiluminescence (ECL), a process in which the coupled HRP catalyzes the oxidation of its substrate luminol. This reaction emits light proportional to the amounts of bound target protein.

To this end, luminol and peroxide solution (Amersham ECL Prime Western Blotting Detection Reagent, GE Healthcare) were mixed in a ratio of 1:1 and added to the membrane. After incubation for 1 min at RT, the produced light was detected with the Fusion SL Detection System (Vilber Lourmat, Eberhardzell, Germany).

Table 13 Secondary antibodies

Name	Species	Supplier	#	Dilution
Anti-Chicken IgG-HRP	goat	Jackson ImmunoResearch	103-035-155	1:5,000
Anti-Mouse IgG-HRP	goat	Jackson ImmunoResearch	115-035-071	1:5,000
Anti-Rabbit IgG-HRP	goat	Jackson ImmunoResearch	111-035-003	1:5,000

4.6. Statistical analyses

Unless otherwise stated, all experiments in this thesis were performed in at least three biological replicates. Microsoft Excel (Microsoft Office 2017, Microsoft, Albuquerque, New Mexico, USA) or SigmaPlot Version 13 (Systat Software, Erkrath, Germany) were used to calculate mean values and standard deviations. Statistical significance was determined by one-sample Student's *t*-test for foldchange data and by two-sided Student's *t*-test for comparing two unpaired samples using SigmaPlot. P-values of ≤ 0.05 (*), ≤ 0.01 (**), ≤ 0.001 (***) were considered statistically significant.

Appendix

Appendix

List of plasmids

Table 14 Plasmids

Plasmid	Purpose	Target gene/ protein	Source
pBluescript II (pBS)	Carrier DNA	-	Stratagene
pcDNA3.1/NAG-1	Protein expression	GDF15	[62]
pCEP4	Expression of proteins or shRNAs	-	Thermo Fisher
pCEP4_GDF15	Protein expression	GDF15	See 4.3.5
pCEP4_GDF15(N70A)	Protein expression	GDF15 (N70A)	See 4.3.5
pCEP_sh	Control for shRNA expression	-	[272]
pCEP_shContr-1	Expression of control shRNA	-	[273]
pCEP_shGDF15.1	Expression of shRNA	*GDF15*	See 4.3.5
pCEP_shGDF15.3	Expression of shRNA	*GDF15*	See 4.3.5
pCEP_shGDF15.4	Expression of shRNA	*GDF15*	See 4.3.5
pCEP_shGDF15.5	Expression of shRNA	*GDF15*	See 4.3.5
pCEP_shNeg	Expression of control shRNA	-	[273]
pLenti_CRISPRv1	Expression of gRNA and Cas9		Addgene
pLenti_CRISPRv1_sgGDF15_1	Expression of Cas9 and gRNA	*GDF15*	See 4.3.5
pLenti_CRISPRv1_sgGDF15_2	Expression of Cas9 and gRNA	*GDF15*	See 4.3.5
pLenti_CRISPRv1_sgGDF15_3	Expression of Cas9 and gRNA	*GDF15*	See 4.3.5
pNAG1-GFP_N70A	Protein expression	GDF15 (N70A)-GFP	[97]
pSUPER	Expression of shRNA		[264]
pSUPER_contr-1	Expression of control shRNA	-	[274]
pSUPER_neg	Expression of control shRNA	-	[274]
pSUPER_shGDF15.1	Expression of shRNA	*GDF15*	See 4.3.5
pSUPER_shGDF15.3	Expression of shRNA	*GDF15*	See 4.3.5
pSUPER_shGDF15.4	Expression of shRNA	*GDF15*	See 4.3.5
pSUPER_shGDF15.5	Expression of shRNA	*GDF15*	See 4.3.5

List of figures

List of tables

Abbreviations

Abbreviation	Full form
Amp	ampicillin
ATF3	activating transcription factor 3
ATF4	activating transcription factor 4
ATF6	activating transcription factor 6
Bcl-2	B-cell lymphoma 2
BD	Becton Dickinson
BiP/GRP78	binding immunoglobulin protein/glucose-regulated protein 78
BMI	body mass index
BMP	Bone morphogenetic protein
BSA	bovine serum albumin
C/EBPβ	CCAAT enhancer binding protein beta
Cas9	CRISPR-associated protein 9
CCS	cell culture supernatant
cDNA	copy DNA
CFA	colony formation assay
CHOP	C/EBP homologous protein
CIN	cervical intraepithelial neoplasia
Cis	cisplatin, *cis*-diamminedichloridoplatinum(II)
cl.	cleaved
CPT	camptothecin
CRISPR	clustered regularly interspaced short palindromic repeats
DAPI	4',6-diamidino-2-pheylindole
DDIT3	DNA damage-inducible transcript 3
DF	DharmaFECT
DMSO	dimethyl sulfoxide
Doxo	doxorubicin
DR4	death receptor 4
DR5	death receptor 5
DREAM	dimerization partner, RB-like, E2F and MuvB
E6AP	E6-associated protein
ECL	enhanced chemiluminescence
ECM	extracellular matrix
EGR1	early growth response 1
eIF2α	eukaryotic initiation factor 2 alpha

ELF3	E74 like ETS transcription factor 3
EMT	epithelial-mesenchymal transition
EP	electrophoresis buffer
ER	endoplasmic reticulum
ERAD	ER-associated degradation
ERK	extracellular signal-regulated kinase
et al.	*et alii*
exp.	exposed
FCS	fetal calf serum
GADD34	growth arrest and DNA damage-inducible protein 34
GDF15	growth differentiation factor 15
gDNA	genomic DNA
gRNA	guide RNA
HPV	human papillomavirus
HRP	horseradish peroxidase
hTERT	human telomerase reverse transcriptase
HuR	human antigen R
HygB	hygromycin B
IC50	half maximal inhibitory concentration
IGF1	insulin-like growth factor
indels	insertions and deletions
IRE1α	inositol-requiring enzyme 1 alpha
KO	knockout
LB	Lysogeny Broth
LCR	long control region
LTBP1	latent TGFβ-binding protein 1
m.	mature
MAPK	mitogen-activated protein kinase
ME	medium exchange
MIC-1	macrophage inhibitory cytokine-1
miR	microRNA
MMP	mitochondrial membrane potential
MMP9	matrix metallopeptidase 9
mRNA	messenger RNA
NAG-1	NSAID-activated gene-1
NanoDrop	NanoDrop ND-1000 spectrophotometer

NAPA	N-ethylmaleimide-sensitive factor attachment protein alpha
NF-κB	nuclear factor “kappa-light-chain-enhancer” of activated B-cells
NEB	New England Biolabs
NSAID	non-steroidal anti-inflammatory drug
ORF	open reading frame
PARP	poly(ADP-ribose) polymerase
PBS	phosphate-buffered saline
pBS	pBluescript II
PCR	polymerase chain reaction
PCSK	proprotein convertase subtilisin/kexin
PDI	protein disulfide isomerase
PDZ	post synaptic density protein 95, disc large homolog 1, zonula occludens-1 protein
PERK	protein kinase R-like ER kinase
PI	propidium iodide
PI3K	phosphatidylinositol-4,5-bisphosphate 3-kinase
PKB	protein kinase B
PLAB	placental bone morphogenetic protein
PLC-γ	phosphoinositide phospholipase C gamma
PPAR-γ	peroxisome proliferator-activated receptor gamma
pRB	retinoblastoma protein
PSG	100 U/ml penicillin, 0.1 mg/ml streptomycin, 2 mM L-glutamine
PTGFB	placental transformation growth factor beta
PUMA	p53 upregulated modulator of apoptosis
PVDF	polyvinylidene difluoride
qRT-PCR	quantitative real-time PCR
RED	restriction enzyme digest
RNAi	RNA interference
RT	room temperature
SDS	sodium dodecyl sulfate
SDS-PAGE	SDS-polyacrylamide gel electrophoresis
SERCA	sarco-endoplasmic reticulum Ca^{2+}-ATPase
shRNA	short-hairpin RNA
siRNA	small interfering RNA
Smad	Sma, Mad (Mothers against decapentaplegic)
SSide	sulindac sulfide
TG	thapsigargin

TGFBR	transforming growth factor beta receptor
TGF-β	transforming growth factor beta
TIMP3	tissue inhibitor of metalloproteinase 3
TM	tunicamycin
TUNEL	terminal deoxynucleotidyl transferase dUTP nick end labelling
uncl.	uncleaved
UPR	unfolded protein response
VLP	virus-like particle
XBP1	X-box binding protein 1
Yip1A	Yip1 interacting factor homolog A

The one-letter code for nucleotides was applied according to declarations by the International Union of Pure and Applied Chemistry (IUPAC).

Units and prefixes

Units

%	percent
°C	degree Celsius
Da	Dalton
g	gravitational acceleration
g	gram
h	hour
l	liter
M	molar, mol/l
m	meter
min	minute
mol	mole
s	second
U	enzyme activity unit
V	volt

Prefixes

Symbol	Prefix	Factor
p	pico	10^{-12}
n	nano	10^{-9}
µ	micro	10^{-6}
m	milli	10^{-3}
c	centi	10^{-2}
k	kilo	10^{3}

References

1. Bray, F. *et al.* Global cancer statistics 2018: GLOBOCAN estimates of incidence and mortality worldwide for 36 cancers in 185 countries. *CA: A Cancer Journal for Clinicians* **68**, 394–424 (2018).
2. Dürst, M., Gissmann, L., Ikenberg, H. & zur Hausen, H. A papillomavirus DNA from a cervical carcinoma and its prevalence in cancer biopsy samples from different geographic regions. *Proceedings of the National Academy of Sciences of the United States of America* **80**, 3812–5 (1983).
3. de Martel, C., Georges, D., Bray, F., Ferlay, J. & Clifford, G. M. Global burden of cancer attributable to infections in 2018: a worldwide incidence analysis. *The Lancet Global Health* **8**, e180–e190 (2020).
4. Hasche, D., Vinzón, S. E. & Rösl, F. Cutaneous papillomaviruses and non-melanoma skin cancer: Causal agents or innocent bystanders? *Frontiers in Microbiology* **9**, 1–19 (2018).
5. Bravo, I. G., Crusius, K. & Alonso, A. The E5 protein of the human papillomavirus type 16 modulates composition and dynamics of membrane lipids in keratinocytes. *Archives of virology* **150**, 231–46 (2005).
6. Bernard, H. U. *et al.* Classification of papillomaviruses (PVs) based on 189 PV types and proposal of taxonomic amendments. *Virology* **401**, 70–79 (2010).
7. Sharma, S. & Munger, K. The Role of Long Noncoding RNAs in Human Papillomavirus-associated Pathogenesis. *Pathogens* **9**, 289 (2020).
8. Bouvard, V. *et al.* A review of human carcinogens--Part B: biological agents. *The lancet oncology* **10**, 321–322 (2009).
9. Butz, K. & Hoppe-Seyler, F. Transcriptional control of human papillomavirus (HPV) oncogene expression: composition of the HPV type 18 upstream regulatory region. *Journal of Virology* **67**, 6476–6486 (1993).
10. Doorbar, J. Molecular biology of human papillomavirus infection and cervical cancer. *Clinical Science* **110**, 525–541 (2006).
11. Bergvall, M., Melendy, T. & Archambault, J. The E1 proteins. *Virology* **445**, 35–56 (2013).
12. McBride, A. A. The Papillomavirus E2 proteins. *Virology* **445**, 57–79 (2013).
13. Vande Pol, S. B. & Klingelhutz, A. J. Papillomavirus E6 oncoproteins. *Virology* **445**, 115–137 (2013).
14. Roman, A. & Munger, K. The papillomavirus E7 proteins. *Virology* **445**, 138–168 (2013).
15. DiMaio, D. & Petti, L. M. The E5 proteins. *Virology* **445**, 99–114 (2013).

16. Schwarz, E. *et al.* Structure and transcription of human papillomavirus sequences in cervical carcinoma cells. *Nature* **314**, 111–114 (1985).
17. Doorbar, J. The E4 protein; structure, function and patterns of expression. *Virology* **445**, 80–98 (2013).
18. Buck, C. B., Day, P. M. & Trus, B. L. The papillomavirus major capsid protein L1. *Virology* **445**, 169–174 (2013).
19. Wang, J. W. & Roden, R. B. S. L2, the minor capsid protein of papillomavirus. *Virology* **445**, 175–186 (2013).
20. Schiffman, M., Castle, P. E., Jeronimo, J., Rodriguez, A. C. & Wacholder, S. Human papillomavirus and cervical cancer. *Lancet (London, England)* **370**, 890–907 (2007).
21. Schiffman, M. *et al.* Carcinogenic human papillomavirus infection. *Nature Reviews Disease Primers* **2**, 16086 (2016).
22. Gustafsson, L. & Adami, H. O. Natural history of cervical neoplasia: Consistent results obtained by an identification technique. *British Journal of Cancer* **60**, 132–141 (1989).
23. Dürst, M., Dzarlieva-Petrusevska, R. T., Boukamp, P., Fusenig, N. E. & Gissmann, L. Molecular and cytogenetic analysis of immortalized human primary keratinocytes obtained after transfection with human papillomavirus type 16 DNA. *Oncogene* **1**, 251–6 (1987).
24. Walboomers, J. M. *et al.* Human papillomavirus is a necessary cause of invasive cervical cancer worldwide. *The Journal of pathology* **189**, 12–9 (1999).
25. Wentzensen, N., Vinokurova, S. & Von Knebel Doeberitz, M. Systematic review of genomic integration sites of human papillomavirus genomes in epithelial dysplasia and invasive cancer of the female lower genital tract. *Cancer Research* **64**, 3878–3884 (2004).
26. Dooley, K. E., Warburton, A. & McBride, A. A. Tandemly integrated HPV16 can form a brd4-dependent super-enhancer-like element that drives transcription of viral oncogenes. *mBio* **7**, 1–10 (2016).
27. Jeon, S. & Lambert, P. F. Integration of human papillomavirus type 16 DNA into the human genome leads to increased stability of E6 and E7 mRNAs: implications for cervical carcinogenesis. *Proceedings of the National Academy of Sciences* **92**, 1654–1658 (1995).
28. McBride, A. A. & Warburton, A. The role of integration in oncogenic progression of HPV-associated cancers. *PLoS Pathogens* **13**, 1–7 (2017).
29. Butz, K. *et al.* siRNA targeting of the viral E6 oncogene efficiently kills human papillomavirus-positive cancer cells. *Oncogene* **22**, 5938–5945 (2003).
30. Hall, A. H. S. & Alexander, K. A. RNA Interference of Human Papillomavirus Type 18 E6 and E7 Induces Senescence in HeLa Cells. *Journal of Virology* **77**, 6066–6069

(2003).

31. Jabbar, S. F., Abrams, L., Glick, A. & Lambert, P. F. Persistence of high-grade cervical dysplasia and cervical cancer requires the continuous expression of the human papillomavirus type 16 E7 oncogene. *Cancer Research* **69**, 4407–4414 (2009).
32. Yamato, K. *et al.* New highly potent and specific E6 and E7 siRNAs for treatment of HPV16 positive cervical cancer. *Cancer Gene Therapy* **15**, 140–153 (2008).
33. Hoppe-Seyler, K., Bossler, F., Braun, J. A., Herrmann, A. L. & Hoppe-Seyler, F. The HPV E6/E7 Oncogenes: Key Factors for Viral Carcinogenesis and Therapeutic Targets. *Trends in Microbiology* **26**, 158–168 (2018).
34. Gheit, T. Mucosal and Cutaneous Human Papillomavirus Infections and Cancer Biology. *Frontiers in Oncology* **9**, (2019).
35. Hawley-Nelson, P., Vousden, K. H., Hubbert, N. L., Lowy, D. R. & Schiller, J. T. HPV16 E6 and E7 proteins cooperate to immortalize human foreskin keratinocytes. *The EMBO journal* **8**, 3905–10 (1989).
36. Duensing, S. & Münger, K. Mechanisms of genomic instability in human cancer: Insights from studies with human papillomavirus oncoproteins. *International Journal of Cancer* **109**, 157–162 (2004).
37. Frolov, M. V. & Dyson, N. J. Molecular mechanisms of E2F-dependent activation and pRB-mediated repression. *Journal of Cell Science* **117**, 2173–2181 (2004).
38. Gheit, T. Mucosal and cutaneous human papillomavirus infections and cancer biology. *Frontiers in Oncology* **9**, (2019).
39. Boyer, S. N., Wazer, D. E. & Band, V. E7 protein of human papilloma virus-16 induces degradation of retinoblastoma protein through the ubiquitin-proteasome pathway. *Cancer Research* **56**, 4620–4624 (1996).
40. Fischer, M., Uxa, S., Stanko, C., Magin, T. M. & Engeland, K. Human papilloma virus E7 oncoprotein abrogates the p53-p21-DREAM pathway. *Scientific Reports* **7**, 1–11 (2017).
41. Aubrey, B. J., Kelly, G. L., Janic, A., Herold, M. J. & Strasser, A. How does p53 induce apoptosis and how does this relate to p53-mediated tumour suppression? *Cell Death and Differentiation* **25**, 104–113 (2018).
42. Scheffner, M., Huibregtse, J. M., Vierstra, R. D. & Howley, P. M. The HPV-16 E6 and E6-AP complex functions as a ubiquitin-protein ligase in the ubiquitination of p53. *Cell* **75**, 495–505 (1993).
43. Kühne, C., Gardiol, D., Guarnaccia, C., Amenitsch, H. & Banks, L. Differential regulation of human papillomavirus E6 by protein kinase A: Conditional degradation of human discs large protein by oncogenic E6. *Oncogene* **19**, 5884–5891 (2000).
44. Liu, X. *et al.* HPV E6 protein interacts physically and functionally with the cellular

telomerase complex. *Proceedings of the National Academy of Sciences of the United States of America* **106**, 18780–18785 (2009).

45. Appleby, P. *et al.* Carcinoma of the cervix and tobacco smoking: Collaborative reanalysis of individual data on 13,541 women with carcinoma of the cervix and 23,017 women without carcinoma of the cervix from 23 epidemiological studies. *International Journal of Cancer* **118**, 1481–1495 (2006).
46. Rajkumar, T. *et al.* Cervical carcinoma and reproductive factors: Collaborative reanalysis of individual data on 16,563 women with cervical carcinoma and 33,542 women without cervical carcinoma from 25 epidemiological studies. *International Journal of Cancer* **119**, 1108–1124 (2006).
47. Collaboration, I., Studies, E. & Cancer, C. Cervical cancer and hormonal contraceptives: collaborative reanalysis of individual data for 16 573 women with cervical cancer and 35 509 women without cervical cancer from 24 epidemiological studies. *The Lancet* **370**, 1609–1621 (2007).
48. Bzhalava, D., Guan, P., Franceschi, S., Dillner, J. & Clifford, G. A systematic review of the prevalence of mucosal and cutaneous human papillomavirus types. *Virology* **445**, 224–231 (2013).
49. Lehtinen, M. & Dillner, J. Clinical trials of human papillomavirus vaccines and beyond. *Nature reviews. Clinical oncology* **10**, 400–10 (2013).
50. Macartney, K. K., Chiu, C., Georgousakis, M. & Brotherton, J. M. L. Safety of human papillomavirus vaccines: A review. *Drug Safety* **36**, 393–412 (2013).
51. Takla, A. *et al.* Background paper for the recommendation of HPV vaccination for boys in Germany. *Bundesgesundheitsblatt - Gesundheitsforschung - Gesundheitsschutz* **61**, 1170–1186 (2018).
52. Pouyanfard, S. & Müller, M. Human papillomavirus first and second generation vaccines-current status and future directions. *Biological chemistry* **398**, 871–889 (2017).
53. Bruni, L. *et al.* Global estimates of human papillomavirus vaccination coverage by region and income level: A pooled analysis. *The Lancet Global Health* **4**, e453–e463 (2016).
54. Cullmann, C. *et al.* Oncogenic human papillomaviruses block expression of the B-cell translocation gene-2 tumor suppressor gene. *International Journal of Cancer* **125**, 2014–2020 (2009).
55. Cohen, P. A., Jhingran, A., Oaknin, A. & Denny, L. Cervical cancer. *The Lancet* **393**, 169–182 (2019).
56. Chen, S. H. & Chang, J. Y. New insights into mechanisms of cisplatin resistance: From tumor cell to microenvironment. *International Journal of Molecular Sciences* **20**, (2019).
57. Pal, A. & Kundu, R. Human Papillomavirus E6 and E7: The Cervical Cancer Hallmarks and Targets for Therapy. *Frontiers in Microbiology* **10**, (2020).

58. Westrich, J. A., Warren, C. J. & Pyeon, D. Evasion of host immune defenses by human papillomavirus. *Virus Research* **231**, 21–33 (2017).
59. Dymalla, S. *et al.* A novel peptide motif binding to and blocking the intracellular activity of the human papillomavirus E6 oncoprotein. *Journal of Molecular Medicine* **87**, 321–331 (2009).
60. Kuner, R. *et al.* Identification of cellular targets for the human papillomavirus E6 and E7 oncogenes by RNA interference and transcriptome analyses. 1253–1262 (2007). doi:10.1007/s00109-007-0230-1
61. Yokoyama-Kobayashi, M., Saeki, M., Sekine, S. & Kato, S. Human cDNA encoding a novel TGF-beta superfamily protein highly expressed in placenta. *Journal of biochemistry* **122**, 622–6 (1997).
62. Baek, S. J., Kim, K.-S., Nixon, J. B., Wilson, L. C. & Eling, T. E. Cyclooxygenase Inhibitors Regulate the Expression of a TGF-beta Superfamily Member That Has Proapoptotic and Antitumorigenic Activities. *Mol. Pharmacol.* **59**, 901–908 (2001).
63. Hromas, R. *et al.* PLAB, a novel placental bone morphogenetic protein. *Biochimica et Biophysica Acta - Gene Structure and Expression* **1354**, 40–44 (1997).
64. Lawton, L. N. *et al.* Identification of a novel member of the TGF-beta superfamily highly expressed in human placenta. *Gene* **203**, 17–26 (1997).
65. Paralkar, V. M. *et al.* Cloning and characterization of a novel member of the transforming growth factor-β/bone morphogenetic protein family. *Journal of Biological Chemistry* **273**, 13760–13767 (1998).
66. Bootcov, M. R. *et al.* MIC-1, a novel macrophage inhibitory cytokine, is a divergent member of the TGF-beta superfamily. *Proceedings of the National Academy of Sciences of the United States of America* **94**, 11514–9 (1997).
67. Yamaguchi, K. *et al.* Molecular characterisation of canine nonsteroidal anti-inflammatory drug-activated gene (NAG-1). *Veterinary Journal* **175**, 89–95 (2008).
68. Hsiao, E. C. *et al.* Characterization of Growth-Differentiation Factor 15, a Transforming Growth Factor beta Superfamily Member Induced following Liver Injury. *Molecular and Cellular Biology* **20**, 3742–3751 (2000).
69. Uhlén, M. *et al.* Tissue-based map of the human proteome. *Science* **347**, (2015).
70. Appierto, V. *et al.* Analysis of gene expression identifies PLAB as a mediator of the apoptotic activity of fenretinide in human ovarian cancer cells. *Oncogene* **26**, 3952–3962 (2007).
71. Hinoi, E. *et al.* Positive regulation of osteoclastic differentiation by growth differentiation factor 15 upregulated in osteocytic cells under hypoxia. *Journal of Bone and Mineral Research* **27**, 938–949 (2012).
72. Wang, T. *et al.* GDF 15 is a heart-derived hormone that regulates body growth . *EMBO*

Molecular Medicine **9**, 1150–1164 (2017).

73. Chen, Y. *et al.* Activation of Nonsteroidal Anti-Inflammatory Drug-Activated Activated Protein Kinase Revealed a Isochaihulactone-Triggered Apoptotic Pathway in Human Lung Cancer A549 Cells. *Pharmacology* **323**, 746–756 (2007).
74. Patel, S. *et al.* GDF15 Provides an Endocrine Signal of Nutritional Stress in Mice and Humans. *Cell Metabolism* **29**, 707-718.e8 (2019).
75. Böttner, M. *et al.* Characterization of the rat, mouse, and human genes of growth/differentiation factor-15/macrophage inhibiting cytokine-1 (GDF-15/MIC-1). *Gene* **237**, 105–11 (1999).
76. Tan, M., Wang, Y., Guan, K. & Sun, Y. PTGF-beta, a type beta transforming growth factor (TGF-beta) superfamily member, is a p53 target gene that inhibits tumor cell growth via TGF-beta signaling pathway. *Proceedings of the National Academy of Sciences of the United States of America* **97**, 109–14 (2000).
77. Park, S. H. *et al.* Two in-and-out modulation strategies for endoplasmic reticulum stress-linked gene expression of pro-apoptotic macrophage-inhibitory cytokine 1. *Journal of Biological Chemistry* **287**, 19841–19855 (2012).
78. Chung, H. K. *et al.* Growth differentiation factor 15 is a myomitokine governing systemic energy homeostasis. *Journal of Cell Biology* **216**, 149–165 (2017).
79. Lee, S. H., Krisanapun, C. & Baek, S. J. NSAID-activated gene-1 as a molecular target for capsaicin-induced apoptosis through a novel molecular mechanism involving GSK3β, C/EBPβ and ATF3. *Carcinogenesis* **31**, 719–728 (2010).
80. Baek, S. J. *et al.* Cyclooxygenase Inhibitors Induce the Expression of the Tumor Suppressor Gene EGR-1, Which Results in the Up-Regulation of NAG-1, an Antitumorigenic Protein. *Molecular Pharmacology* **67**, 356–64 (2004).
81. Baek, S. J., Horowitz, J. M. & Eling, T. E. Molecular cloning and characterization of human nonsteroidal anti-inflammatory drug-activated gene promoter. Basal transcription is mediated by Sp1 and Sp3. *Journal of Biological Chemistry* **276**, 33384–33392 (2001).
82. Kadowaki, M. *et al.* DNA methylation-mediated silencing of nonsteroidal anti-inflammatory drug-activated gene (NAG-1/GDF15) in glioma cell lines. *International Journal of Cancer* **130**, 267–277 (2012).
83. Martinez, J. M. *et al.* Drug-Induced Expression of Nonsteroidal Anti-Inflammatory Drug-Activated Gene/Macrophage Inhibitory Cytokine-1/Prostate-Derived Factor, a Putative Tumor Suppressor, Inhibits Tumor Growth. *Journal of Pharmacology and Experimental Therapeutics* **318**, 899–906 (2006).
84. Yamaguchi, K., Lee, S.-H., Eling, T. E. & Baek, S. J. A novel peroxisome proliferator–activated receptor γ ligand, MCC-555, induces apoptosis via posttranscriptional

regulation of NAG-1 in colorectal cancer cells. *Molecular Cancer Therapeutics* **5**, 1352–1361 (2006).

85. Newman, D. *et al.* Differential regulation of nonsteroidal anti-inflammatory drug-activated gene in normal human tracheobronchial epithelial and lung carcinoma cells by retinoids. *Molecular Pharmacology* **63**, 557–564 (2003).
86. Zhang, X. *et al.* GL-V9 induced upregulation and mitochondrial localization of NAG-1 associates with ROS generation and cell death in hepatocellular carcinoma cells. *Free Radical Biology and Medicine* **112**, 49–59 (2017).
87. Bauskin, A. R. A. R. A. R. *et al.* The propeptide of macrophage inhibitory cytokine (MIC-1), a TGF-beta superfamily member, acts as a quality control determinant for correctly folded MIC-1. *The EMBO journal* **19**, 2212–20 (2000).
88. Fairlie, W. D. *et al.* The Propeptide of the Transforming Growth Factor-β Superfamily Member, Macrophage Inhibitory Cytokine-1 (MIC-1), Is a Multifunctional Domain That Can Facilitate Protein Folding and Secretion. *Journal of Biological Chemistry* **276**, 16911–16918 (2001).
89. Li, J. J. *et al.* Growth Differentiation Factor 15 Maturation Requires Proteolytic Cleavage by PCSK3, -5, and -6. *Molecular and Cellular Biology* **38**, (2018).
90. Hsu, J. Y. *et al.* Non-homeostatic body weight regulation through a brainstem-restricted receptor for GDF15. *Nature* **550**, 255–259 (2017).
91. Bauskin, A. R. *et al.* The propeptide of macrophage inhibitory cytokine (MIC-1), a TGF-β superfamily member, acts as a quality control determinant for correctly folded MIC-1. *The EMBO Journal* **19**, 2212–2220 (2000).
92. Sha, X., Brunner, A. M., Purchio, A. F. & Gentry, L. E. Transforming growth factor β1: Importance of glycosylaytion and acidic proteases for processing and secretion. *Molecular Endocrinology* **3**, 1090–1098 (1989).
93. Gray, A. & Mason, A. Requirement for activin A and transforming growth factor-beta 1 pro-regions in homodimer assembly. *Science* **247**, 1328–1330 (1990).
94. Fairlie, W. D. *et al.* The propeptide of the transforming growth factor-beta superfamily member, macrophage inhibitory cytokine-1 (MIC-1), is a multifunctional domain that can facilitate protein folding and secretion. *The Journal of biological chemistry* **276**, 16911–8 (2001).
95. Bauskin, A. R. *et al.* The TGF-β Superfamily Cytokine MIC-1/GDF15: Secretory Mechanisms Facilitate Creation of Latent Stromal Stores. *Journal of Interferon & Cytokine Research* **30**, 389–397 (2010).
96. Bauskin, A. R. *et al.* The propeptide mediates formation of stromal stores of PROMIC-1: role in determining prostate cancer outcome. *Cancer research* **65**, 2330–6 (2005).
97. Min, K. *et al.* NAG-1/GDF15 accumulates in the nucleus and modulates transcriptional

regulation of the Smad pathway. *Oncogene* **35**, 377–388 (2016).

98. Li, J. J. *et al.* Growth Differentiation Factor 15 Maturation Requires Proteolytic Cleavage by PCSK3, -5, and -6. *Molecular and cellular biology* **38**, 1–11 (2018).
99. Xu, J. *et al.* GDF15/MIC-1 functions as a protective and antihypertrophic factor released from the myocardium in association with SMAD protein activation. *Circulation Research* **98**, 342–350 (2006).
100. Heger, J. *et al.* Growth differentiation factor 15 acts anti-apoptotic and pro-hypertrophic in adult cardiomyocytes. *Journal of Cellular Physiology* **224**, 120–126 (2010).
101. Johnen, H. *et al.* Tumor-induced anorexia and weight loss are mediated by the TGF-β superfamily cytokine MIC-1. *Nature Medicine* **13**, 1333–1340 (2007).
102. Lu, J. M., Wang, C. Y., Hu, C., Fang, Y. J. & Mei, Y. A. GDF-15 enhances intracellular Ca2+by increasing Cav1.3 expression in rat cerebellar granule neurons. *Biochemical Journal* **473**, 1895–1904 (2016).
103. Lee, J. *et al.* Reconstitution of TGFBR2-Mediated Signaling Causes Upregulation of GDF-15 in HCT116 Colorectal Cancer Cells. *PLOS ONE* **10**, e0131506 (2015).
104. Olsen, O. E. *et al.* TGF-β contamination of purified recombinant GDF15. *PLoS ONE* **12**, 1–10 (2017).
105. Emmerson, P. J. *et al.* The metabolic effects of GDF15 are mediated by the orphan receptor GFRAL. *Nature Medicine* **23**, 1215–1219 (2017).
106. Mullican, S. E. *et al.* GFRAL is the receptor for GDF15 and the ligand promotes weight loss in mice and nonhuman primates. *Nature Medicine* **23**, 1150–1157 (2017).
107. Yang, L. *et al.* GFRAL is the receptor for GDF15 and is required for the anti-obesity effects of the ligand. *Nature Medicine* **23**, 1158–1166 (2017).
108. Mullican, S. E. & Rangwala, S. M. Uniting GDF15 and GFRAL: Therapeutic Opportunities in Obesity and Beyond. *Trends in Endocrinology and Metabolism* **29**, 560–570 (2018).
109. Tsui, K. *et al.* Growth differentiation factor-15: a p53- and demethylation-upregulating gene represses cell proliferation, invasion and tumorigenesis in bladder carcinoma cells. *Scientific Reports* **5**, 12870 (2015).
110. Kalli, M., Minia, A., Plia, V., Fotis, C. & Leonidas, G. A. Solid stress-induced migration is mediated by GDF15 through Akt pathway activation in pancreatic cancer cells. 1–12 (2019). doi:10.1038/s41598-018-37425-6
111. Yang, H., Park, S. H., Choi, H. J. & Moon, Y. The integrated stress response-associated signals modulates intestinal tumor cell growth by NSAID-activated gene 1 (NAG-1/MIC-1/PTGF-β). *Carcinogenesis* **31**, 703–711 (2010).
112. Wollert, K. C., Kempf, T. & Wallentin, L. Growth Differentiation Factor 15 as a Biomarker in Cardiovascular Disease. *Clinical Chemistry* **63**, 140–151 (2017).

113. Adela, R. & Banerjee, S. K. GDF-15 as a target and biomarker for diabetes and cardiovascular diseases: A translational prospective. *Journal of Diabetes Research* **2015**, (2015).
114. Corre, J., Hébraud, B. & Bourin, P. Concise Review: Growth Differentiation Factor 15 in Pathology: A Clinical Role? *STEM CELLS Translational Medicine* **2**, 946–952 (2013).
115. Welsh, J. B. *et al.* Large-scale delineation of secreted protein biomarkers overexpressed in cancer tissue and serum. *Proceedings of the National Academy of Sciences* **100**, 3410–3415 (2003).
116. Wiklund, F. E. *et al.* Macrophage inhibitory cytokine-1 (MIC-1/GDF15): A new marker of all-cause mortality. *Aging Cell* **9**, 1057–1064 (2010).
117. Daniels, L. B., Clopton, P., Laughlin, G. A., Maisel, A. S. & Barrett-Connor, E. Growth-differentiation factor-15 is a robust, independent predictor of 11-year mortality risk in community-dwelling older adults: The rancho bernardo study. *Circulation* **123**, 2101–2110 (2011).
118. Wang, X. *et al.* hNAG-1 increases lifespan by regulating energy metabolism and insulin/IGF-1/mTOR signaling. *Aging* **6**, 690–704 (2014).
119. Ho, J. E. *et al.* Clinical and genetic correlates of growth differentiation factor 15 in the community. *Clinical Chemistry* **58**, 1582–1591 (2012).
120. Moore, A. G. *et al.* The transforming growth factor-β superfamily cytokine macrophage inhibitory cytokine-1 is present in high concentrations in the serum of pregnant women. *Journal of Clinical Endocrinology and Metabolism* **85**, 4781–4788 (2000).
121. Kleinert, M. *et al.* Exercise increases circulating GDF15 in humans. *Molecular Metabolism* **9**, 187–191 (2018).
122. Kelly, J. A., Scott Lucia, M. & Lambert, J. R. p53 controls prostate-derived factor/macrophage inhibitory cytokine/NSAID-activated gene expression in response to cell density, DNA damage and hypoxia through diverse mechanisms. *Cancer Letters* **277**, 38–47 (2009).
123. Li, P. X. *et al.* Placental transforming growth factor-β is a downstream mediator of the growth arrest and apoptotic response of tumor cells to DNA damage and p53 overexpression. *Journal of Biological Chemistry* **275**, 20127–20135 (2000).
124. Baek, S. J., Wilson, L. C. & Eling, T. E. Resveratrol enhances the expression of non-steroidal anti-inflammatory drug-activated gene (NAG-1) by increasing the expression of p53. *Carcinogenesis* **23**, 425–434 (2002).
125. Wilson, L. C., Baek, S. J., Call, A. & Eling, T. E. Nonsteroidal anti-inflammatory drug-activated gene (NAG-1) is induced by genistein through the expression of P53 in colorectal cancer cells. *International Journal of Cancer* **105**, 747–753 (2003).
126. Baek, S. J., Kim, J.-S., Nixon, J. B., DiAugustine, R. P. & Eling, T. E. Expression of

NAG-1, a transforming growth factor-beta superfamily member, by troglitazone requires the early growth response gene EGR-1. *The Journal of biological chemistry* **279**, 6883–92 (2004).

127. Wang, X., Baek, S. J. & Eling, T. E. The diverse roles of nonsteroidal anti-inflammatory drug activated gene (NAG-1/GDF15) in cancer. *Biochemical Pharmacology* **85**, 597–606 (2013).
128. Sasahara, A. *et al.* An autocrine/paracrine circuit of growth differentiation factor (GDF) 15 has a role for maintenance of breast cancer stem-like cells. *Impact journals* **8**, 24869–24881 (2017).
129. Tsai, V. W. W., Husaini, Y., Sainsbury, A., Brown, D. A. & Breit, S. N. The MIC-1/GDF15-GFRAL Pathway in Energy Homeostasis: Implications for Obesity, Cachexia, and Other Associated Diseases. *Cell Metabolism* **28**, 353–368 (2018).
130. Mimeault, M. & Batra, S. K. Divergent molecular mechanisms underlying the pleiotropic functions of macrophage inhibitory cytokine-1 in cancer. *Journal of Cellular Physiology* **224**, 626–635 (2010).
131. Jäger, R., Bertrand, M. J. M., Gorman, A. M., Vandenabeele, P. & Samali, A. The unfolded protein response at the crossroads of cellular life and death during endoplasmic reticulum stress. *Biology of the Cell* **104**, 259–270 (2012).
132. Urra, H., Dufey, E., Avril, T., Chevet, E. & Hetz, C. Endoplasmic Reticulum Stress and the Hallmarks of Cancer. *Trends in Cancer* **2**, 252–262 (2016).
133. Hetz, C. The unfolded protein response: Controlling cell fate decisions under ER stress and beyond. *Nature Reviews Molecular Cell Biology* **13**, 89–102 (2012).
134. Hu, H., Tian, M., Ding, C. & Yu, S. The C/EBP homologous protein (CHOP) transcription factor functions in endoplasmic reticulum stress-induced apoptosis and microbial infection. *Frontiers in Immunology* **10**, 1–13 (2019).
135. Ubeda, M. *et al.* Stress-induced binding of the transcriptional factor CHOP to a novel DNA control element. *Molecular and Cellular Biology* **16**, 1479–1489 (1996).
136. Storm, M., Sheng, X., Arnoldussen, Y. J. & Saatcioglu, F. Prostate cancer and the unfolded protein response. *Oncotarget* **7**, 54051–54066 (2016).
137. Cubillos-Ruiz, J. R., Bettigole, S. E. & Glimcher, L. H. Tumorigenic and Immunosuppressive Effects of Endoplasmic Reticulum Stress in Cancer. *Cell* **168**, 692–706 (2017).
138. Mügge, F. L. B. & Silva, A. M. Endoplasmic reticulum stress response in the roadway for the effects of non-steroidal anti-inflammatory drugs. *Endoplasmic Reticulum Stress in Diseases* **2**, 1–17 (2015).
139. Liggett, J. L., Zhang, X., Eling, T. E. & Baek, S. J. Anti-tumor activity of non-steroidal anti-inflammatory drugs: Cyclooxygenase-independent targets. *Cancer Letters* **346**,

217–224 (2014).

140. Baek, S. J. & Eling, T. Growth differentiation factor 15 (GDF15): A survival protein with therapeutic potential in metabolic diseases. *Pharmacology and Therapeutics* **198**, 46–58 (2019).
141. Murielle, M. & Batra, S. K. Divergent molecular mechanisms underlying the pleiotropic functions of macrophage inhibitory cytokine-1 in cancer. *Journal of Cellular Physiology* **224**, 626–635 (2010).
142. Vaňhara, P., Hampl, a, Kozubík, a & Souček, K. Growth/differentiation factor-15: prostate cancer suppressor or promoter? *Prostate cancer and prostatic diseases* **15**, 320–8 (2012).
143. Emmerson, P. J., Duffin, K. L., Chintharlapalli, S. & Wu, X. GDF15 and Growth Control. *Frontiers in Physiology* **9**, 1–7 (2018).
144. Li, C. *et al.* GDF15 promotes EMT and metastasis in colorectal cancer. *Oncotarget* **7**, 860–72 (2016).
145. Roth, P. *et al.* GDF-15 contributes to proliferation and immune escape of malignant gliomas. *Clinical Cancer Research* **16**, 3851–3859 (2010).
146. Boyle, G. M. *et al.* Macrophage inhibitory cytokine-1 is overexpressed in malignant melanoma and is associated with tumorigenicity. *Journal of Investigative Dermatology* **129**, 383–391 (2009).
147. Lee, D. H. *et al.* Macrophage inhibitory cytokine-1 induces the invasiveness of gastric cancer cells by up-regulating the urokinase-type plasminogen activator system. *Cancer Research* **63**, 4648–4655 (2003).
148. Wang, T. *et al.* YAP promotes breast cancer metastasis by repressing growth differentiation factor-15. *Biochimica et Biophysica Acta - Molecular Basis of Disease* **1864**, 1744–1753 (2018).
149. Lambert, J. R. *et al.* Prostate derived factor in human prostate cancer cells: Gene induction by vitamin D via a p53-dependent mechanism and inhibition of prostate cancer cell growth. *Journal of Cellular Physiology* **208**, 566–574 (2006).
150. Albertoni, M. *et al.* Anoxia induces macrophage inhibitory cytokine-1 (MIC-1) in glioblastoma cells independently of p53 and HIF-1. *Oncogene* **21**, 4212–4219 (2002).
151. Zhang, Z. *et al.* Opposing effects of PI3K/Akt and smad-dependent signaling pathways in NAG-1-induced glioblastoma cell apoptosis. *PLoS ONE* **9**, 1–7 (2014).
152. Zimmers, T. A., Gutierrez, J. C. & Koniaris, L. G. Loss of GDF-15 abolishes Sulindac chemoprevention in the Apc Min/+ mouse model of intestinal cancer. *Journal of Cancer Research and Clinical Oncology* **136**, 571–576 (2010).
153. Jang, T. J., Kang, H. J., Kim, J. R. & Yang, C. H. Non-steroidal anti-inflammatory drug activated gene (NAG-1) expression is closely related to death receptor-4 and -5

induction, which may explain sulindac sulfide induced gastric cancer cell apoptosis. *Carcinogenesis* **25**, 1853–1858 (2004).

154. Hsu, E. M., McNicol, P. J., Guijon, F. B. & Paraskevas, M. Quantification of HPV-16 E6-E7 transcription in cervical intraepithelial neoplasia by reverse transcriptase polymerase chain reaction. *International Journal of Cancer* **55**, 397–401 (1993).
155. Scheffner, M., Werness, B. A., Huibregtse, J. M., Levine, A. J. & Howley, P. M. The E6 oncoprotein encoded by human papillomavirus types 16 and 18 promotes the degradation of p53. *Cell* **63**, 1129–36 (1990).
156. Hengstermann, A. *et al.* Growth suppression induced by downregulation of E6-AP expression in human papillomavirus-positive cancer cell lines depends on p53. *Journal of virology* **79**, 9296–300 (2005).
157. Tsai, V. W. W. W., Lin, S., Brown, D. A., Salis, A. & Breit, S. N. Anorexia-cachexia and obesity treatment may be two sides of the same coin: Role of the TGF-b superfamily cytokine MIC-1/GDF15. *International Journal of Obesity* **40**, 193–7 (2016).
158. Akella, N. M., Ciraku, L. & Reginato, M. J. Fueling the fire: Emerging role of the hexosamine biosynthetic pathway in cancer. *BMC Biology* **17**, 1–14 (2019).
159. Watson, J. V, Chambers, S. H. & Smith, P. J. A pragmatic approach to the analysis of DNA histograms with a definable G1 peak. *Cytometry* **8**, 1–8 (1987).
160. González, A., Jiménez, A., Vázquez, D., Davies, J. E. & Schindler, D. Studies on the mode of action of hygromycin B, an inhibitor of translocation in eukaryotes. *Biochimica et biophysica acta* **521**, 459–69 (1978).
161. Wemhoff, S., Klassen, R., Beetz, A. & Meinhardt, F. DNA Damage Responses Are Induced by tRNA Anticodon Nucleases and Hygromycin B. *PLOS ONE* **11**, e0157611 (2016).
162. Gaggelli, E. *et al.* Coordination pattern, solution structure and DNA damage studies of the copper(II) complex with the unusual aminoglycoside antibiotic hygromycin B. *Dalton transactions (Cambridge, England : 2003)* **39**, 9830–9837 (2010).
163. Hsiang, Y. H., Hertzberg, R., Hecht, S. & Liu, L. F. Camptothecin induces protein-linked DNA breaks via mammalian DNA topoisomerase I. *The Journal of biological chemistry* **260**, 14873–8 (1985).
164. Basch, H., Krauss, M., Stevens, W. J. & Cohen, D. Binding of Pt(NH3)32+ to nucleic acid bases. *Inorganic Chemistry* **25**, 684–688 (1986).
165. Bodley, A. *et al.* DNA topoisomerase II-mediated interaction of doxorubicin and daunorubicin congeners with DNA. *Cancer research* **49**, 5969–78 (1989).
166. Mandic, A., Hansson, J., Linder, S. & Shoshan, M. C. Cisplatin induces endoplasmic reticulum stress and nucleus-independent apoptotic signaling. *Journal of Biological Chemistry* **278**, 9100–9106 (2003).

167. Hetz, C., Chevet, E. & Harding, H. P. Targeting the unfolded protein response in disease. *Nature Publishing Group* **12**, 703–719 (2013).
168. Heifetz, A., Keenan, R. W. & Elbein, A. D. Mechanism of Action of Tunicamycin on the UDP-GlcNAc:Dolichyl-Phosphate GlcNAc-1 -Phosphate Transferase. *Biochemistry* **18**, 2186–2192 (1979).
169. Thastrup, O., Cullen, P. J., Drobak, B. K., Hanley, M. R. & Dawson, A. P. Thapsigargin, a tumor promoter, discharges intracellular Ca2+ stores by specific inhibition of the endoplasmic reticulum Ca2+-ATPase. *Proceedings of the National Academy of Sciences of the United States of America* **87**, 2466–2470 (1990).
170. Sørensen, H. T. *et al.* Risk of cancer in a large cohort of nonaspirin NSAID users: A population-based study. *British Journal of Cancer* **88**, 1687–1692 (2003).
171. Friel, G. *et al.* Aspirin and Acetaminophen Use and the Risk of Cervical Cancer. *Journal of Lower Genital Tract Disease* **19**, 189–193 (2015).
172. Tsutsumi, S. *et al.* Endoplasmic reticulum stress response is involved in nonsteroidal anti-inflammatory drug-induced apoptosis. *Cell Death and Differentiation* **11**, 1009–1016 (2004).
173. Karl, T. *et al.* Sulindac induces specific degradation of the HPV oncoprotein E7 and causes growth arrest and apoptosis in cervical carcinoma cells. *Cancer letters* **245**, 103–11 (2007).
174. Shams-Eldeen, M. A., Vallner, J. J. & Needham, T. E. Interaction of Sulindac and Metabolite with Human Serum Albumin. *Journal of Pharmaceutical Sciences* **67**, 1077–1080 (1978).
175. Jeong, H. K. *et al.* Cyclooxygenase inhibitors induce apoptosis in sinonasal cancer cells by increased expression of nonsteroidal anti-inflammatory drug-activated gene. *International Journal of Cancer* **122**, 1765–1773 (2008).
176. Kim, J. S., Baek, S. J., Sali, T. & Eling, T. E. The conventional nonsteroidal anti-inflammatory drug sulindac sulfide arrests ovarian cancer cell growth via the expression of NAG-1/MIC-1/GDF-15. *Molecular Cancer Therapeutics* **4**, 487–493 (2005).
177. Hanahan, D. & Weinberg, R. A. The Hallmarks of Cancer. *Cell* **100**, 57–70 (2000).
178. Kelley, M. L., Keiger, K. E., Lee, C. J. & Huibregtse, J. M. The Global Transcriptional Effects of the Human Papillomavirus E6 Protein in Cervical Carcinoma Cell Lines Are Mediated by the E6AP Ubiquitin Ligase. *Journal of Virology* **79**, 3737–3747 (2005).
179. Thierry, F. *et al.* A Genomic Approach Reveals a Novel Mitotic Pathway in Papillomavirus Carcinogenesis. *Cancer Research* **64**, 895–903 (2004).
180. Wan, F. *et al.* Gene expression changes during HPV-mediated carcinogenesis: A comparison between an in vitro cell model and cervical cancer. *International Journal of Cancer* **123**, 32–40 (2008).

181. Nees, M. *et al.* Papillomavirus Type 16 Oncogenes Downregulate Expression of Interferon-Responsive Genes and Upregulate Proliferation-Associated and NF- B-Responsive Genes in Cervical Keratinocytes. *Journal of Virology* **75**, 4283–4296 (2001).
182. Yang, Y. *et al.* Transcription factor C/EBP homologous protein in health and diseases. *Frontiers in Immunology* **8**, (2017).
183. Denoyelle, C. *et al.* Anti-oncogenic role of the endoplasmic reticulum differentially activated by mutations in the MAPK pathway. *Nature Cell Biology* **8**, 1053–1063 (2006).
184. Huber, A. L. *et al.* P58IPK-Mediated Attenuation of the Proapoptotic PERK-CHOP Pathway Allows Malignant Progression upon Low Glucose. *Molecular Cell* **49**, 1049–1059 (2013).
185. Thomas, M. C. & Chiang, C. M. E6 oncoprotein represses p53-dependent gene activation via inhibition of protein acetylation independently of inducing p53 degradation. *Molecular Cell* **17**, 251–264 (2005).
186. Bernat, A., Avvakumov, N., Mymryk, J. S. & Banks, L. Interaction between the HPV E7 oncoprotein and the transcriptional coactivator p300. *Oncogene* **22**, 7871–7881 (2003).
187. Ohoka, N., Hattori, T., Kitagawa, M., Onozaki, K. & Hayashi, H. Critical and functional regulation of CHOP (C/EBP homologous protein) through the N-terminal portion. *Journal of Biological Chemistry* **282**, 35687–35694 (2007).
188. Moremen, K. W., Tiemeyer, M. & Nairn, A. V. Vertebrate protein glycosylation: Diversity, synthesis and function. *Nature Reviews Molecular Cell Biology* **13**, 448–462 (2012).
189. Abd El-Aziz, S. H., Endo, Y., Miyamaori, H., Takino, T. & Sato, H. Cleavage of growth differentiation factor 15 (GDF15) by membrane type 1-matrix metalloproteinase abrogates GDF15-mediated suppression of tumor cell growth. *Cancer Science* **98**, 1330–1335 (2007).
190. Warburg, O., Wind, F. & Negelein, E. THE METABOLISM OF TUMORS IN THE BODY. *The Journal of General Physiology* **8**, 519–530 (1927).
191. Shalev, A. *et al.* Oligonucleotide microarray analysis of intact human pancreatic islets: Identification of glucose-responsive genes and a highly regulated TGFβ signaling pathway. *Endocrinology* **143**, 3695–3698 (2002).
192. Vaupel, P. & Mayer, A. Hypoxia in cancer: Significance and impact on clinical outcome. *Cancer and Metastasis Reviews* **26**, 225–239 (2007).
193. Kocher, R. A. Effects of a Low Lysine Diet on the Growth of Spontaneous Mammary Tumors in Mice and on the N2 Balance in Man. *Cancer Research* **4**, 251–256 (1944).
194. Cellarier, E. *et al.* Methionine dependency and cancer treatment. *Cancer Treatment Reviews* **29**, 489–499 (2003).
195. Kim, K. H. *et al.* Growth differentiation factor 15 ameliorates nonalcoholic steatohepatitis and related metabolic disorders in mice. *Scientific Reports* **8**, 1–14 (2018).

196. Iurlaro, R. *et al.* Glucose Deprivation Induces ATF4-Mediated Apoptosis through TRAIL Death Receptors. *Molecular and Cellular Biology* **37**, 1–17 (2017).
197. Jones, R. G. *et al.* AMP-activated protein kinase induces a p53-dependent metabolic checkpoint. *Molecular Cell* **18**, 283–293 (2005).
198. Okoshi, R. *et al.* Activation of AMP-activated protein kinase induces p53-dependent apoptotic cell death in response to energetic stress. *Journal of Biological Chemistry* **283**, 3979–3987 (2008).
199. Garufi, A. & D'Orazi, G. High glucose dephosphorylates serine 46 and inhibits p53 apoptotic activity. *Journal of Experimental and Clinical Cancer Research* **33**, 1–10 (2014).
200. Li, D., Zhang, H. & Zhong, Y. Hepatic GDF15 is regulated by CHOP of the unfolded protein response and alleviates NAFLD progression in obese mice. *Biochemical and biophysical research communications* **498**, 388–394 (2018).
201. Han, J. *et al.* ER-stress-induced transcriptional regulation increases protein synthesis leading to cell death. *Nature Cell Biology* **15**, 481–490 (2013).
202. Marciniak, S. J. *et al.* CHOP induces death by promoting protein synthesis and oxidation in the stressed endoplasmic reticulum. *Genes and Development* **18**, 3066–3077 (2004).
203. Behrman, S., Acosta-alvear, D. & Walter, P. A CHOP-regulated microRNA controls rhodopsin expression. **192**, 919–927 (2011).
204. Teng, M. S. *et al.* A GDF15 3′ UTR variant, rs1054564, results in allele-specific translational repression of GDF15 by hsa-miR-1233-3p. *PLoS ONE* **12**, 1–15 (2017).
205. Guo, T. M. *et al.* Predictive value of microRNA-132 and its target gene NAG-1 in evaluating therapeutic efficacy of non-steroidal anti-inflammatory drugs treatment in patients with ankylosing spondylitis. *Clinical Rheumatology* **37**, 1281–1293 (2018).
206. Li, J., Lee, B. & Lee, A. S. Endoplasmic Reticulum Stress-induced Apoptosis. *Journal of Biological Chemistry* **281**, 7260–7270 (2006).
207. Lin, W.-C. *et al.* Endoplasmic Reticulum Stress Stimulates p53 Expression through NF-κB Activation. *PLoS ONE* **7**, e39120 (2012).
208. Zappavigna, S. *et al.* Anti-Inflammatory Drugs as Anticancer Agents. *International Journal of Molecular Sciences* **21**, 2605 (2020).
209. Tewari, D., Majumdar, D., Vallabhaneni, S. & Bera, A. K. Aspirin induces cell death by directly modulating mitochondrial voltage-dependent anion channel (VDAC). *Scientific Reports* **7**, 45184 (2017).
210. Kim, K. Y., Seol, J. Y., Jeon, G. & Nam, M. J. The combined treatment of aspirin and radiation induces apoptosis by the regulation of bcl-2 and caspase-3 in human cervical cancer cell. *Cancer letters* **189**, 157–66 (2003).
211. Yueling, W., Hongmin, Z., Lin, L. & Jiangfen, W. Effect of aspirin alone or combined with

cisplatin on human cervical carcinoma HeLa cells. *Journal of Medical Colleges of PLA* **25**, 11–18 (2010).

212. Saha, B. *et al.* Restoration of tumor suppressor p53 by differentially regulating pro-and anti-p53 networks in HPV-18-infected cervical cancer cells. *Oncogene* **31**, 173–186 (2012).
213. Kim, S. H. *et al.* Erratum: GADD153 mediates celecoxib-induced apoptosis in cervical cancer cells (Carcinogenesis). *Carcinogenesis* **28**, 223–231 (2007).
214. Xiang, S. *et al.* Aspirin inhibits ErbB2 to induce apoptosis in cervical cancer cells. *Medical Oncology* **27**, 379–387 (2010).
215. Setiawati, A. Celecoxib , a COX-2 Selective Inhibitor , Induces Cell Cycle Arrest at the G2 / M Phase in HeLa Cervical Cancer Cells. **17**, 1655–1659 (2016).
216. Zimmermann, K. C., Waterhouse, N. J., Goldstein, J. C., Schuler, M. & Green, D. R. Aspirin Induces Apoptosis through Release of Cytochrome c from Mitochondria. *Neoplasia* **2**, 505–513 (2002).
217. Kutuk, O. & Basaga, H. Aspirin inhibits TNFα- and IL-1-induced NF-κB activation and sensitizes HeLa cells to apoptosis. *Cytokine* **25**, 229–237 (2004).
218. Vaish, V., Piplani, H., Rana, C., Vaiphei, K. & Sanyal, S. N. NSAIDs may regulate EGR-1-mediated induction of reactive oxygen species and non-steroidal anti-inflammatory drug-induced gene (NAG)-1 to initiate intrinsic pathway of apoptosis for the chemoprevention of colorectal cancer. *Molecular and Cellular Biochemistry* **378**, 47–64 (2013).
219. Kim, K. S. *et al.* Cyclooxygenase inhibitors induce apoptosis in oral cavity cancer cells by increased expression of nonsteroidal anti-inflammatory drug-activated gene. *Biochemical and Biophysical Research Communications* **325**, 1298–1303 (2004).
220. Dell'Omo, G. *et al.* Inhibition of SIRT1 deacetylase and p53 activation uncouples the anti-inflammatory and chemopreventive actions of NSAIDs. *British Journal of Cancer* **120**, 537–546 (2019).
221. Baek, S. J. Dual Function of Nonsteroidal Anti-Inflammatory Drugs (NSAIDs): Inhibition of Cyclooxygenase and Induction of NSAID-Activated Gene. *Journal of Pharmacology and Experimental Therapeutics* **301**, 1126–1131 (2002).
222. Xu, Y., Wang, C. & Li, Z. A new strategy of promoting cisplatin chemotherapeutic efficiency by targeting endoplasmic reticulum stress. *Molecular and clinical oncology* **2**, 3–7 (2014).
223. Shen, L. *et al.* Calcium efflux from the endoplasmic reticulum regulates cisplatin-induced apoptosis in human cervical cancer HeLa cells. *Oncology Letters* **11**, 2411–2419 (2016).
224. Altena, R. *et al.* Growth differentiation Factor 15 (GDF-15) plasma levels increase during bleomycin- And cisplatin-based treatment of testicular cancer patients and relate to

endothelial damage. *PLoS ONE* **10**, 1–15 (2015).

225. Kerley-Hamilton, J. S., Pike, A. M., Li, N., DiRenzo, J. & Spinella, M. J. A p53-dominant transcriptional response to cisplatin in testicular germ cell tumor-derived human embyronal carcinoma. *Oncogene* **24**, 6090–6100 (2005).
226. Ravera, M. *et al.* Antiproliferative activity of Pt(IV) conjugates containing the non-steroidal anti-inflammatory drugs (NSAIDs) Ketoprofen and Naproxen. *International Journal of Molecular Sciences* **20**, 1–18 (2019).
227. Luethy, J. D. & Holbrook, N. J. Activation of the gadd153 promoter by genotoxic agents: a rapid and specific response to DNA damage. *Cancer research* **52**, 5–10 (1992).
228. Gately, D. P., Sharma, A., Christen, R. D. & Howell, S. B. Cisplatin and taxol activate different signal pathways regulating cellular injury-induced expression of GADD153. *British Journal of Cancer* **73**, 18–23 (1996).
229. Ellinger-Ziegelbauer, H. *et al.* Characterization and interlaboratory comparison of a gene expression signature for differentiating genotoxic mechanisms. *Toxicological Sciences* **110**, 341–352 (2009).
230. Zhao, J. *et al.* The common stress responsive transcription factor ATF3 binds genomic sites enriched with p300 and H3K27ac for transcriptional regulation. *BMC Genomics* **17**, 1–14 (2016).
231. Wang, H., Mo, P., Ren, S. & Yan, C. Activating transcription factor 3 activates p53 by preventing E6-associated protein from binding to E6. *Journal of Biological Chemistry* **285**, 13201–13210 (2010).
232. Hegyesi, H., R., J., Sandor, N., Schilling-Toth, B. & Safrany, G. Validation of Growth Differentiation Factor (GDF-15) as a Radiation Response Gene and Radiosensitizing Target in Mammary Adenocarcinoma Model. *Breast Cancer - Recent Advances in Biology, Imaging and Therapeutics* (2012). doi:10.5772/21019
233. Kim, K. S. *et al.* Expression and regulation of nonsteroidal anti-inflammatory drug-activated gene (NAG-1) in human and mouse tissue. *Gastroenterology* **122**, 1388–1398 (2002).
234. Li, S., Ma, Y. M., Zheng, P. S. & Zhang, P. GDF15 promotes the proliferation of cervical cancer cells by phosphorylating AKT1 and Erk1/2 through the receptor ErbB2. *Journal of Experimental and Clinical Cancer Research* **37**, 1–14 (2018).
235. Naeger, L. K. *et al.* Bovine papillomavirus E2 protein activates a complex growth-inhibitory program in p53-negative HT-3 cervical carcinoma cells that includes repression of cyclin A and cdc25A phosphatase genes and accumulation of hypophosphorylated retinoblastoma protein. *Cell Growth and Differentiation* **10**, 413–422 (1999).
236. Scheffner, M., Munger, K., Byrne, J. C. & Howley, P. M. The state of the p53 and

retinoblastoma genes in human cervical carcinoma cell lines. **88**, 5523–5527 (1991).

237. Tate, J. G. *et al.* COSMIC: The Catalogue Of Somatic Mutations In Cancer. *Nucleic Acids Research* **47**, D941–D947 (2019).
238. Li, J. *et al.* Mutants TP53 p.R273H and p.R273C but not p.R273G Enhance Cancer Cell Malignancy. *Human Mutation* **35**, 575–584 (2014).
239. Luo, C., Fan, W., Jiang, Y., Zhou, S. & Cheng, W. Glucose-related protein 78 expression and its effects on cisplatin-resistance in cervical cancer. *Medical Science Monitor* **24**, 2197–2209 (2018).
240. Li, P. *et al.* Caspase-9: Structure, mechanisms and clinical application. *Oncotarget* **8**, 23996–24008 (2017).
241. Sopov, I. *et al.* Detection of cancer-related gene expression profiles in severe cervical neoplasia. *International Journal of Cancer* **112**, 33–43 (2004).
242. Holley, R. W. & Kiernan, J. A. Control of the initiation of DNA synthesis in 3T3 cells: low-molecular weight nutrients. *Proceedings of the National Academy of Sciences of the United States of America* **71**, 2942–2945 (1974).
243. Stylianopoulos, T. The Solid Mechanics of Cancer and Strategies for Improved Therapy. *Journal of Biomechanical Engineering* **139**, 1–10 (2017).
244. Hou, H. *et al.* Tunicamycin potentiates cisplatin anticancer efficacy through the dpagt1/akt/abcg2 pathway in mouse xenograft models of human hepatocellular carcinoma. *Molecular Cancer Therapeutics* **12**, 2874–2884 (2013).
245. Xu, Y. *et al.* Inhibition of autophagy enhances cisplatin cytotoxicity through endoplasmic reticulum stress in human cervical cancer cells. *Cancer Letters* **314**, 232–243 (2012).
246. Shi, Y. *et al.* Starvation-induced activation of ATM/Chk2/p53 signaling sensitizes cancer cells to cisplatin. *BMC Cancer* **12**, (2012).
247. Gerina-Berzina, A. *et al.* Determination of cisplatin in human blood plasma and urine using liquid chromatography-mass spectrometry for oncological patient s with a variety of fatty tissue mass for prediction of to xicity. *Experimental Oncology* **39**, 124–130 (2017).
248. Cattel, L., De Simone, M., Passera, R., Verlengo, M. C. & Delprino, L. Pharmacokinetics of cisplatin in semi-closed hyperthermic peritoneal perfusion (HPP) for treatment of peritoneal carcinomatosis. *Anticancer Research* **24**, 2041–2045 (2004).
249. Xu, Y. *et al.* Tolerance to endoplasmic reticulum stress mediates cisplatin resistance in human ovarian cancer cells by maintaining endoplasmic reticulum and mitochondrial homeostasis. *Oncology Reports* **34**, 3051–3060 (2015).
250. Xu, D. *et al.* Increased sensitivity to apoptosis upon endoplasmic reticulum stress-induced activation of the unfolded protein response in chemotherapy-resistant malignant pleural mesothelioma. *British Journal of Cancer* **119**, 65–75 (2018).

251. Andersen, T. B., López, C. Q., Manczak, T., Martinez, K. & Simonsen, H. T. Thapsigargin-From Thapsia L. to Mipsagargin. *Molecules* **20**, 6113–6127 (2015).
252. Jago, M. V. & Culvenor, C. C. Tunicamycin and corynetoxin poisoning in sheep. *Australian veterinary journal* **64**, 232–235 (1987).
253. Finnie, J. W. & O'Shea, J. D. Pathological and pathogenetic changes in the central nervous system of guinea pigs given tunicamycin. *Acta Neuropathologica* **75**, 411–421 (1988).
254. Kim, B. *et al.* Curcumin induces ER stress-mediated apoptosis through selective generation of reactive oxygen species in cervical cancer cells. *Molecular Carcinogenesis* **55**, 918–928 (2016).
255. Comitato, R. *et al.* Tocotrienols induce endoplasmic reticulum stress and apoptosis in cervical cancer cells. *Genes and Nutrition* **11**, 1–15 (2016).
256. Niyonizigiye, I., Ngabire, D., Patil, M. P., Singh, A. A. & Kim, G. Do. In vitro induction of endoplasmic reticulum stress in human cervical adenocarcinoma HeLa cells by fucoidan. *International Journal of Biological Macromolecules* **137**, 844–852 (2019).
257. Qiao, Y. *et al.* Associations between aspirin use and the risk of cancers: A meta-analysis of observational studies. *BMC Cancer* **18**, (2018).
258. Umar, A., Steele, V. E., Menter, D. G. & Hawk, E. T. Mechanisms of nonsteroidal anti-inflammatory drugs in cancer prevention. *Seminars in Oncology* **43**, 65–77 (2016).
259. Grabosch, S. M., Shariff, O. M. & Helm, C. W. Non-steroidal anti-inflammatory agents to induce regression and prevent the progression of cervical intraepithelial neoplasia. *Cochrane Database of Systematic Reviews* **2018**, (2018).
260. Bunz, F. *et al.* Requirement for p53 and p21 to sustain G2 arrest after DNA damage. *Science (New York, N.Y.)* **282**, 1497–501 (1998).
261. Chen, C. & Okayama, H. High-efficiency transformation of mammalian cells by plasmid DNA. *Molecular and Cellular Biology* **7**, 2745–2752 (1987).
262. Hanahan, D. Studies on transformation of Escherichia coli with plasmids. *Journal of Molecular Biology* **166**, 557–580 (1983).
263. Sambrook, J. & Russell, D. W. Preparation of Plasmid DNA by Alkaline Lysis with SDS: Maxipreparation. *CSH protocols* **2006**, (2006).
264. Brummelkamp, T. R., Bernards, R. & Agami, R. A system for stable expression of short interfering RNAs in mammalian cells. *Science* **296**, 550–553 (2002).
265. Jinek, M. *et al.* A Programmable Dual-RNA-Guided DNA Endonuclease in Adaptive Bacterial Immunity. *Science* **337**, 816–821 (2012).
266. Horvath, P. & Barrangou, R. CRISPR/Cas, the immune system of Bacteria and Archaea. *Science* **327**, 167–170 (2010).
267. Sanjana, N. E., Shalem, O. & Zhang, F. Improved vectors and genome-wide libraries

for CRISPR screening. *Nature Methods* **11**, 783–784 (2014).

268. Livak, K. J. & Schmittgen, T. D. Analysis of Relative Gene Expression Data Using Real-Time Quantitative PCR and the 2−ΔΔCT Method. *Methods* **25**, 402–408 (2001).
269. Bradford, M. M. A rapid and sensitive method for the quantitation of microgram quantities of protein utilizing the principle of protein-dye binding. *Analytical Biochemistry* **72**, 248–254 (1976).
270. Laemmli, U. K. Cleavage of structural proteins during the assembly of the head of bacteriophage T4. *Nature* **227**, 680–5 (1970).
271. Towbin, H., Staehelin, T. & Gordon, J. Electrophoretic transfer of proteins from polyacrylamide gels to nitrocellulose sheets: procedure and some applications. *Proceedings of the National Academy of Sciences* **76**, 4350–4354 (1979).
272. Cullmann, C. *et al.* Oncogenic human papillomaviruses block expression of the B-cell translocation gene-2 tumor suppressor gene. *International Journal of Cancer* **125**, 2014–2020 (2009).
273. Leitz, J. *et al.* Oncogenic Human Papillomaviruses Activate the Tumor-Associated Lens Epithelial-Derived Growth Factor (LEDGF) Gene. *PLoS Pathogens* **10**, e1003957 (2014).
274. Holland, D. *et al.* Activation of the enhancer of zeste homologue 2 gene by the human papillomavirus E7 oncoprotein. *Cancer Research* **68**, 9964–9972 (2008).